

TITLE TBD

A Thesis
Presented to
The Division of Mathematics and Natural Sciences
Reed College

In Partial Fulfillment
of the Requirements for the Degree
Bachelor of Arts

Kees Benkendorfer

May 2021

Approved for the Division
(Physics)

Andrew Larkoski

Acknowledgements

I want to thank a few people.

Preface

This is an example of a thesis setup to use the reed thesis document class.

List of Abbreviations

LHC	Large Hadron Collider
mMDT	Modified Mass Drop Tagger
QCD	Quantum Chromodynamics
QFT	Quantum Field Theory
SCET	Soft-Collinear Effective Theory

Table of Contents

Introduction	.	.	.	1
0.1	The physics of elementary particles	.	.	1
0.1.1	The Standard Model	.	.	1
0.1.2	(In)completeness of the Standard Model	.	.	3
0.1.3	Collider experiments	.	.	4
0.2	Thesis goals	.	.	7
0.2.1	Scientific	.	.	7
0.2.2	Pedagogical	.	.	9
0.3	Technical and notational conventions	.	.	9
Chapter 1: Technical introduction	.	.	.	13
1.1	Quantum Chromodynamics (QCD)	.	.	13
1.1.1	Approximate scale invariance	.	.	14
1.2	Groomed heavy hemisphere mass	.	.	15
1.2.1	Jets	.	.	16
1.2.2	Cross sections	.	.	17
1.2.3	Heavy hemisphere mass	.	.	18
1.2.4	Jet Grooming	.	.	19
1.3	Calculational techniques	.	.	23
1.3.1	Soft-Collinear Effective Theory (SCET)	.	.	23
1.3.2	Dimensional regularization	.	.	23
1.3.3	Resummation	.	.	24
Chapter 2: Leading-order calculation	.	.	.	25
2.1	Soft gluon	.	.	26
2.1.1	Setup	.	.	26
2.1.2	Calculation	.	.	30
2.2	Collinear gluon	.	.	31
2.2.1	Setup	.	.	31
2.2.2	Calculation	.	.	34
2.3	Soft-collinear gluon	.	.	34
2.4	Putting it all together	.	.	35
Chapter 3: Factorization formula	.	.	.	39
3.1	Setup	.	.	40

3.2	Power counting	41
3.2.1	Resolved soft emission	41
3.2.2	Ungroomed extra-soft unresolved radiation	42
3.2.3	Collinear radiation	42
3.3	Factorization	43
Chapter 4: All-orders calculation	45
4.1	Resummation	45
4.1.1	Strategy	46
4.1.2	Anomalous dimension	47
4.1.3	Solving the renormalization group equation	48
4.1.4	Full resummed result	51
4.2	Soft function	53
4.2.1	Setup	53
4.2.2	Coordinate choice	56
4.2.3	Computation, transformation, and Laurent series	59
4.2.4	Anomalous dimension	60
4.2.5	Resumming the soft function	61
Conclusion	65
Appendix A: Soft function integral	67
Appendix B: The dilogarithm function	73
References	75

Abstract

The preface pretty much says it all.

Dedication

You can have a dedication here if you wish.

Introduction

0.1 The physics of elementary particles

Modern particle physics is, ultimately, the result of a confluence of an ancient problem and an ancient technique. The problem: how does nature work on the most fundamental level? The technique: to smash objects together and see what comes out.

Of course, thousands of years of scientific development have led us to a more nuanced and sophisticated understanding than, say, the early atomic theories of Democritus and Lucretius — though echoes of these theories remain. We now understand¹ that almost all visible matter and almost all observed forces are, at root, manifestations of interactions between 17 fundamental particles (though there may yet be more). We conceive of these particles as excitations in fields which permeate space-time — this conception is known as quantum field theory.²

The goal of elementary particle physics³ is to understand these particles and fields at the deepest level.⁴ We would like to lay a complete framework, understanding their nature and their interactions to such an extent that one could, in principle, derive from first principles an explanation for any observed physical phenomenon. The field is a long way from that goal, but much progress has been made over the past centuries. Let us begin by summarizing what we know so far.

0.1.1 The Standard Model

The 17 known particles are organized in a framework called the Standard Model of particle physics [2, 3], displayed in schematic form in Fig. 1.

There are 12 particles, called **fermions**, which are the fundamental components of matter. These in turn are subdivided into **quarks** and **leptons**. Quarks, with names such as ‘up,’ ‘down,’ and ‘strange,’ combine in turn to form **hadrons** — among the hadrons are familiar composite particles like protons and neutrons.

The remaining 5 particles, called **bosons**, mediate interactions between particles.

¹Or at least, believe to understand

²Space-time itself is a geometric entity — we perceive this geometry as the force of gravity, acting on both human and cosmic scales — described by the theory of General Relativity.

³Also known simply as particle physics or high-energy physics

⁴Some particle theorists are also trying to unite quantum field theory with General Relativity. Whether they will ever succeed remains to be seen, but they do lots of pretty math

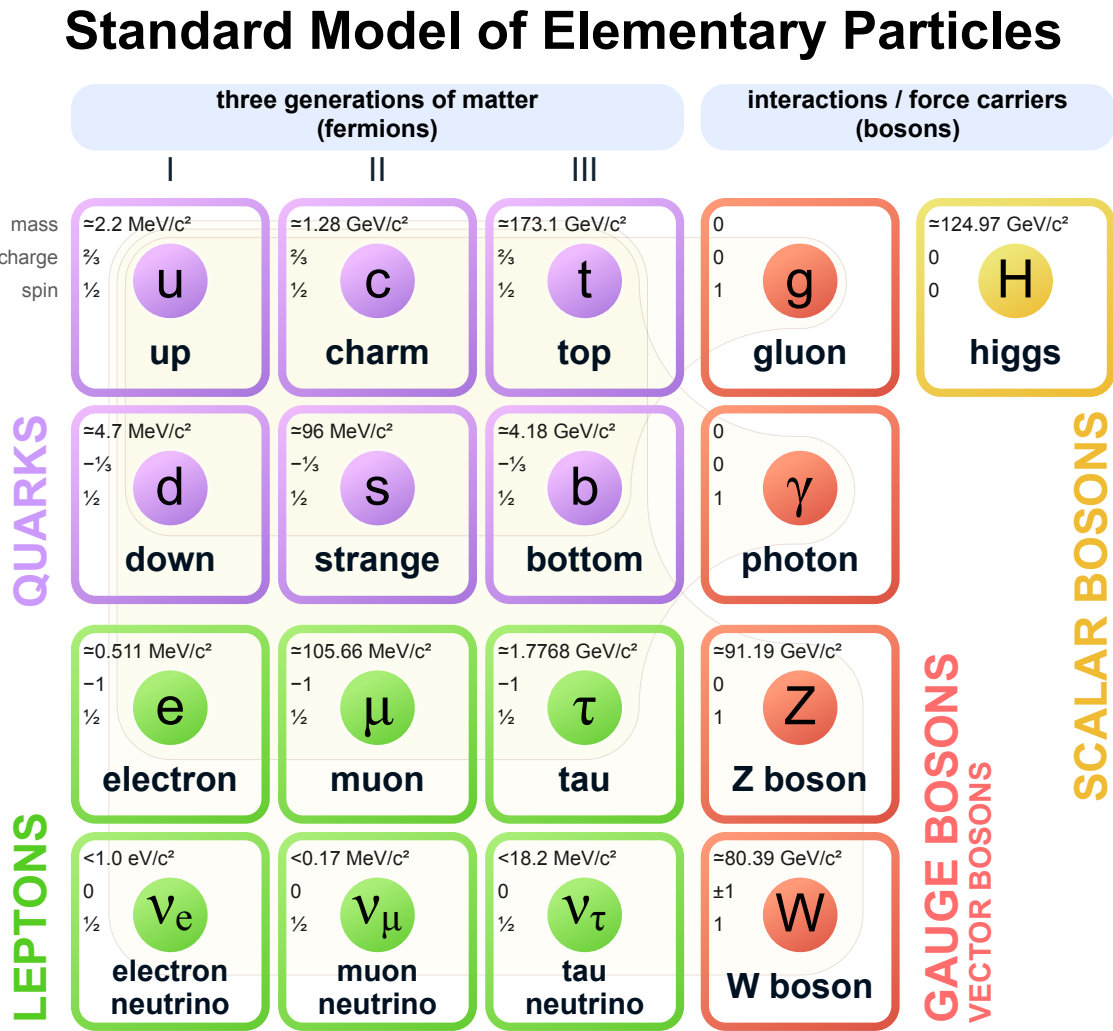


Figure 1: Diagram of the Standard Model of particle physics, as it currently stands. From [1]

Four of these are responsible for three of the forces of nature: the **gluon** is responsible for the strong force; the **photon** is responsible for the electromagnetic force; and the **W and Z bosons** are responsible for the weak force. In terms of familiar phenomena, the strong force is what binds together the nuclei of atoms; the electromagnetic force is what makes possible most of chemistry, electronics, and modern technology; and the weak force is responsible for the decay of unstable nuclei and particles. The final boson, the **Higgs boson**, is responsible for giving mass to most of the fundamental particles, and in a technical sense is the keystone which holds the Standard Model together.

In the Standard Model, each fermion is beholden to some subset of these bosons. The neutrinos experience the weak force and so interact via the W and Z bosons. The electron, muon, and tau experience the weak force as well, but they can also interact electromagnetically through exchange of photons. The quarks experience all of the fundamental forces, and can interact via any of the force-carrying bosons. It is the interaction of quarks and gluons through the strong force which will occupy most of this thesis.

0.1.2 (In)completeness of the Standard Model

The Standard Model is a remarkable theory. It explains many observed phenomenon with unparalleled accuracy — in fact, the Standard Model explanation of electromagnetism, called quantum electrodynamics, is the most precise physical theory ever constructed, making predictions that agree to less than 1 part per billion [2]. Experiment after experiment has confirmed predictions of the Standard Model, and in this sense it is a triumph of 20th-century physics.

In the present century, however, the strength of the theory is a significant problem in the field — for we know that the Standard Model is incomplete. While the theory is successful at describing small-scale physics, it is not nearly as successful on a cosmic scale: it has been observed that 84.4% of all matter in the universe is unknown to us and invisible except by gravitational signatures [4]. We would like to understand the composition of this so-called ‘dark matter.’ There are also more earthly hints that the Standard Model is incomplete. Among these, one of the most famous is the existence of neutrino masses. While the Standard Model describes neutrinos as massless particles, the Super-Kamiokande experiment discovered evidence in 1998 that neutrinos have a (tiny) non-zero mass [5] — these observations have since been verified by numerous other experiments [4]. Finally, there are aesthetic considerations. The Standard Model, as it currently stands, has a multitude of parameters (e.g., the masses of different particles) that currently have no basis in the theory; they must be supplied externally. If possible, we would like to be able to predict these parameters eventually.⁵

Thus, the Standard Model is incomplete. What can we do about that? There are two primary approaches to finding a solution:

⁵One can hardly say they understand something if, when asked why a particular detail is just so, their response is no more sophisticated than “That’s just the way it is.”

1. **Searches for new particles:** one strategy is to design experiments that attempt to generate and detect new, previously unobserved particles. This is a well-worn technique in particle physics, responsible for many of the advances in the field over the last 20th century. Famous examples of new-particle discoveries include the J/ψ in 1974 [6, 7], the discovery of the top quark in 1995 [8, 9], and the discovery of the Higgs boson in 2012 [10, 11]. Historically, whenever new experimental frontiers have been explored, new discoveries have followed, and with them, new understanding. This is not, of course, a guarantee that such will continue in the future.⁶ Nevertheless, it is the underlying (if simplified) philosophy for many new particle searches at modern experiments.
2. **Precision measurements of Standard Model parameters:** another, complementary strategy is to measure parameters of the Standard Model very precisely and then compare these measurements to theoretical predictions. These parameters could be anything from particle masses, to the strength of coupling constants, to the probability of a particular event after a particular interaction. If a discrepancy emerges, then that is a clue about where to consider modifying the Standard Model. Note, however, that to put a precise experimental measurement into a proper context, it is necessary to have at hand a precise theory. If we could measure, say, the mass of the muon⁷ to 1 part in 10^{20} , it would do us no good if the theoretical prediction were only confident to 1 part in 10^5 . Theory and experiment must both be sufficiently advanced to take full advantage of a precise measurement.

This thesis is situated firmly in the latter camp. We will be interested in precision theoretical predictions of a particular observable, called the ‘groomed heavy hemisphere mass mass,’ measured in high-energy electron-positron collisions. More will be said on this topic in due time.

0.1.3 Collider experiments

Although this thesis is theoretical in nature, it will be helpful to have some familiarity with the experiments whose outcomes we would like to predict. There is an enormous variety of experiments in particle physics, and it would be neither feasible nor helpful to discuss them all here. Instead, let us examine the two modern experiments most pertinent for our study to come. These experiments are called **ATLAS (A large Toroidal LHC ApparatuS)** and **CMS (Compact Muon Solenoid)**.⁸

Both of these are located at the Large Hadron Collider (LHC) at CERN in Geneva, Switzerland. The name of this collider is appropriate. Beams of protons are accelerated to around 99.9998% of the speed of light using a circular ring approximately

⁶Past performance is not a guarantee of future returns.

⁷Compared to the state of the art, this would be an outrageously precise measurement. The mass of the muon is currently accepted to be 105.658 374 5(24) MeV [4], which is a precision of approximately 1 part in 10^8 .

⁸Acronyms in particle physics get very unwieldy very quickly. But look how much fun they are!

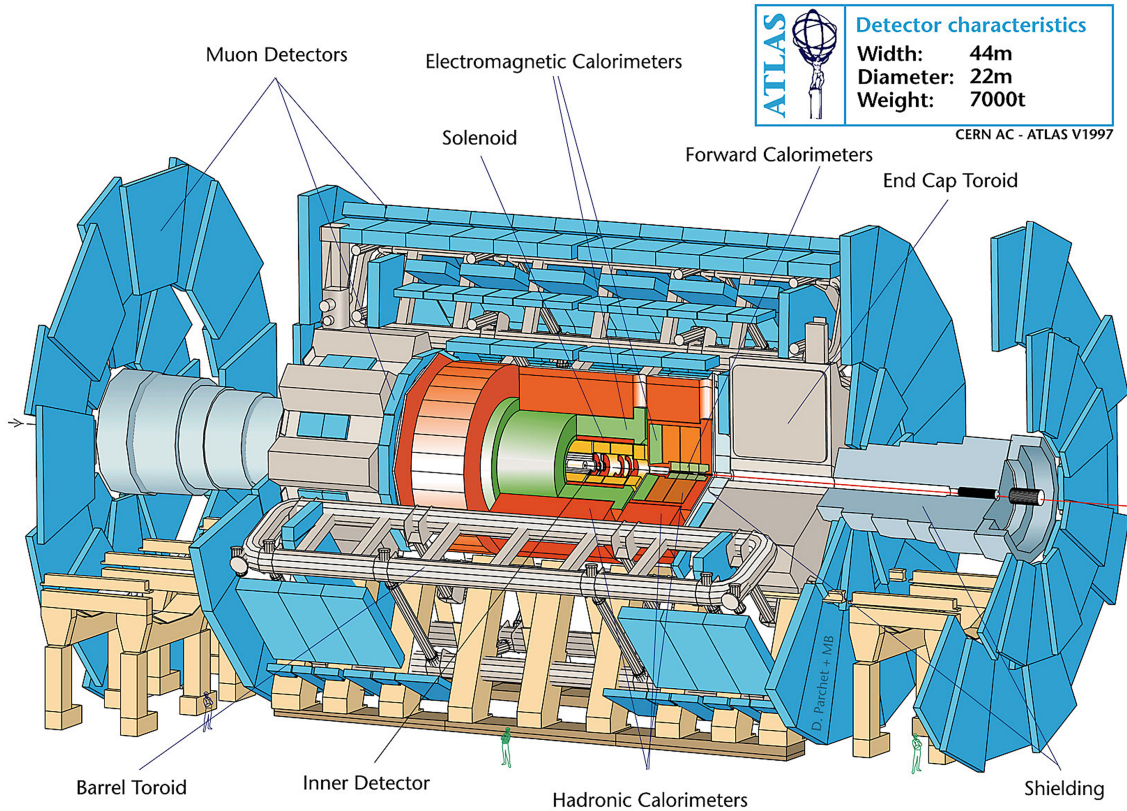


Figure 2: Schematic of the ATLAS experiment. For a sense of scale, note the people depicted along the bottom. Image from CERN [12]

27 km in circumference.⁹ Two beams circulate in the collider at a time, one traveling clockwise, the other counterclockwise. These beams are then maneuvered into collisions at four points around the ring, each located in the center of a massive, purpose-built experiment (in addition to ATLAS and CMS, there are two other experiments, called ALICE and LHCb). That is when the magic begins — the collision of these protons at high energy produces, through fundamental interactions, a huge variety of particles. By observing these particles, we hope to learn something about the interactions that brought them into being.

ATLAS and CMS are designed as multi-purpose experiments which detect all the products of the proton-proton collisions (or at least, they try to detect them). A schematic of the ATLAS detector is displayed in Fig. 2, and a schematic of CMS is displayed in Fig. 3. These detectors are built in layers surrounding the **interaction point**, with each layer serving a dedicated purpose. These layers can be summarized as follows [2]:

1. In the center of each detector is the **beam pipe**. This is where collisions take place.

⁹The ring straddles the French-Swiss border.

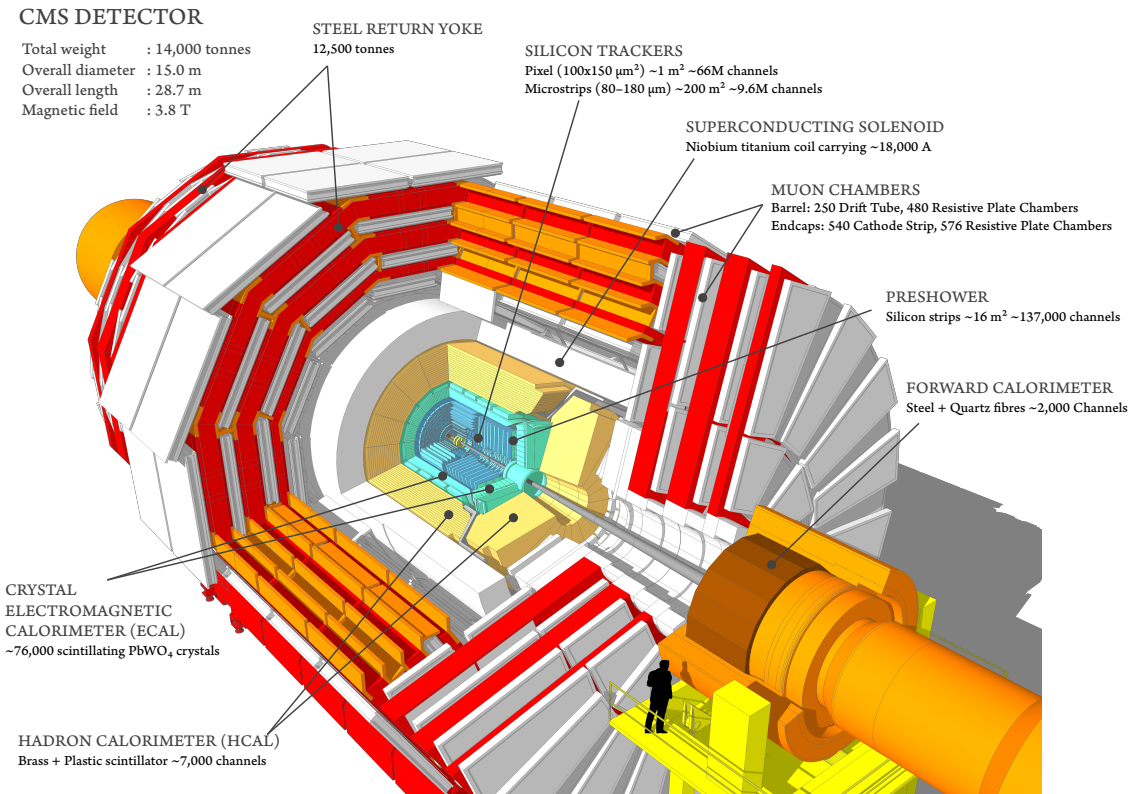


Figure 3: Schematic of the CMS experiment. Note the person on the far right for scale. Image from [13]

2. Immediately surrounding the beam pipe is a **tracking system**. The objective of this system is to track particles as they fly away from the interaction point. From these tracks, we can glean information about the energy, charge, and type of the particles.
3. Outside the tracking system is a **calorimetry system**. These are divided into two parts, the **electromagnetic calorimeter** and the **hadronic calorimeter**. The calorimetry system records information about the energy of particles. It works by absorbing this energy directly. The electromagnetic calorimeter is designed to most efficiently absorb particles which interact primarily through electromagnetism: electrons, photons, and the like. The hadronic calorimeter is designed to absorb hadrons like protons and neutrons.
4. High-energy muons often escape all inner layers of the detector. Their properties are measured using **muon detectors** which line the detector's exterior.

Using these systems, ATLAS and CMS are able to measure the outcome of more than a billion collision events per second [14]. This data gets stored and processed

at data centers distributed globally.¹⁰ Typical searches and measurements at these experiments then look for statistical signatures of interesting physics. This could be anything from an unexpected excess of events in a particular region of phase space (for a particle search) to the probability distribution of observing particular values of particle parameters (for Standard Model measurements).

0.2 Thesis goals

The objectives of this thesis can be divided into two categories: scientific and pedagogical. It will be necessary to properly balance the two. Our scientific focus will be rather technical, and too much emphasis on this would cloud the narrative and make it difficult to learn from the work. The other side of this coin is that, to achieve the pedagogical goals of the thesis, we will have to complete only a partial calculation. This is not a complete loss — what we achieve will be meaningful in its own right, and we will not have to suffer unnecessary tedium. Nevertheless, I warn the reader in advance that the story will be left incomplete.

But enough digression — what are the goals?

0.2.1 Scientific

The primary scientific objective of the thesis will be to complete an all-orders calculation of the distribution of groomed heavy hemisphere mass in $e^+e^- \rightarrow \text{jets}$ events, in the limit that the jet mass is approximately equal to the grooming cutoff. There are several moving parts here:

1. **$e^+e^- \rightarrow \text{jets}$ events:** We are going to consider collider events in which electrons and positrons annihilate to produce quarks and gluons. At high energies, because of the nature of the strong force, quarks and gluons manifest themselves in a detector as **jets**, or collimated sprays of hadronic particles. Note that these are not the type of collision events observed at the LHC, which is a proton-proton collider. Electron-positron annihilation is much easier to handle theoretically, and it turns out that we can generalize our results to pp collisions without much difficulty.
2. **Heavy hemisphere mass:** We are interested in an observable called heavy hemisphere mass. To compute heavy hemisphere mass, one can divide a collision event into two hemispheres, measure the mass of both hemispheres, and then take the greater of the two masses.
3. **Groomed:** When measuring an observable like jet mass, modern experiments like ATLAS and CMS must take into account significant amounts of background radiation from simultaneous events in the detector. One common technique is to perform ‘jet grooming,’ in which undesirable radiation is algorithmically removed from a jet. We will consider a particular grooming algorithm called the

¹⁰The scale of ATLAS and CMS is absolutely mind-boggling.

Modified Mass Drop Tagger (mMDT) [15], in which radiation with energy below some threshold is ignored. Such grooming can significantly alter the distribution of an observable, and it has important experimental and theoretical advantages. Understanding the effect of grooming on observables like jet mass is an active area of research.

4. **The limit:** Jets are a phenomenon of the strong force, and the theory of the strong force is rather unwieldy. It is therefore difficult to accurately predict an entire observable distribution with only one calculation. While the distribution of groomed heavy hemisphere mass is well understood in the low-mass limit [16, 17, 18] and in the high-mass regime [19], little study has been performed in the regime where the mass is approximately equal to the mMDT energy cutoff. Nevertheless, interesting physics occurs in this region — whereas events throughout the distribution all rely on the production of two back-to-back quarks, this region is the one in which a third (gluon) emission just begins to be resolved above the grooming threshold. Thus, this region is our focus.
5. **Calculation:** Just as we must perform calculations in particular limits to work with the strong force, so we must also perform calculations perturbatively, as a series expansion in the strong coupling constant α_s . That is, if we want to compute an observable ω , it is not usually feasible¹¹ to do so with perfect precision. Instead, we can expand ω in α_s ,

$$\omega(\alpha_s) = \omega_0 + \omega_1 \alpha_s + \omega_2 \alpha_s^2 + \dots = \sum_{n=0}^{\infty} \omega_n \alpha_s^n. \quad (1)$$

Then, to compute ω to a particular desired accuracy, we can simply compute the coefficients ω_i up to a particular order in α_s . Unfortunately, α_s is not a particularly small quantity, taking a value of order 0.1.¹² This means it often takes several terms to obtain a reasonable degree of accuracy.

6. **All-orders:** That said, we are aiming to achieve an all-orders calculation of the groomed heavy hemisphere mass. This does *not* mean that we will determine the distribution to infinite precision (i.e., infinite order in α_s). Instead, it means that we will derive an expression which can be used to push to *arbitrary accuracy* in α_s , given the proper accuracy of inputs (and the proper degree of mathematical sophistication). Thus, by an ‘all-orders calculation,’ we mean that we will develop a *framework* for achieving precision results. The term ‘all-orders’ also refers to the fact that our calculation will account for the influence of large logarithms at every order in α_s through the process of resummation.

A more complete development of these foundational concepts will be provided in Chapter 1.

¹¹At least with current theoretical techniques

¹²The strong coupling constant is not actually a constant...it changes with the energy of observation. This process is called the **running** of the strong coupling [2]. At the mass of the Z boson, $\alpha_s(m_Z) = 0.1179(10)$ [4].

0.2.2 Pedagogical

The primary pedagogical goal of this thesis is to understand the inner workings of a particular class of precision calculations in modern high-energy physics. The scientific objectives described above require a set of advanced theoretical tools which are interesting in their own right, but difficult to understand except through examples and context. Such tools include:

1. **Dimensional regularization:** There will be times when we must evaluate an integral which diverges when computed in the usual 4 dimensions (3 spatial dimensions and one temporal). We will get around this problem by performing such calculations in $d = 4 - 2\epsilon$ dimensions for some small ϵ [3]. The result will still diverge if we send $\epsilon \rightarrow 0$, but operating in this way will allow us to see the divergences explicitly, and cancel them as appropriate.
2. **Resummation:** A naïve series expansion of the distribution which we want to compute is plagued by corrections that take the form of logarithms of ratios of differing energy scales (e.g., the energy scale of a jet versus the energy scale of background radiation). When these scales are sufficiently different, the logarithm of their ratio becomes very large. Resummation is the process of getting a theoretical handle on these logarithmic corrections [2]. The primary thrust of this thesis can be viewed, in a sense, as one large resummation calculation.
3. **Soft and collinear effective theory (SCET):** Quantum field theory (QFT) is a remarkable description of the (subatomic) universe, but for our purposes it is too much machinery. Instead of using the full theory, we will make use of a low-energy effective theory called ‘soft and collinear effective theory’ (SCET). SCET is essentially a limiting case of full QFT, useful in the regime which we will occupy ourselves. As a simpler theory, SCET has some useful properties that we will exploit.

0.3 Technical and notational conventions

Before we embark, we must lay some mathematical ground rules. First, we hold Planck’s constant and the speed of light to be equal to unity: $\hbar = c = 1$. It turns out that non-unity values of these quantities are, for our purposes, redundant; when converting a given quantity back to SI units, the appropriate factors of c and \hbar can be intuited from context. The result is that all quantities will be measured in units of energy. Physics where we will be working is at the GeV scale and higher. Therefore, to a high degree of accuracy, we will assume all particles to be massless.

Unless otherwise stated (and we *will* eventually state otherwise), we will work in 4 dimensions, comprising the usual three spatial dimensions and one temporal dimension. Vectors in 4 dimensions (called four-vectors) are denoted by a Greek-letter index and take the form

$$p^\mu = (p^0, p^1, p^2, p^3). \quad (2)$$

The 0-th component of a four-vector is its ‘time’ (or equivalent) component, and the others are the ‘spatial’ (or equivalent) components. Thus, for example, a four-vector representing position would be

$$x^\mu = (t, x, y, z), \quad (3)$$

while a four-momentum has the components

$$p^\mu = (E, p_x, p_y, p_z) \quad (4)$$

with energy taking the place of time. It is sometimes convenient to refer to lower-dimensional pieces of a four-vector (usually two or three of the spatial components). When doing so, we will denote the sub-vector using a bold-face letter:

$$p^\mu = (E, \mathbf{p}), \quad \mathbf{p} = (p_x, p_y, p_z). \quad (5)$$

As is standard in high-energy physics, we will neglect the effects of gravity and assume we are working in a flat space-time. When combining four-vectors, we will therefore use the ‘mostly minus’ metric¹³

$$\eta^{\mu\nu} = \begin{pmatrix} 1 & 0 & 0 & 0 \\ 0 & -1 & 0 & 0 \\ 0 & 0 & -1 & 0 \\ 0 & 0 & 0 & -1 \end{pmatrix}. \quad (6)$$

We will also employ the Einstein summation notation, in which one sums over repeated indices in an expression (known as ‘contracting’ the index). Hence, for $p^\mu = (p^0, \mathbf{p})$ and $k_\mu = (k_0, \mathbf{k})$, we have

$$k_\mu p^\mu = k_0 p^0 + k_1 p^1 + k_2 p^2 + k_3 p^3. \quad (7)$$

With our choice of metric, there is little mechanical difference between a contravariant and a covariant four-vector; one picks up a formal minus sign in the spatial components, but that is all. We will, therefore, not distinguish between the two, and we will interchange upper and lower indices freely, bearing in mind that contracting an index negates the spatial terms of the sum. Hence, for $p^\mu = (p^0, \mathbf{p})$ and $k^\mu = (k^0, \mathbf{k})$, we will write¹⁴

$$k^\mu p_\mu = k_\mu p^\mu = k^\mu p^\mu = k_\mu p_\mu = k^0 p^0 - \mathbf{k} \cdot \mathbf{p}. \quad (8)$$

The final term is the standard dot product between the three-vectors. This choice enables us to abuse notation in a convenient manner: we will often drop the Greek sub/superscript on four-vectors, and use the standard notation of linear algebra to indicate their contraction:

$$k \cdot p = k^0 p^0 - \mathbf{k} \cdot \mathbf{p}. \quad (9)$$

¹³Also known as the ‘West Coast’ metric, among other names. The ‘East Coast’ metric takes the opposite sign convention. Our convention here is clearly the correct one, as it results in naturally positive masses.

¹⁴Sorry, Joel.

Let us end with a reminder about the connection between these four-vectors and the physical world. Suppose a particle has a momentum four-vector p^μ . Transforming our frame of reference to the particle's rest frame, we could write $p^\mu = (E, 0, 0, 0)$, where E is the particle's energy. But then, recalling the famous relation $E = mc^2 = m$ (since we set $c = 1$), we have

$$p^2 = p \cdot p = E^2 = m^2. \quad (10)$$

Thus, the square of a particle's four-momentum yields its squared mass. Recall now that we are assuming all particles to be massless; therefore, for any 'on-shell' particle (that is, a particle that could exist on its own and not just in some quantum fluctuation), we see that $p^2 = 0$, and also that $E^2 = \mathbf{p} \cdot \mathbf{p}$.¹⁵ This will greatly simplify our calculations later on.

With these details out of the way, let us proceed.

¹⁵This is not strictly an accurate proof of these properties, since massless particles move at the speed of light and one cannot boost into a light-like reference frame using Lorentz transformations. But the spirit of the argument is right, and the result is the same regardless.

Chapter 1

Technical introduction

It will be helpful to first develop a basic level of understanding about the groomed hemisphere mass distribution which we wish to calculate. In order to understand calculations which deal with the strong force, we must first study the theory of quantum chromodynamics (QCD), albeit at a superficial level. This will lead us naturally into a discussion of jet grooming, followed by a discussion of the calculational framework under which we will work, called Soft-Collinear Effective Theory (SCET). Then, after touching briefly on some specific techniques we will use later, we will be ready to start calculating.

1.1 Quantum Chromodynamics (QCD)

Recall that, in the Standard Model, quarks and gluons interact with each other via the strong force. The theory of the strong force is called quantum chromodynamics (QCD). In the context of quantum field theory, QCD can be described by the Lagrangian [2]

$$\mathcal{L}_{\text{QCD}} = -\frac{1}{4}F_{\mu\nu}^a F^{\mu\nu a} + \bar{\psi}i\gamma \cdot D\psi, \quad (1.1)$$

where $F_{\mu\nu}^a$ is the Yang-Mills field strength tensor, ψ is a spinor (describing quarks), and γ is a particular set of matrices. D is the covariant derivative defined by

$$D_\mu = \partial_\mu - igA_\mu^a T^a, \quad (1.2)$$

with g the strong force coupling, A_μ^a a field describing gluons, and T^a the matrices of the Lie algebra $\mathfrak{su}(3)$. The precise details of this theory are not important for our purposes. What is valuable is to contrast the QCD Lagrangian with the Lagrangian of quantum electrodynamics (QED), which describes electromagnetism.¹ This Lagrangian is [2]

$$\mathcal{L}_{\text{QED}} = -\frac{1}{4}F_{\mu\nu}F^{\mu\nu} + \bar{\psi}(i\gamma \cdot \partial - m - e\gamma \cdot A)\psi, \quad (1.3)$$

where A_μ is the vector potential of the photon, ψ describes fermions, and $F_{\mu\nu}$ is the electromagnetic field strength tensor. The value e is the electromagnetic coupling (or,

¹Electromagnetism is, hopefully, more familiar and intuitive to you than the strong force.

from a different perspective, the charge of the electron), and m is the mass of the electron.

Notice that Eqs. 1.1 and 1.3 are remarkably similar in structure. This hints at a fundamental similarity between the two theories. Both describe particles which carry a charge, as well as a massless force carrier which mediates interactions between particles with charge. In QED, that charge is the familiar electric charge; in QCD, it is called **color** charge.²³

The primary difference between these two theories lies in their field strength tensors. In QED, the field strength tensor is [2]

$$F_{\mu\nu} = \partial_\mu A_\nu - \partial_\nu A_\mu. \quad (1.4)$$

The result is that, in Lorentz gauge $\partial \cdot A = 0$,

$$\partial^2 A^\nu = 0, \quad (1.5)$$

which reveals the familiar fact that electromagnetism obeys the principle of superposition [2]. In contrast, the field strength tensor for QCD is [2]

$$F_{\mu\nu}^a = \partial_\mu A_\nu^a - \partial_\nu A_\mu^a + g f^{abc} A_\mu^b A_\nu^c. \quad (1.6)$$

Here, f^{abc} are the structure constants of the $\mathfrak{su}(3)$ algebra. Notice that the QCD field strength tensor has a third term relative to the QED field strength tensor. This term is quadratic in the gluon field, with the result that QCD is a highly nonlinear theory [2].

Physically, this means that gluons interact with themselves! This is a bizarre property which makes QCD simultaneously difficult to work with and very rich in structure. We will see a direct manifestation of this phenomenon in Sec. 1.2.1.

1.1.1 Approximate scale invariance

For our purposes, one of the most important consequences of the structure of the QCD Lagrangian is that the theory is (approximately) scale invariant. What this means is that, if we shift the energy scale of a system governed by QCD, its dynamics are unchanged.

To see this, one can observe the action of the QCD Lagrangian under a scale dilation $x^\mu \rightarrow \lambda x^\mu$. In the limit of massless quarks, the QCD action is [2]

$$S[A_\mu^a, \psi] = \int d^4x \left[-\frac{1}{4} F_{\mu\nu}^a F^{\mu\nu a} + \bar{\psi} i\gamma \cdot D\psi \right]. \quad (1.7)$$

Under the dilation $x^\mu \rightarrow \lambda x^\mu$, the action transforms as [2]

$$\begin{aligned} S[A_\mu^a, \psi] &\rightarrow \int d^4x \lambda^4 \left[-\frac{1}{4} \lambda^{-2} F_{\mu\nu}^a \lambda^{-2} F^{\mu\nu a} + \lambda^{-3/2} \bar{\psi} i\gamma \cdot D\lambda^{-1} \psi \lambda^{-3/2} \right] \\ &= S[A_\mu^a, \psi]. \end{aligned} \quad (1.8)$$

²Hence the name quantum **chromodynamics**

³Incidentally, the color charge of QCD has absolutely nothing to do with color as we usually think of it. It is simply a whimsical name.

Scale invariance is another remarkable feature of QCD, which will become important in Sec. 1.2.1.

You will notice, however, that we said the scale invariance is only approximate. That is because the argument outlined above depends on the assumption that the strong coupling g in the field strength tensor, Eq. 1.6, is a constant. It turns out that this is not the case. For quantum mechanical reasons, the coupling of the strong force is affected by the temporary production of virtual particles; at different energies, these effects result in different corrections. This is known as the **running coupling** of the strong force.⁴ For an intuitive description of the mechanics of this effect, see Ref. [2].

We need to take into account the running of the strong coupling when we perform calculations in QCD. Defining the strong coupling to be

$$\alpha_s = \frac{g^2}{4\pi}, \quad (1.9)$$

the running of the coupling is described by the β -function, defined by [2]

$$\beta(\alpha_s) = \mu \frac{\partial \alpha_s}{\partial \mu} \quad (1.10)$$

for an energy scale μ . The β -function can be computed perturbatively in α_s ; more information about this, including specific values, is given in Sec. 4.1.3. Where the running of the strong coupling is important, we will write $\alpha_s(\mu)$ to mean the coupling at a particular scale.

While the running of the strong coupling is an important effect for precision calculations, its effect is small at high energies, so we can still consider QCD to be scale invariant to a reasonable degree of accuracy.

As remarkable as scale invariance is, it has a significant downside from the perspective of QCD calculations. Many calculations of interest, like the distribution of groomed heavy hemisphere jet masses which we will calculate, impose scales onto the theory (such as the scale of the energy cutoff in jet grooming). In a sense, when one tries to impose a scale onto a scale-invariant theory like QCD, the theory fights back. Logarithms of ratios of scales emerge in the calculation that can grow very large if the scales are far apart, and it is important to account for these effects [2, 20]. Our calculation will use the technique of **resummation** to account for these large logarithms in a consistent manner.

1.2 Groomed heavy hemisphere mass

Now that we have a basic understanding of the theory of QCD, it is time to learn what we are trying to study.

⁴The same effect actually occurs in QED, with the provocative result that the charge of the electron, as we typically conceive of it, is not actually constant.

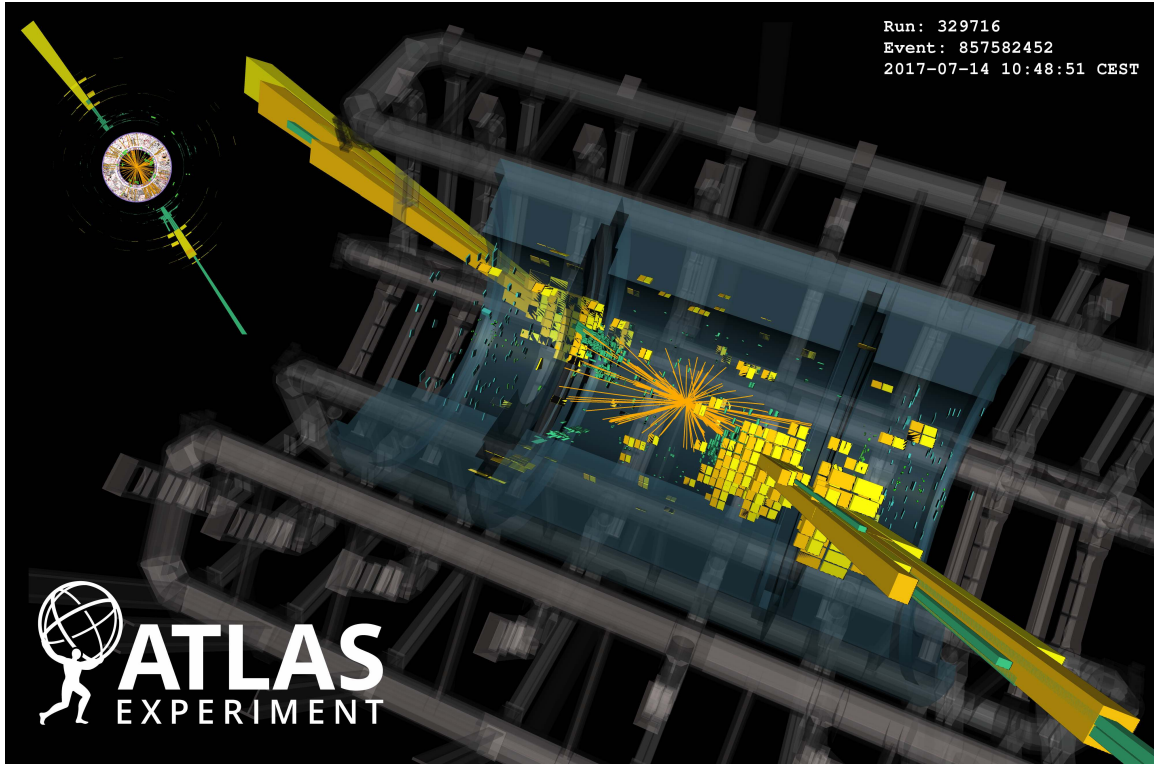


Figure 1.1: An event captured by the ATLAS detector in 2017 in which two jets are produced. From [21]

1.2.1 Jets

Two oddities of QCD discussed in Sec. 1.1 — the gluon self-interaction and the scale invariance of QCD — conspire to generate a unique experimental phenomenon called **jets**. As a high-energy quark or gluon propagates, it radiates gluons, which in turn might produce quark-antiquark pairs, which then radiate gluons, and so on. Because QCD is scale invariant, as we ‘zoom in’ on the emissions,⁵ we will see the same structure emerge at all scales. That is, when a color-charged particle is produced at high energy, there will be an arbitrary number of emissions alongside that particle [2].

As we discussed above, however, QCD is not truly scale-invariant, and as more particles are emitted the energy of each individual particle decreases. Eventually, the energy falls to the GeV scale and below, at which point **hadronization** occurs — quarks and gluons settle into bound states like protons, neutrons, and pions. The end result of all this is that we never see an individual quark or gluon in a detector. Instead, we see collimated streams of these hadronic particles, to which the term ‘jet’ refers.

Figure 1.1 shows an example of the production of two jets in a proton-proton collision in the ATLAS experiment at the Large Hadron Collider. The solid bars

⁵By changing either the length or the energy scale

represent particle energies measured in the hadronic calorimeter. Notice that the energy is deposited in strongly collimated streams, as predicted.

1.2.2 Cross sections

We would like to compute properties of jets in electron-positron collisions. But what are the actual objects we can work with?

In high-energy physics, the standard experimental strategy is to perform many particle collisions, observe the results of each collision, and then make observations about these results *en masse*. Because of the probabilistic nature of quantum mechanics, there is little to be learned from individual events. Instead, questions in the field require statistical answers drawn from massive datasets.

One basic question one could reasonably ask in this context is “What is the probability of event X occurring?” We describe this probability as a **cross section** $\sigma(X)$.⁶ Cross sections are measured in units of area called **barns**, with $1 \text{ b} = 10 \times 10^{-24} \text{ cm}^2$.⁷

If it is not interesting enough to measure the probability of a specific process occurring, one might instead ask about the distribution of a cross section over a particular observable. If we want to measure the distribution of x in a collision event, then we could measure the **differential cross section** $d\sigma/dx$. If cross sections are essentially probabilities, then differential cross sections are probability distributions — they tell us the probability of that the variable x will take on a set of values. Integrating over x would return the total cross section σ .

Cross sections can be either inclusive or exclusive. An **inclusive** cross section is one which allows for a particular event *alongside anything else*. For example, suppose we are interested in the production of a quark-antiquark pair in electron-positron collisions, but do not care if additional particles are produced:

$$e^+ e^- \rightarrow q\bar{q} + X \tag{1.11}$$

for some arbitrary particles X . Then the cross section $\sigma(e^+ e^- \rightarrow q\bar{q} + X)$ is inclusive [2]. The production of additional particles comes with reduced probability, so the inclusive cross section is a reasonable approximation for the event $e^+ e^- \rightarrow q\bar{q}$.

On the other hand, suppose that we wanted to perform precision studies of quark production in electron-positron annihilation and therefore demand that other particles in the final state have certain features

$$e^+ e^- \rightarrow q\bar{q} + (\text{particles with certain qualities}). \tag{1.12}$$

⁶The origin of the term comes from early experiments which measured the probability of two particles colliding with or scattering off of each other. The term ‘cross section’ was an attempt to draw an analogy to the classical problem of two macroscopic objects colliding. The probability that they will hit each other is proportional to their cross-sectional area.

⁷The origin of the unit ‘barn’ comes from the Manhattan project, where the problem *du jour* was to calculate the probability that neutrons would, say, cause fission events in materials like uranium. It turns out that the probability of neutron absorption by U-235 is on the order of 1 b, and this probability was deemed to be ‘as big as a barn’. There is another side to the story involving unfortunate names and bathroom humor, which can be read in Ref. [22].

These demands result in a restriction of the allowed phase space of final states, so we call this an **exclusive** cross section. It becomes important to account for all energy scales imposed by these restrictions — it is these energy scales which can give rise to large logarithms which must be resummed [2].

Cross sections can be computed using **Fermi's Golden Rule** [2, 3],

$$\sigma = \mathcal{N} \int d\Pi_{\text{LIPS}} |\mathcal{M}|^2, \quad (1.13)$$

where \mathcal{N} is a normalizing constant. $d\Pi_{\text{LIPS}}$ is called the Lorentz-invariant phase space measure. It ranges over all the possible four momenta of the n final-state particles, each with momentum p_i^μ . It is defined to be

$$d\Pi_{\text{LIPS}} = (2\pi)^4 \delta^4 \left(P - \sum_{i=1}^n p_i \right) \prod_{i=1}^n \frac{d^4 p_i}{(2\pi)^3} \delta(p_i^2 - m_i^2), \quad (1.14)$$

where P is the total four-momentum of the initial-state particles. The first Dirac delta function enforces conservation of momentum, while the second enforces that every final-state particle is **on-shell**, meaning essentially that it is real. An on-shell particle with momentum p and mass m satisfies $p^2 = m^2$.⁸

The last term in Eq. 1.13 is called the *S*-matrix element, or, more commonly, just the **matrix element**. The *S*-matrix is the scattering matrix which encodes all possible transitions from an initial state to a final state [2]. Thus, for initial-state particles $p_1^i, p_2^i, \dots, p_m^i$ and final-state particles $p_1^f, p_2^f, \dots, p_n^f$, the matrix element is

$$\langle p_1^i p_2^i \cdots p_m^i | p_1^f p_2^f \cdots p_n^f \rangle. \quad (1.15)$$

While Eq. 1.13 allows for the calculation of a total cross section, it must be slightly modified to compute a differential cross section. To measure an observable x , we must introduce a measurement term of the form

$$\delta_x = \delta(x - f(p_1, p_2, \dots, p_n)) \quad (1.16)$$

where $f(p_1, p_2, \dots, p_n)$ is a function of the final-state momenta. Integrating over this delta function inserts the observable in place of the function f of the momenta. Thus, the version of Fermi's Golden Rule which we will use is

$$\frac{d\sigma}{dx} = \mathcal{N} \int d\Pi_{\text{LIPS}} |\mathcal{M}|^2 \delta_x.$$

(1.17)

1.2.3 Heavy hemisphere mass

One of the most basic properties of anything is its mass, so it is reasonable that we might want to know the distribution of possible jet masses. This can both provide information about the physics of jets and assist in precision measurements of quantities like the strong coupling α_s .

⁸It is possible, quantum mechanically, for particles to exist for a brief period of time *off-shell*. We call these virtual particles, and they are important for high-order corrections in many calculations. In fact, it is these off-shell virtual particles which generate the running of the strong coupling α_s .

Although the state-of-the-art collider, the LHC, collides protons on protons, this experimental arrangement is problematic for precision measurements.⁹ Protons are composite particles — each consists of two up quarks and one down quark — and when they collide it is impossible to know even which fundamental particles interacted with which other particles, let alone to know their momenta or energies. In short, proton-proton collisions are a (useful) mess. By contrast, electrons and positrons are fundamental particles, and parameters of their collisions can be very well-controlled in colliders. For these and other reasons, electron-positron collisions are viewed as the ultimate precision tool.¹⁰

It also happens (for similar reasons) that electron-positron collisions are much easier to account for theoretically than proton-proton collisions. We are therefore going to consider $e^+e^- \rightarrow \text{jets}$ events.

We wish to measure the heavy hemisphere mass ρ , which will be defined shortly. In the limit $\rho \ll 1$, the leading contribution to the distribution comes from the emission of a back-to-back quark-antiquark pair (such an event is visible in Fig. 1.1). The mass of each hemisphere can be measured separately as the sum of all particles in the hemisphere. If hemisphere i has mass m_i and energy E_i , the hemisphere mass ratio of interest is defined to be

$$\rho_i = \left(\frac{m_i}{E_i} \right)^2. \quad (1.18)$$

The heavy hemisphere mass ratio is simply the larger of the two:

$$\rho = \max[\rho_1, \rho_2] = \left(\frac{m_h}{E_h} \right)^2, \quad (1.19)$$

with m_h the mass of the heavier hemisphere and E_h its energy. Our target distribution will be the differential cross section $d\sigma/d\rho$.

1.2.4 Jet Grooming

The story is not quite done, as we still need to take jet grooming into account. Jet grooming is a primarily experimental technique used to obtain clean data. Particle collisions and measurements do not happen on their own — since the probability of a collision between particles in a collider is low, the particles are collided in large bunches to ensure at least one collision event per beam crossing. As technology has improved, collision probabilities have been brought higher, which means that an increasing number of collisions happen per crossing.

⁹Though it is excellent for the discovery of new particles, which was the founding mission of the LHC.

¹⁰There are other problems, though, namely that synchrotron radiation makes it all but impossible to develop an e^+e^- collider which could reach energies above a few hundred GeV. Other leptons have nice collisional properties, though, while their higher mass limits the problems with energy loss during acceleration. For this reason, there is a growing discussion about building a muon-antimuon collider in the coming decades — if the funding could be found! There are also plenty of technical challenges with this idea that need to be solved first.

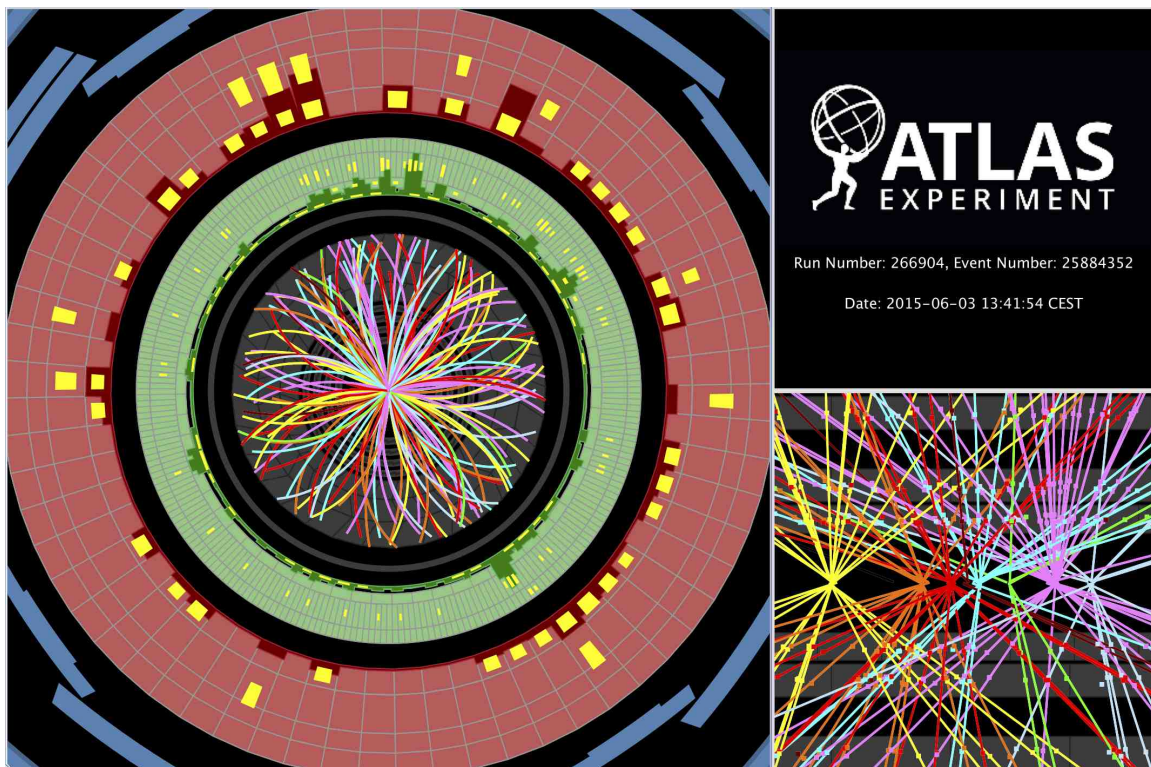


Figure 1.2: An event captured by the ATLAS detector in 2015 which exhibits moderate pileup. From [23]

When multiple collisions happen simultaneously in the detector, the situation is called **pileup**. An example of an event with moderate pileup¹¹ is displayed in Fig. 1.2. Notice how particles from each interaction stray into other interactions, possibly contaminating data on those interactions. This is not a problem for something like the tracking system, which can reproduce a particle's track to identify which interaction generated it; but for the calorimetry system, which is the primary way to measure jet masses, it is very difficult to disentangle these interactions.

Particle physicists have developed a number of **jet grooming** techniques to study jet properties while minimizing these effects. The basic idea of a jet groomer is to cut away particles with undesirable properties.

We will focus on one, which is a slightly modified version of the Modified Mass Drop Tagger (mMDT) [15]. The algorithm is as follows [17]:

1. Divide the event into two hemispheres
2. For each hemisphere, run the Cambridge/Aachen jet algorithm [24, 25]:
 - (a) Create a table T of the energies E_i of particles and an ordering variable $R_{ij}^2 = \Delta\eta_{ij}^2 + \Delta\phi_{ij}^2$, where i and j range over all particles, ϕ is the azimuthal angle, and η is pseudorapidity.¹² Set some cutoff R_0 .
 - (b) If T contains only one item, store this item as a jet and return the jets
 - (c) Select particles (i, j) which minimize R_{ij}^2
 - (d) Do the following:
 - If $R_{ij}^2 < R_0$, delete i and j from T . Create a new particle (ij) with momentum $p_{ij} = p_i + p_j$, recompute relevant values of the ordering variable, and add (ij) to T
 - If $R_{ij}^2 \geq R_0$, store i and j as jets and delete them from T
 - (e) Repeat, starting at step (b)

In summary, the Cambridge/Aachen algorithm clusters sequentially particles by angular proximity.

3. Pick some $0 \leq z_{\text{cut}} < 1/2$. Starting in one hemisphere at the widest angle, iterate through the pairs of particles (or sets of particles) returned in step (2). For each pair of particles i, j , test whether

$$\frac{\min [E_i, E_j]}{E_i + E_j} > z_{\text{cut}}. \quad (1.21)$$

¹¹In fact, the pileup of this event is fairly low by today's standards. Within the next decade, after the LHC undergoes its High Luminosity upgrade, as many as dozens of collisions could happen per bunch crossing.

¹²Pseudorapidity is defined as

$$\eta = -\log\left(\tan\frac{\theta}{2}\right), \quad (1.20)$$

where θ is the polar angle from the beam axis. As the angle of the particle approaches the beam axis, $\eta \rightarrow \infty$.

If it is true, stop and return all particles remaining in the hemisphere. If not, remove the lower energy set of particles. Repeat this step until the hemisphere passes the cut.

4. Repeat step (3) for the other hemisphere.

The intuition behind the mMDT groomer is that it removes particles whose energy fraction falls below z_{cut} , unless the particles are at a smaller angle than one which passed the cut. Most stray background radiation will appear with low energy at a wide angle relative to the core of the jet — an mMDT groomer removes this radiation.

Of course, we also run the risk that some of the radiation from the jet itself will be cut by the groomer. That is why we need to calculate the jet mass distribution in the presence of mMDT grooming, since the groomer will modify the shape of the ungroomed distribution. High-precision calculations have already been performed in the limit $\rho \ll z_{\text{cut}} \ll 1$ [18, 16, 17], as well as at fixed order (which is accurate for large ρ) [19]. As of yet, the distribution is not well-understood in the limit $\rho \sim z_{\text{cut}} \ll 1$, though this is an important region physically, as the relative size of the two scales is no longer dramatically different [26]. This, then is the goal:

We wish to calculate the differential cross section $d\sigma/d\rho$, with ρ defined by Eq. 1.19, in $e^+e^- \rightarrow \text{jets}$ events in the presence of mMDT grooming. We will work in the limit $\rho \sim z_{\text{cut}} \ll 1$.

While it might be reasonable to worry that the grooming algorithm will make the calculation more difficult (it introduces another external scale z_{cut} , after all), it turns out that there are theoretical benefits to jet grooming, in addition to the experimental ones. A common problem in the calculation of jet observables is the presence of **non-global logarithms**, which are large logarithms of scales from radiation external to the jet.¹³ This could be, for example, due to background radiation which radiates particles into the jet as it passes. The presence of non-global logarithms has made it difficult to compute the ungroomed jet mass distribution to high accuracy [15]. However, it turns out that mMDT grooming eliminates the radiation which could give rise to non-global logarithms, which enables us to achieve higher accuracy than might otherwise be feasible [15, 18].

This is not the only benefit. It also turns out that the groomed jet mass is more sensitive to the strong coupling α_s than the ungroomed version [26]. If our goal is to measuring α_s using jet masses — and this would be a valiant goal, as it would be a novel way to measure the coupling and therefore a strong verification of the Standard Model — then this provides another reason to be interested in the groomed distribution.

Thus, though we may gain some degree of complication in our calculation from the grooming algorithm, it is well worth the cost. Now let us figure out how to compute it.

¹³This is the theoretical justification for hating background radiation.

1.3 Calculational techniques

1.3.1 Soft-Collinear Effective Theory (SCET)

The machinery of quantum field theory is, in some sense, too powerful. While the theory is extremely effective at predicting observations in nature, it is also unwieldy. Getting from the QCD Lagrangian of Eq. 1.1 to a precision calculation of the groomed heavy hemisphere mass would be simultaneously very difficult and not very enlightening.

Luckily for us, QCD simplifies in the low-energy, or **soft**, limit in which we will be working (since we are taking $\rho \ll 1$). In this limit, we can replace QCD with a low-energy effective theory called Soft-Collinear Effective Theory (SCET) [27, 28, 29, 30, 31, 32, 33]. The precise details of SCET are unimportant for our purposes — for more information, see Refs. [3] or [20].

What we will use is the framework which SCET provides for factorizing cross sections. In general, the differential cross section for an $e^+e^- \rightarrow 3$ jets event takes on a factorized form like [34, 18]

$$\frac{d^2\sigma}{d\rho_1 d\rho_2} = H(Q^2) \otimes S(\rho_1, \rho_2, z_{\text{cut}}) \otimes J_q(\rho_1) \otimes J_g(\rho_1, z_{\text{cut}}) \otimes J_{\bar{q}}(\rho_2), \quad (1.22)$$

where here ρ_1 and ρ_2 are the normalized masses of the two hemispheres. $H(Q^2)$ is a hard function describing $e^+e^- \rightarrow$ jets; $S(\rho_1, \rho_2, z_{\text{cut}})$ is a function describing soft radiation; and the J_i are jet functions describing the production of collinear radiation in a jet about particle i (in this case, i could be a quark q , antiquark \bar{q} , or gluon g).

This factorization will be key for developing an all-orders calculation of the groomed heavy hemisphere mass, as it enables us to resum large logarithms. Much more on the factorization theorem will be discussed in Chapter 3.

1.3.2 Dimensional regularization

Beyond the framework of SCET, we will work using a technique called **dimensional regularization**.¹⁴ At its heart, dimensional regularization is a scheme for analytically isolating the divergences in divergent integrals.

This is done by decreasing the dimension of the calculation by some small amount $\epsilon > 0$ — we will work in $d = 4 - 2\epsilon$ dimensions instead of the usual 4. The effect is to siphon divergences in the original integral into poles at $\epsilon = 0$. The result is still divergent if we send $\epsilon \rightarrow 0$, but now it is contained in a single term which can be manipulated and possibly removed. Effectively, dimensional regularization provides one answer the question: “How can we, in a self-consistent way, remove divergences which cancel?”

As an example, take the integral

$$\int_1^\infty \frac{dx}{x}. \quad (1.23)$$

¹⁴Developed by 't Hooft and Veltman in the 1970s [35]

This integral is, of course, divergent in one dimension. But now suppose we choose to work in $d = 1 - \epsilon$ dimensions. The integral becomes (ignoring the normalization)

$$\int_1^\infty \frac{dx}{x} \rightarrow \mu^\epsilon \int_1^\infty \frac{dx}{x^{1+\epsilon}} \quad (1.24)$$

for some arbitrary scale μ . The scale μ is necessary because the original integral is dimensionless, so the dimension carried by the new $x^{-\epsilon}$ term must be eliminated. Now performing the integral yields

$$\mu^\epsilon \int_1^\infty \frac{dx}{x^{1+\epsilon}} = \frac{\mu^\epsilon}{\epsilon} = \frac{1}{\epsilon} + \log \mu + \epsilon \log^2 \mu + \mathcal{O}(\epsilon^2). \quad (1.25)$$

Notice that the divergence has emerged as single term: $1/\epsilon$. Now if there were another term in the calculation which, when expanded in ϵ , carried a $-1/\epsilon$, the divergences would manifestly cancel. We could then safely take $\epsilon \rightarrow 0$ with a finite result at the end.

Of course, the examples which we will see in practice are a little more complicated, but the basic strategy is the same. Our first encounter with dimensional regularization in the wild will take place in Chapter 2.

1.3.3 Resummation

The last piece of technical machinery we will use is the technique of **resummation**. As we have previously mentioned, the presence of multiple energy scales in certain calculations in QCD results in the emergence of logarithms of ratios of those energy scales [2, 20]. If these scales differ greatly, their ratio will be large, and so will the corresponding logarithms. It is possible, and indeed necessary, to tame these terms by accounting for them at **all orders**. This is the process of resummation. The actual mechanics will make more sense in context, so we will delay further discussion until Sec. 4.1.

We are now ready to put our knowledge to work and start calculating. We will begin, in Chapter 2, with the relatively simple task of deriving a fixed-order distribution for the groomed heavy hemisphere mass. This will give us some physical intuition about the distribution, as well as some practice applying our new calculational techniques. From there, we will proceed to derive an all-orders result in Chapters 3 and 4.

Chapter 2

Leading-order calculation

In order to develop an intuition for the mathematical tools we will put to use in the all-orders calculation of groomed heavy hemisphere mass, let us first compute the first-order (or rather, first *nontrivial* order) distribution of the observable. A simple electron-positron production with the production of two quark jets, $e^+e^- \rightarrow q\bar{q}$, would produce a constant distribution: the mass of the heavy hemisphere would simply be half of the final mass. The lowest-order nontrivial distribution corresponds to an $e^+e^- \rightarrow q\bar{q}g$ event, in which an electron and positron annihilate to produce a quark-antiquark pair, off of which a single gluon is emitted. The location of the gluon in phase space sets the heavy hemisphere mass. This process is depicted in a Feynman diagram in Fig. 2.1.

We will work in the limit that the heavy hemisphere mass ρ is approximately equal to the mMDT cutoff z_{cut} , which is itself small: $\rho \sim z_{\text{cut}} \ll 1$. We will utilize the strategy of regions [20] to compute the distribution. This is necessary because the distribution is essentially singular in the limit of interest [TODO: is this accurate?]. The method of regions entails computing the distribution in all singular regions of phase space, then summing the results at the end to generate the full distribution.¹ There are three singular regions of phase space:

1. The **soft region**, in which the gluon is emitted with low energy.
2. The **collinear region**, in which the gluon is emitted collinear to the quark or

¹The fact that this works is rather magical.

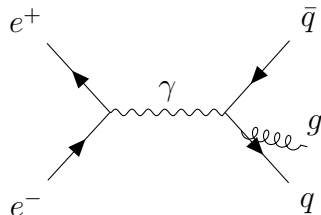


Figure 2.1: Feynman diagram of an $e^+e^- \rightarrow q\bar{q}g$ event.

antiquark.

3. The **soft-collinear region**, in which the gluon is both low-energy and collinear to the quark or antiquark. This region is covered by both the soft and the collinear calculations, so we must subtract it away to avoid double-counting.

If we label these cross sections σ_{soft} , $\sigma_{\text{collinear}}$, and $\sigma_{\text{soft-collinear}}$, respectively, then the full cross distribution will be

$$\frac{d\sigma}{d\rho} = \frac{d\sigma_{\text{soft}}}{d\rho} + \frac{d\sigma_{\text{collinear}}}{d\rho} + \frac{d\sigma_{\text{soft-collinear}}}{d\rho}. \quad (2.1)$$

Let us calculate these components now.

2.1 Soft gluon

2.1.1 Setup

For now, we assume a soft (i.e., low-energy) gluon. Recall that the (normalized) heavy hemisphere mass is defined to be

$$\rho = \left(\frac{m_h}{E_h} \right)^2 \quad (2.2)$$

with m_h the mass of the more massive hemisphere and E_h its energy.

We first need to sort out the kinematics of the event. Let us shift our reference frame so that the quark has momentum

$$p_1^\mu = \frac{Q_q}{2}(1, 0, 0, 1) \quad (2.3)$$

and the antiquark has momentum

$$p_2^\mu = \frac{Q_q}{2}(1, 0, 0, -1), \quad (2.4)$$

and let the gluon have momentum k^μ . The soft-gluon limit means that the energy of the gluon is $k^0 \ll 1$. In this case, the quarks carry most of the energy, so we can approximate $Q_q \approx Q$, the total energy of the event. Furthermore, let us assume that the gluon is emitted in the hemisphere containing the quark (the problem is symmetric under quark-antiquark exchange, so we will simply multiply the cross section by 2 at the end to account for this assumption). Then the momentum of the heavy hemisphere is

$$p_h = p_1 + k, \quad (2.5)$$

so the heavy hemisphere has mass

$$\begin{aligned} m_h^2 &= p_h^2 = (p_{1,0} + k_0)^2 - (k_1)^2 - (k_2)^2 - (p_{1,3} + k_3)^2 \\ &= 2p_{1,0}k_0 - 2p_{1,3}k_3 + p_1^2 + k^2 \\ &= Q(k_0 - k_3). \end{aligned} \quad (2.6)$$

The last line follows because we assume every particle to be massless, such that $p_1^2 = k^2 = 0$.² Now let us introduce the **light-cone coordinates**

$$k^+ \equiv k^0 - k^3 \quad k^- \equiv k^0 + k^3, \quad (2.7)$$

this can be written simply as

$$m_h^2 = Qk^+. \quad (2.8)$$

The energy of the heavy hemisphere is

$$E_h = p_{1,0} + k_0 = \frac{Q}{2} + k_0 \approx \frac{Q}{2}, \quad (2.9)$$

since, for a soft gluon, $k_0 \ll Q/2$. The heavy hemisphere mass is therefore

$$\rho = \frac{Qk^+}{Q^2/4} = \frac{4k^+}{Q}. \quad (2.10)$$

This means that we will need to insert the measurement function

$$\delta\left(\rho - \frac{4k^+}{Q}\right) \quad (2.11)$$

into Fermi's Golden Rule.

With the kinematics under our belt, let us think about the effects of an mMDT groomer. For the simple case of only 3 particles, the groomer only keeps pairs of particles i and j for which [15, 17]

$$\frac{\min [E_i, E_j]}{E_i + E_j} > z_{\text{cut}}. \quad (2.12)$$

This must be true for the quark and gluon; since the gluon has lower energy than the quark, this necessitates that

$$\frac{k_0}{E_h} = \frac{(k^+ + k^-)/2}{Q/2} > z_{\text{cut}}, \quad (2.13)$$

or

$$k^+ + k^- > Q z_{\text{cut}}. \quad (2.14)$$

Moreover, since we are assuming that the gluon shares a hemisphere with the quark, we must also have $k_3 > 0$, which requires

$$k^- - k^+ > 0. \quad (2.15)$$

Equations 2.14 and 2.15 generate the phase space constraints

$$\Theta(k^+ + k^- - Q z_{\text{cut}}) \Theta(k^- - k^+). \quad (2.16)$$

²This is a reasonably accurate assumption for the energies accessible by colliders, and makes our calculations much easier. The gluon is actually massless regardless of the theoretical assumptions made.

When we insert these into Fermi's Golden Rule, the differential cross section takes the form

$$\frac{d\sigma_{\text{soft}}}{d\rho} = 2 \int d\text{LIPS} |\mathcal{M}|^2 \delta\left(\rho - \frac{4k^+}{Q}\right) \Theta(k^+ + k^- - Q z_{\text{cut}}) \Theta(k^- - k^+). \quad (2.17)$$

Here, $d\text{LIPS}$ is a differential element of Lorentz-invariant phase space, and \mathcal{M} is the matrix element governing the $e^+e^- \rightarrow q\bar{q}g$ process.

Assuming a soft gluon, the matrix element is well-known in the literature (see Eqs. 87 and 88 of [36]):

$$|\mathcal{M}|^2 = 4\pi\alpha_s\sigma_0 C_F \mu^{2\epsilon} \frac{p_1 \cdot p_2}{(p_1 \cdot k)(p_2 \cdot k)}. \quad (2.18)$$

Here, α_s is the strong coupling constant³, σ_0 is the cross section for $e^+e^- \rightarrow q\bar{q}$, C_F is the quadratic Casimir of the fundamental representation of color (taken to be $C_F = 4/3$ for our purposes [4]), and μ is a mass scale introduced to ensure that the differential cross section will remain dimensionless in $d = 4 - 2\epsilon$ dimensions. Inserting the values of p_1 , p_2 , and k , we have

$$|\mathcal{M}|^2 = 4\pi\alpha_s\sigma_0 C_F \mu^{2\epsilon} \frac{2}{k^+ k^-}. \quad (2.19)$$

Now we must unpack the Lorentz-invariant phase space element $d\text{LIPS}$. Working in d dimensions, the standard form is

$$d\text{LIPS} = \frac{d^d k}{(2\pi)^{d-1}} \delta(k^2) \Theta(k_0), \quad (2.20)$$

where the Dirac delta and Heaviside functions ensure that the gluon is on-shell (i.e., real) with positive energy. If $\epsilon = 0$, we would have

$$d^d k = d^4 k = dk_0 dk_1 dk_2 dk_3. \quad (2.21)$$

When we transform to light-cone coordinates with $(k_0, k_3) \rightarrow (k^+, k^-)$, the Jacobian of the transformation is

$$\frac{\partial(k_0, k_3)}{\partial(k^+, k^-)} = \begin{pmatrix} 1/2 & 1/2 \\ -1/2 & 1/2 \end{pmatrix}, \quad (2.22)$$

so

$$dk_0 dk_3 = \left| \det \frac{\partial(k_0, k_3)}{\partial(k^+, k^-)} \right| dk^+ dk^- = \frac{1}{2} dk^+ dk^-. \quad (2.23)$$

Now let $k_\perp = (k_1, k_2)$ be the transverse components of the gluon momentum. For $\epsilon \neq 0$, we imagine that these transverse components are the ones which bleed into the modified dimensions. Therefore, after noticing that

$$\delta(k^2) = \delta(k_0^2 - k_3^2 - k_\perp^2) = \delta(k^+ k^- - k_\perp^2), \quad (2.24)$$

³Which is not really a constant

we have

$$d\text{LIPS} = \frac{dk^+ dk^- d^{d-2} k_\perp}{2(2\pi)^{d-1}} \delta(k^+ k^- - k_\perp^2) \Theta(k^+ + k^-). \quad (2.25)$$

Now it is convenient to transfer the $2 - 2\epsilon$ dimensions of k_\perp into spherical coordinates, so that

$$d^{d-2} k_\perp = k_\perp^{d-3} dk_\perp d\Omega_{d-2} \quad (2.26)$$

with Ω_{d-2} the solid angle of the $(d-2)$ -dimensional unit sphere. Since none of the terms in the cross section of Eq. 2.17 or matrix element of Eq. 2.19 have angular dependence, we can go ahead and integrate the solid angle:

$$\int d\Omega_{d-2} = \frac{2\pi^{(d-2)/2}}{\Gamma(\frac{d-2}{2})} \quad (2.27)$$

with $\Gamma(x)$ the gamma function; this identity comes from Eq. B.28 of [3]. Therefore,

$$d\text{LIPS} = \frac{2\pi^{(d-2)/2}}{\Gamma(\frac{d-2}{2})} \frac{dk^+ dk^- dk_\perp}{2(2\pi)^{d-1}} k_\perp^{d-3} \delta(k^+ k^- - k_\perp^2) \Theta(k^+ + k^-). \quad (2.28)$$

As a final step, we can resolve this delta function:

$$\delta(k^+ k^- - k_\perp^2) = \frac{1}{\sqrt{k^+ k^-}} \delta\left(k_\perp - \sqrt{k^+ k^-}\right). \quad (2.29)$$

Then integrating over k_\perp yields

$$\int dk_\perp \frac{k_\perp^{d-3}}{2\sqrt{k^+ k^-}} \delta\left(k_\perp - \sqrt{k^+ k^-}\right) = (k^+ k^-)^{(d-4)/2}. \quad (2.30)$$

Putting everything together, inserting $d = 4 - 2\epsilon$, and simplifying, we are left with

$$d\text{LIPS} = \frac{(4\pi)^\epsilon}{\Gamma(1-\epsilon)8\pi^2} \frac{dk^+ dk^-}{(k^+ k^-)^\epsilon} \Theta(k^+ + k^-). \quad (2.31)$$

Notice that a factor of $(k^+ k^-)^\epsilon$ has been introduced — this is what will help us capture divergences as we work and cancel them at the end. Finally, we will work using a convention known as **modified minimal subtraction**, under which we will throw away factors of $(4\pi)^\epsilon$ and set the Euler-Mascheroni constant to be $\gamma_E \rightarrow 0$ when it appears (this does not affect the final result, but will make calculations slightly less unwieldy). Under this scheme, we have

$$d\text{LIPS} = \frac{1}{\Gamma(1-\epsilon)8\pi^2} \frac{dk^+ dk^-}{(k^+ k^-)^\epsilon} \Theta(k^+ + k^-). \quad (2.32)$$

as our final phase space element.

Combining Eqs. 2.17, 2.19, and 2.32 then yields the full cross section:

$$\frac{1}{4\pi\alpha_s\sigma_0 C_F} \frac{d\sigma_{\text{soft}}}{d\rho} = \frac{\mu^{2\epsilon}}{\Gamma(1-\epsilon)2\pi^2} \int \frac{dk^+ dk^-}{(k^+ k^-)^{1+\epsilon}} \delta\left(\rho - \frac{4k^+}{Q}\right) \Theta(k^+ + k^-) \times \Theta(k^+ + k^- - Q z_{\text{cut}}) \Theta(k^- - k^+). \quad (2.33)$$

2.1.2 Calculation

The integral of Eq. 2.33 is relatively straightforward to evaluate. The first step is to resolve the Dirac delta:

$$\delta\left(\rho - \frac{4k^+}{Q}\right) = \frac{Q}{4}\delta\left(k^+ - \frac{Q\rho}{4}\right). \quad (2.34)$$

The integrating over k^+ yields

$$\begin{aligned} \frac{1}{4\pi\alpha_s\sigma_0 C_F} \frac{d\sigma_{\text{soft}}}{d\rho} &= \frac{\mu^{2\epsilon}}{\Gamma(1-\epsilon)2\pi^2\rho} \frac{1}{\rho} \left(\frac{4}{Q\rho}\right)^\epsilon \int \frac{dk^-}{(k^-)^{1+\epsilon}} \Theta\left(\frac{Q\rho}{4} + k^-\right) \\ &\quad \times \Theta\left(\frac{Q\rho}{4} + k^- - Qz_{\text{cut}}\right) \Theta\left(k^- - \frac{Q\rho}{4}\right). \end{aligned} \quad (2.35)$$

Now, the integrand is only non-zero when

$$k^- > -\frac{Q\rho}{4} \quad k^- > Q\left(z_{\text{cut}} - \frac{\rho}{4}\right) \quad k^- > \frac{Q\rho}{4}. \quad (2.36)$$

If the second and third requirements are satisfied, then so is the first, so we can ignore it. To deal with the others, notice that each is stricter for different values of ρ : if $\rho < 2z_{\text{cut}}$, then

$$Q\left(z_{\text{cut}} - \frac{\rho}{4}\right) > \frac{Q\rho}{4}, \quad (2.37)$$

and the opposite is true if $\rho > 2z_{\text{cut}}$. We can therefore break the integral into two pieces:

$$\begin{aligned} &\int \frac{dk^-}{(k^-)^{1+\epsilon}} \Theta\left(\frac{Q\rho}{4} + k^-\right) \Theta\left(\frac{Q\rho}{4} + k^- - Qz_{\text{cut}}\right) \Theta\left(k^- - \frac{Q\rho}{4}\right) \\ &= \Theta(\rho - 2z_{\text{cut}}) \int_{Q\rho/4}^{\infty} \frac{dk^-}{(k^-)^{1+\epsilon}} + \Theta(2z_{\text{cut}} - \rho) \int_{Q(z-\rho/4)}^{\infty} \frac{dk^-}{(k^-)^{1+\epsilon}}. \end{aligned} \quad (2.38)$$

If we take $\epsilon > 0$, then these integrals yield a finite result:

$$\begin{aligned} \frac{1}{4\pi\alpha_s\sigma_0 C_F} \frac{d\sigma_{\text{soft}}}{d\rho} &= \frac{\mu^{2\epsilon}}{\Gamma(1-\epsilon)2\pi^2\rho} \frac{1}{\rho} \left(\frac{4}{Q\rho}\right)^\epsilon \frac{1}{\epsilon} \left[\Theta(\rho - 2z_{\text{cut}}) \left(\frac{Q\rho}{4}\right)^{-\epsilon} \right. \\ &\quad \left. + \Theta(2z_{\text{cut}} - \rho) \left(Q\left(z_{\text{cut}} - \frac{\rho}{4}\right)\right)^{-\epsilon} \right]. \end{aligned} \quad (2.39)$$

Notice how dimensional regularization helped us achieve this calculation: without the regulating $(k^-)^\epsilon$, the integrals would have diverged without an upper bound on the value of k^- (which, physically, has no upper bound). Our result is still manifestly divergent if we send $\epsilon \rightarrow 0$, but at least we can see the divergence. This is the power of the technique.

We can pull out the divergence even more cleanly if we perform a Laurent expansion⁴ in ϵ . We will send $\epsilon \rightarrow 0$ at the end anyway, so we only care about terms

⁴Like a Taylor expansion, but possibly including negative exponents

through order $\mathcal{O}(\epsilon^0)$; anything below this order generates divergences, and anything above this order will vanish. Performing the expansion yields

$$\boxed{\frac{1}{4\pi\alpha_s\sigma_0C_F}\frac{d\sigma_{\text{soft}}}{d\rho} = \frac{1}{2\pi^2\rho}\left[\frac{1}{\epsilon} + \Theta(\rho - 2z_{\text{cut}})2\log\left(\frac{4\mu}{Q\rho}\right)\right.} \\ \left. + \Theta(2z_{\text{cut}} - \rho)\left[\log\left(\frac{4\mu^2}{Q\rho}\right) - \log\left(Qz_{\text{cut}} - \frac{Q\rho}{4}\right)\right]\right] + \mathcal{O}(\epsilon). \quad (2.40)$$

From this expansion, we see that the soft contribution to the cross section diverges as

$$\lim_{\epsilon \rightarrow 0} \frac{d\sigma_{\text{soft}}}{d\rho} \sim \frac{2\alpha_s\sigma_0C_F}{\pi\rho\epsilon}. \quad (2.41)$$

Stop reading and appreciate this for a minute — it is remarkable! By pushing our calculation out of the standard 4 dimensions, we are able to learn about structure that was inaccessible to us in our 4-dimensional perspective.

This technique, moreover, is not only beautiful from a mathematical point of view; it will be extremely useful to have analytically extracted the divergences in this way. At the end of the calculation, we will find that they all cancel each other out. It is rather magical.

2.2 Collinear gluon

Now that we have computed the contribution from a soft gluon, let us move on to the next singular region of phase space: a gluon collinear to the quark or antiquark.

2.2.1 Setup

For this calculation, we will use a different system of coordinates: the gluon's hemisphere energy fraction and angle from the quark. To derive these coordinates, we first define the phase-space coordinates

$$x_i = \frac{2p_i \cdot Q}{Q^2} \quad (2.42)$$

where $i = 1, 2, 3$ ranges over the three particles of the event and $Q = p_1 + p_2 + p_3$ is the total four-momentum of the event. Let x_1 be the energy fraction of the quark, x_2 be the energy fraction of the antiquark, and x_3 be the energy fraction of the gluon. Also let $k = p_3$ be the momentum of the gluon. Notice that

$$x_1 + x_2 + x_3 = \frac{2(p_1 + p_2 + p_3) \cdot Q}{Q^2} = 2. \quad (2.43)$$

In the collinear limit, each hemisphere carries half the momentum and energy (in order to conserve the net-zero initial momentum of the collision). Assume now that

the gluon is emitted in the same hemisphere as the quark (we will again multiply the result by a factor of 2 to compensate). Then, in the collinear limit, we have

$$x_1 + x_3 \rightarrow 1. \quad (2.44)$$

Now we will introduce the gluon's energy fraction

$$z \equiv \frac{x_3}{x_1 + x_3} \approx x_3, \quad (2.45)$$

where the final step holds in the collinear limit. The quark's hemisphere energy fraction is

$$1 - z = \frac{x_1}{x_1 + x_3} \approx x_1. \quad (2.46)$$

This is equivalent to the assumption that the quark four-momentum p_1 and the gluon four-momentum k are collinear along some vector \bar{p}_1 :

$$k = z\bar{p}_1 \quad p_1 = (1 - z)\bar{p}_1. \quad (2.47)$$

Now let θ be the angle between the quark and the gluon. Notice that

$$1 - x_2 = \frac{Q^2 - 2p_2 \cdot Q}{Q^2} = \frac{2p_1 \cdot k}{Q^2} = \frac{x_1 x_3}{2}(1 - \cos \theta). \quad (2.48)$$

In the collinear limit $\theta \ll 1$, we have $\cos \theta \approx 1 - \theta^2/2$, so this means that

$$\frac{2p_1 \cdot k}{Q^2} = \frac{x_1 x_3}{4} \theta^2 = \frac{z(1 - z)}{4} \theta^2. \quad (2.49)$$

Then the heavy hemisphere mass is

$$m_h^2 = (p_1 + k)^2 = 2p_1 \cdot k = \frac{z(1 - z)}{4} \theta^2 Q^2, \quad (2.50)$$

where again we have $p_1^2 = k^2 = 0$. Since the hemisphere energy is half the total energy, $E_h = Q/2$, the observable we are looking for is then

$$\rho = \frac{m_h^2}{E_h^2} = z(1 - z) \theta^2. \quad (2.51)$$

The measurement function in Fermi's Golden Rule will then be

$$\delta(\rho - z(1 - z) \theta^2) = \frac{1}{z(1 - z)} \delta\left(\theta^2 - \frac{\rho}{z(1 - z)}\right). \quad (2.52)$$

The quark and gluon only pass the mMDT groomer if [17]

$$\frac{\min [E_1, E_3]}{E_1 + E_3} > z_{\text{cut}}. \quad (2.53)$$

This means that we require

$$\min[x_1, x_3] = \min[z, 1-z] > z_{\text{cut}}. \quad (2.54)$$

Thus, the grooming constraint on the cross section takes the form

$$\Theta(\min[z, 1-z] - z_{\text{cut}}). \quad (2.55)$$

In phase space coordinates, the matrix element for $e^+e^- \rightarrow q\bar{q}g$ is [26]

$$|\mathcal{M}|^2 = \frac{\alpha_s \sigma_0 C_F}{2\pi} \frac{x_1^2 + x_2^2}{(1-x_1)(1-x_2)}. \quad (2.56)$$

After performing the the change of variables discussed above and introducing the appropriate Jacobian factor, this reduces to

$$|\mathcal{M}|^2 = \frac{\alpha_s \sigma_0 C_F}{2\pi} \frac{1 + (1-z)^2}{z\theta^2}. \quad (2.57)$$

Finally, we must sort out the phase space measure. In $d = 4 - 2\epsilon$ dimensions, the matrix element itself is slightly modified. The phase space integral with the matrix element becomes [37]

$$\begin{aligned} \frac{2\pi}{\alpha_s C_F} \frac{1}{\sigma_0} \sigma_{\text{collinear}} &= \frac{2}{\sqrt{\pi} \Gamma(\frac{1}{2} - \epsilon)} \left(\frac{2\mu}{Q}\right)^{2\epsilon} \int_0^1 dz \int_0^\infty d\theta^2 \int_0^\pi d\phi \sin^{-2\epsilon} \phi \\ &\quad \times (\theta^2)^{-1-\epsilon} z^{-2\epsilon} (1-z)^{-2\epsilon} \left(\frac{1 + (1-z)^2}{z} - \epsilon z\right). \end{aligned} \quad (2.58)$$

A factor of 2 has been introduced to account for the possibility that the gluon might be collinear to either the quark or the antiquark. When we introduce the measurement and grooming terms of Eqs. 2.52 and 2.55, we find that the full differential cross section is

$$\begin{aligned} &\frac{2\pi}{\alpha_s C_F} \frac{1}{\sigma_0} \frac{d\sigma_{\text{collinear}}}{d\rho} \\ &= \frac{2}{\sqrt{\pi} \Gamma(\frac{1}{2} - \epsilon)} \left(\frac{2\mu}{Q}\right)^{2\epsilon} \int_0^1 dz \int_0^\infty d\theta^2 \int_0^\pi d\phi \sin^{-2\epsilon} \phi (\theta^2)^{-1-\epsilon} \\ &\quad \times z^{-2\epsilon} (1-z)^{-2\epsilon} \left(\frac{1 + (1-z)^2}{z} - \epsilon z\right) \\ &\quad \times \frac{1}{z(1-z)} \delta\left(\theta^2 - \frac{\rho}{z(1-z)}\right) \\ &\quad \times \Theta(\min[z, 1-z] - z_{\text{cut}}). \end{aligned} \quad (2.59)$$

2.2.2 Calculation

We can immediately perform the integrals in ϕ ,

$$\int_0^\pi d\phi \sin^{-2\epsilon} \phi = \frac{\sqrt{\pi} \Gamma(\frac{1}{2} - \epsilon)}{\Gamma(1 - \epsilon)}, \quad (2.60)$$

and in θ^2 to find

$$\begin{aligned} \frac{2\pi}{\alpha_s C_F} \frac{1}{\sigma_0} \frac{d\sigma_{\text{collinear}}}{d\rho} &= \frac{2}{\Gamma(1 - \epsilon)} \left(\frac{2\mu}{Q} \right)^{2\epsilon} \frac{1}{\rho^{1+\epsilon}} \int_0^1 dz \frac{1}{z^\epsilon (1-z)^\epsilon} \left(\frac{1 + (1-z)^2}{z} - \epsilon z \right) \\ &\quad \times \Theta(\min[z, 1-z] - z_{\text{cut}}). \end{aligned} \quad (2.61)$$

The Heaviside function is satisfied by ensuring that

$$z_{\text{cut}} < z < 1 - z_{\text{cut}}, \quad (2.62)$$

so

$$\int_0^1 dz \Theta(\min[z, 1-z] - z_{\text{cut}}) = \int_{z_{\text{cut}}}^{1-z_{\text{cut}}} dz. \quad (2.63)$$

The cross section becomes

$$\frac{4\pi}{\alpha_s C_F} \frac{1}{\sigma_0} \frac{d\sigma_{\text{collinear}}}{d\rho} = \frac{2}{\Gamma(1 - \epsilon)} \left(\frac{2\mu}{Q} \right)^{2\epsilon} \frac{1}{\rho^{1+\epsilon}} \int_{z_{\text{cut}}}^{1-z_{\text{cut}}} dz \frac{1}{z^\epsilon (1-z)^\epsilon} \left(\frac{1 + (1-z)^2}{z} - \epsilon z \right). \quad (2.64)$$

This integral does not diverge in 4 dimensions, so we can simply set $\epsilon = 0$.⁵ Thus,

$$\frac{2\pi}{\alpha_s C_F} \frac{1}{\sigma_0} \frac{d\sigma_{\text{collinear}}}{d\rho} = \frac{2}{\rho} \int_{z_{\text{cut}}}^{1-z_{\text{cut}}} dz \frac{1 + (1-z)^2}{z} + \mathcal{O}(\epsilon). \quad (2.65)$$

This comes out to

$$\frac{2\pi}{\alpha_s C_F} \frac{1}{\sigma_0} \frac{d\sigma_{\text{collinear}}}{d\rho} = \frac{2}{\rho} \left[-\frac{3}{2} + 3z_{\text{cut}} + 2 \log\left(\frac{1 - z_{\text{cut}}}{z_{\text{cut}}}\right) \right] + \mathcal{O}(\epsilon). \quad (2.66)$$

2.3 Soft-collinear gluon

The last piece to compute is the soft-collinear limit. This can be achieved by starting from the collinear limit and taking $z \ll 1$. Thus, from Eq. 2.59, we have

$$\begin{aligned} \frac{2\pi}{\alpha_s C_F} \frac{1}{\sigma_0} \frac{d\sigma_{\text{soft-collinear}}}{d\rho} &= \frac{2}{\sqrt{\pi} \Gamma(\frac{1}{2} - \epsilon)} \left(\frac{2\mu}{Q} \right)^{2\epsilon} \int_0^\infty dz \int_0^\infty d\theta^2 \int_0^\pi d\phi \sin^{-2\epsilon} \phi (\theta^2)^{-1-\epsilon} \\ &\quad \times \frac{2}{z^{2+2\epsilon}} \delta\left(\theta^2 - \frac{\rho}{z}\right) \Theta(z - z_{\text{cut}}). \end{aligned} \quad (2.67)$$

⁵This is equivalent to computing the $\mathcal{O}(\epsilon^0)$ term in the Taylor expansion.

The upper bound on z has been replaced by ∞ because, in the $z \ll 1$ limit, the integral should not depend on the particular upper bound.⁶ These integrals can then be computed to find

$$\frac{2\pi}{\alpha_s C_F} \frac{1}{\sigma_0} \frac{d\sigma_{\text{soft-collinear}}}{d\rho} = \frac{4}{\Gamma(1-\epsilon)} \left(\frac{2\mu}{Q}\right)^{2\epsilon} \frac{1}{\rho^{1+\epsilon}} \frac{z_{\text{cut}}^{-\epsilon}}{\epsilon}. \quad (2.68)$$

Performing a Laurent expansion in ϵ yields

$$\boxed{\frac{2\pi}{\alpha_s C_F} \frac{1}{\sigma_0} \frac{d\sigma_{\text{soft-collinear}}}{d\rho} = \frac{4}{\rho} \left[\frac{1}{\epsilon} + \log\left(\frac{4\mu^2}{Q^2 \rho z_{\text{cut}}}\right) \right] + \mathcal{O}(\epsilon)}. \quad (2.69)$$

2.4 Putting it all together

Now we can combine Eqs. 2.40, 2.66, and 2.69 to get a complete result. In particular, we find

$$\begin{aligned} & \frac{2\pi}{\alpha_s C_F} \frac{\rho}{\sigma_0} \left[\frac{d\sigma_{\text{soft}}}{d\rho} + \frac{d\sigma_{\text{collinear}}}{d\rho} - \frac{d\sigma_{\text{soft-collinear}}}{d\rho} \right] \\ &= 4 \left[\frac{1}{\epsilon} + \Theta(\rho - 2z_{\text{cut}}) 2 \log\left(\frac{4\mu}{Q\rho}\right) \right. \\ & \quad \left. + \Theta(2z_{\text{cut}} - \rho) \left[\log\left(\frac{4\mu^2}{Q\rho}\right) - \log\left(Qz_{\text{cut}} - \frac{Q\rho}{4}\right) \right] \right] \\ &+ 2 \left[-\frac{3}{2} + 3z_{\text{cut}} + 2 \log\left(\frac{1-z_{\text{cut}}}{z_{\text{cut}}}\right) - \frac{2}{\epsilon} - 2 \log\left(\frac{4\mu^2}{Q^2 \rho z_{\text{cut}}}\right) \right] + \mathcal{O}(\epsilon). \end{aligned} \quad (2.70)$$

Notice that the divergences in ϵ cancel! We are left with a function which does not diverge if we send $\epsilon \rightarrow 0$, which means we can simply return to 4 dimensions. Also notice that all factors of μ cancel each other out: we can pull a $\log(4\mu^2/Q^2\rho)$ out of the terms with a Heaviside function, which then cancels with the $-\log(4\mu^2/Q^2\rho)$ from the soft-collinear contribution.⁷ This is a nice consistency check, as μ is a completely arbitrary mass scale — it would not make sense for the physical cross section to depend on an arbitrary constant! Thus, simplifying the expression and setting $\epsilon = 0$, we find that

$$\boxed{\frac{2\pi}{\alpha_s C_F} \frac{\rho}{\sigma_0} \frac{d\sigma}{d\rho} = 4\Theta(\rho - 2z_{\text{cut}}) \log\left(\frac{4}{\rho}\right) - 4\Theta(2z_{\text{cut}} - \rho) \log\left(z_{\text{cut}} - \frac{\rho}{4}\right) - 3 + 6z_{\text{cut}} + 4 \log(1 - z_{\text{cut}})}. \quad (2.71)$$

⁶Another way to think about this is that there is in principle no *a priori* upper bound on any variable of integration. We impose a bound according to the physical constraint that $0 < z < 1$. This could be represented in the integral as a term such as $\Theta(1-z)$, but in the limit $z \ll 1$, we have $\Theta(1-z) \approx 1$, so the upper bound vanishes.

⁷Indeed, notice that logarithms of μ appear in conjunction with divergences in ϵ . This is a general feature of our regularization scheme.

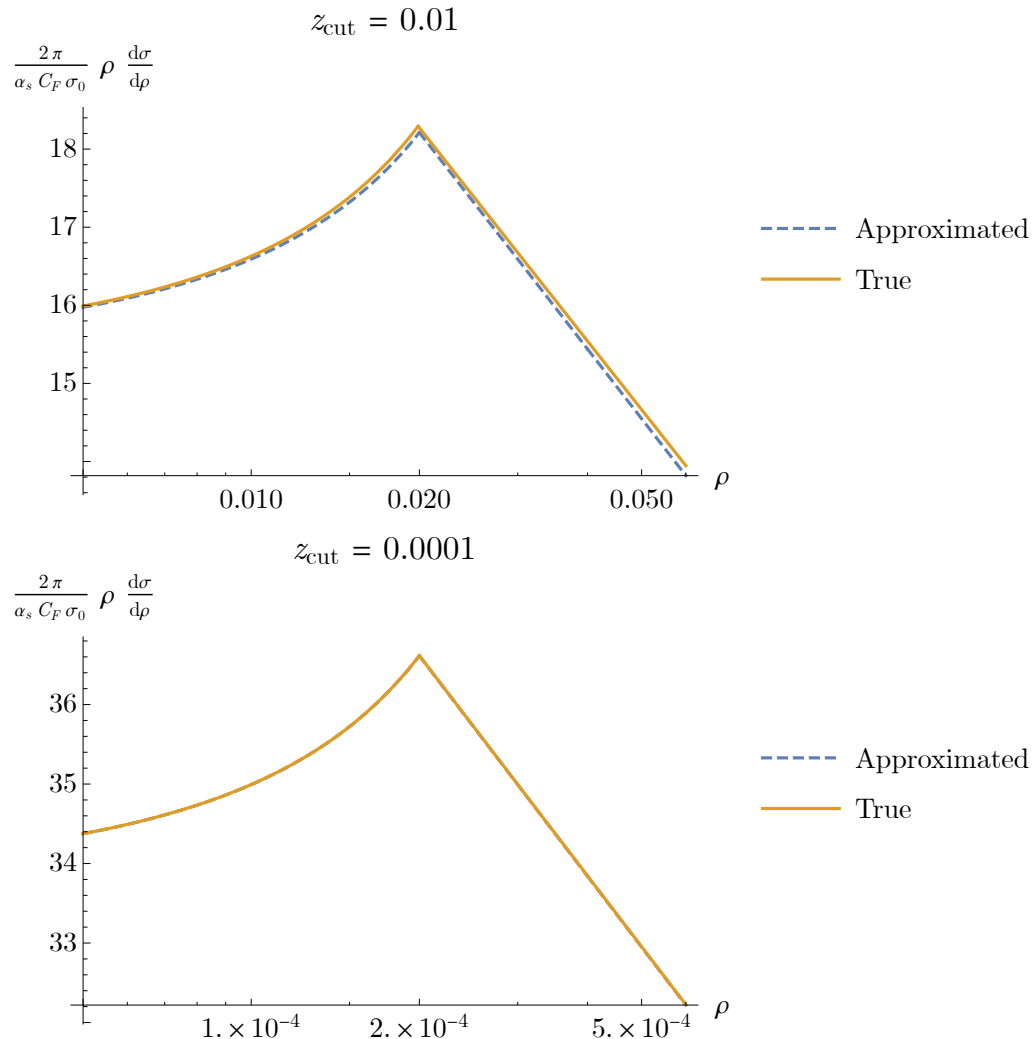


Figure 2.2: True (orange solid line) and approximated (blue dashed line) distribution of groomed heavy hemisphere mass in the limit $\rho \sim z_{\text{cut}} \ll 1$.

For this calculation, the true analytic distribution is known completely and can be used for comparison. From Ref. [26], we have

$$\begin{aligned} \frac{2\pi}{\alpha_s C_F} \frac{1}{\sigma_0} \frac{d\sigma}{d\rho} = & \Theta\left(\frac{3}{4} - \rho\right) \Theta(\rho - (2z_{\text{cut}} - z_{\text{cut}}^2)) \left[-\frac{12(6 - 6\sqrt{1-\rho} + \rho(-8 + 5\sqrt{1-\rho} + 2\rho))}{\rho^3(1-\rho)} \right. \\ & - \frac{2(6 - 6\sqrt{1-\rho} - \rho(5 - 4\sqrt{1-\rho}))}{\rho^2(1-\rho)} \log\left(\frac{\rho}{2 + 2\sqrt{1-\rho} - 3\rho}\right) \Big] \\ & + \Theta(2z_{\text{cut}} - z_{\text{cut}}^2 - \rho) \left[\frac{12(1 - 2z_{\text{cut}})(2 - 2\sqrt{1-\rho} - \rho)^2}{\rho^3(2 - 2\sqrt{1-\rho} - \rho(2 - \sqrt{1-\rho}))} \right. \\ & \left. - \frac{2(6 - 6\sqrt{1-\rho} - \rho(5 - 4\sqrt{1-\rho}))}{\rho^2(1-\rho)} \log\left(\frac{2 - 4z_{\text{cut}}(1 - z_{\text{cut}} - \sqrt{1-\rho}) - 2\sqrt{1-\rho} - \rho}{4z_{\text{cut}}(1 - z_{\text{cut}}) - \rho}\right) \right]. \end{aligned} \quad (2.72)$$

The true result is plotted against the approximation in Fig. 2.2. Notice that, as expected, the approximation gets better both as z_{cut} becomes smaller and as ρ moves closer to z_{cut} .

Now, from the true result, we can then take the limit $\rho \sim z_{\text{cut}} \ll 1$ explicitly to find

$$\begin{aligned} \frac{2\pi}{\alpha_s C_F} \frac{1}{\sigma_0} \frac{d\sigma}{d\rho} = & \Theta(\rho - 2z_{\text{cut}}) \left[-\frac{3}{\rho} + \frac{4}{\rho} \log\left(\frac{4}{\rho}\right) \right] \\ & + \Theta(2z_{\text{cut}} - \rho) \left[-\frac{3}{\rho} - \frac{4}{\rho} \log\left(z_{\text{cut}} - \frac{\rho}{4}\right) \right] \\ = & \Theta(\rho - 2z_{\text{cut}}) \frac{4}{\rho} \log\left(\frac{4}{\rho}\right) \\ & - \Theta(2z_{\text{cut}} - \rho) \frac{4}{\rho} \log\left(z_{\text{cut}} - \frac{\rho}{4}\right) - \frac{3}{\rho}. \end{aligned} \quad (2.73)$$

Notice as well that taking the same limit in Eq. 2.71 yields

$$\frac{2\pi}{\alpha_s C_F} \frac{\rho}{\sigma_0} \frac{d\sigma}{d\rho} = 4\Theta(\rho - 2z_{\text{cut}}) \log\left(\frac{4}{\rho}\right) - 4\Theta(2z_{\text{cut}} - \rho) \log\left(z_{\text{cut}} - \frac{\rho}{4}\right) - 3, \quad (2.74)$$

which is the same result!

Thus, we see that this method works. To compute the distribution in a given limit, it suffices for us to consider only ‘interesting’ regions of phase space, compute their contribution to the distribution, and then combine these contributions in the appropriate manner. The same principle will be applied as we work towards an all-orders calculation.

There, too, we will begin by identifying the singular regions of phase space and the dominant physical contributions in each region. We will need to resum the contributions in each region in order to manage the effects of imposed scales to all orders, but this is simply an additional step in the calculation. Moreover, instead of a simple sum, we will combine functions by convolving them, since we need to appropriately

capture terms at every order in α_s hidden in each function. Despite these complications, however, the core idea is the same, and this simple example provides a general road map as we push forward.⁸

Finally, one should notice in the leading-order distribution the sharp cusp that occurs at $\rho = 2z_{\text{cut}} - z_{\text{cut}}^2$. It looks strange for a reason — this cusp is entirely unphysical. It has been demonstrated that, as higher-order contributions in α_s are added, the cusp becomes smooth [26]. Nevertheless, this oddity should serve as a clue that there is something interesting at play. We will explore the physics further in subsequent chapters.

⁸We could think of this as a map which only contains the location of the interstate highways.

Chapter 3

Factorization formula

Fixed-order calculations like that of Chapter 2 are nice because of their exactness, but because of the relatively large value the strong coupling, $\alpha_s \sim 0.1$, one must go to fairly high orders to obtain precision results. At low orders, the calculations are relatively straightforward, but this quickly ceases to be the case, as the number of event topologies that one must consider increases factorially with the order of α_s . Moreover, and more pressingly, when we compute an exclusive cross section like $\sigma(e^+e^- \rightarrow \text{hemisphere jets})$ in the presence of mMDT grooming, external energy scales are imposed. This is problematic for QCD, which is an intrinsically scale-invariant theory, and our punishment is the appearance of logarithms of scales which might grow large in particular limits, like the limit $\rho \sim z_{\text{cut}} \ll 1$ which we are considering [2]. All this is to say that, while fixed-order calculations are nice for developing intuition for a physical quantity, they have limitations which become quite severe in the regime in which we are interested.

We would therefore like to develop an alternative framework for calculating the distribution of heavy hemisphere mass. The strategy we will settle on is try to develop an **all-orders calculation** of the distribution. This result will take into account contributions at every order of α_s , and provide a mathematical structure for producing arbitrarily accurate predictions, given sufficiently precise inputs. We will get there via the process of **resummation**, which will be discussed in Sec. 4.1 (and, indeed, will occupy most of Chapter 4). In order to prepare for that, we must first lay some groundwork.

The first step on the path to an all-orders calculation is to derive a factorization formula for the heavy hemisphere mass cross section, the goal being to split the cross section into terms which each depend only on a single energy scale. The basic process for doing so is laid out in technical detail in Ref. [20], and an example of a similar flavor to our calculation is provided by Frye et al. in Ref. [18].¹ Once the cross section has been split into functions of single energy scales, the process of resummation can begin.

¹Indeed, the calculation of Frye et al. is a more general factorization of mass-like variables in groomed jets. Setting $\alpha = 2, \beta = 0$ for their two-point energy correlation function $e_2^{(\alpha)}$ under soft drop grooming with angular exponent β yields the mMDT-groomed jet mass ρ . Their factorization is valid in the limit $\rho \ll z_{\text{cut}} \ll 1$, whereas we are interested in the limit $\rho \sim z_{\text{cut}} \ll 1$.

There are two primary steps in developing a factorization formula:

1. **Power counting:** this involves determining the possible radiative modes of an event and their dominant momentum scales. The term ‘power counting’ refers to the fact that for some momentum scale λ , different radiative modes have momenta that scale as different powers of λ .
2. **Factorization and refactorization:** Once the different radiative modes and energy scales are identified, we can use the framework of SCET to split the cross section into a convolution of terms describing different radiative modes. These terms themselves must then be split (refactored) into convolutions of terms, each of which depends, to leading order, only on a single energy scale.

In this chapter, we will follow these steps to derive a factorization formula for the heavy hemisphere mass in the $\rho \sim z_{\text{cut}} \ll 1$ limit.

3.1 Setup

Recall that the hemisphere mass is defined to be

$$\rho = \frac{1}{E_J^2} \sum_{i < j} 2p_i \cdot p_j \quad (3.1)$$

with E_J the jet energy and the sum ranging over all pairs of particles in the jet. Expanding out the dot product, we have

$$\rho = \frac{2}{E_J^2} \sum_{i < j} (E_i E_j - \mathbf{p}_i \cdot \mathbf{p}_j) = \frac{2}{E_J^2} \sum_{i < j} E_i E_j (1 - \cos \theta_{ij}) = \sum_{i < j} 2z_i z_j (1 - \cos \theta_{ij}). \quad (3.2)$$

Here, z_i and z_j are the relative energy fractions of each particle and θ_{ij} is the angle between particles i and j .

Throughout the following discussion, with n^μ the jet direction and \bar{n}^μ the direction opposite the jet, we will describe momenta in light-cone coordinates

$$p^\mu = (p^-, p^+, p_\perp) \quad (3.3)$$

with

$$p^- = \bar{n} \cdot p \qquad \qquad p^+ = n \cdot p \quad (3.4)$$

and p_\perp the components of momentum transverse to n . In these coordinates, the energy fraction with respect to total energy $E_J = Q$ is

$$z = \frac{p^+ + p^-}{2Q} \quad (3.5)$$

and, in the collinear limit, the angle to the jet axis is $\theta \approx p_\perp/p^0$ [18].

In an $e^+e^- \rightarrow \text{jets}$ event, there are two types of emission: resolved and unresolved. The essential difference is that a resolved emission is one which manifests itself as a jet at a particular scale of observation, while an unresolved emission does not. The presence of unresolved emissions can, however, perturb observable values of a resolved emission. [TODO: check that this is a reasonable description]

Suppose now that we have applied an mMDT groomer with energy fraction cutoff z_{cut} . Then every *resolved* emission must satisfy

$$z_i > z_{\text{cut}}, \quad (3.6)$$

while other emissions with $z_i < z_{\text{cut}}$ can only pass the groomer if they are at a sufficiently small angle to a resolved emission.

3.2 Power counting

3.2.1 Resolved soft emission

The primary emission contributing to the jet mass in the limit $\rho \sim z_{\text{cut}} \ll 1$ is a gluon emission z_i sensitive to both ρ and z_{cut} . In the presence of a hard quark (i.e., the jet) with $z_q \sim 1$, leading contributions to the jet mass of Eq. 3.2 is

$$\rho \approx \sum_i 2z_i(1 - \cos \theta_i) \quad (3.7)$$

where θ_i is the angle of emission i from the quark. Considering the case with only one such emission,² we have

$$\rho \approx z_i(1 - \cos \theta_i). \quad (3.8)$$

But since $z_i \sim z_{\text{cut}}$ and $\rho \sim z_{\text{cut}}$, this means that

$$\rho \approx \rho(1 - \cos \theta_i), \quad (3.9)$$

so

$$\cos \theta_i \ll 1. \quad (3.10)$$

This means that

$$\theta_i \sim \frac{\pi}{2}. \quad (3.11)$$

Since this emission is sensitive to $z_{\text{cut}} \ll 1$, we can also conclude that $z_i \ll 1$. Thus, we see that the leading contribution to the cusp region comes from a **resolved soft, wide-angle** gluon. Its momentum scales like

$$p_R \sim z_{\text{cut}} Q(1, 1, 1). \quad (3.12)$$

For future reference, let this gluon have energy fraction z_R and angle θ_R from the quark axis.

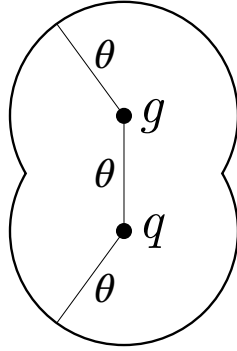


Figure 3.1: Head-on schematic of a quark jet q and a resolved gluon g . If the angle between the quark and the gluon is θ and the gluon (plus all lower-scale unresolved radiation) passes the groomer, then the mMDT groomer will accept all radiation within an angle θ of both the quark and the resolved gluon.

3.2.2 Ungroomed extra-soft unresolved radiation

Unresolved soft emissions can also contribute to the jet mass if they are sufficiently close to the resolved emission or the quark. Suppose there is another emission i with energy fraction z_i at angle θ_i from the jet axis and angle θ_{iR} from the resolved gluon. If $\theta_i < \theta_R$ or $\theta_{iR} < \theta_R$, a situation displayed in Fig. 3.1, then emission i will pass the groomer.

What does this mean for the hemisphere mass? Well, first notice that since $\theta_R \sim \pi/2$, most soft radiation in the hemisphere passes this cut. The effect of these extra-soft emissions, which have $z_i \ll z_R$, is to perturb the mass of the resolved emission, so that the hemisphere mass is approximately

$$\rho \sim z_R + \sum_i z_i (1 - \cos \theta_i). \quad (3.13)$$

The dominant contributions come again from the wide-angle emissions with $1 - \cos \theta_i \sim 1$; these must evidently have an energy scale set by

$$\rho - z_R \sim \sum_i z_i. \quad (3.14)$$

Hence, since $z_R \sim z_{\text{cut}}$, the unresolved extra-soft emissions must scale as

$$p_{S_R} \sim (\rho - z_{\text{cut}}) Q(1, 1, 1). \quad (3.15)$$

3.2.3 Collinear radiation

Finally, we consider radiation collinear to a jet axis with angle $\theta_i \ll 1$. This radiation has $p^- \gg p^+$, which means from Eq. 3.5 that

$$z \approx \frac{p^+}{2Q}. \quad (3.16)$$

²This is the one-loop contribution [TODO: is this accurate?].

Then because the particle must satisfy

$$z_i \theta_i^2 \lesssim \rho, \quad (3.17)$$

we find that [18]

$$\rho \sim \frac{p^+}{Q}. \quad (3.18)$$

If $z \sim 1$, we know that $z \gg z_{\text{cut}}$, so the momentum scales independently of z_{cut} . Hence, the scaling of these **collinear** modes is [18]

$$p_c \sim Q(1, \rho, \rho^{1/2}). \quad (3.19)$$

In a hemisphere where the resolved emission stops the mMDT groomer, this is the only collinear radiation that contributes.

If on the other hand $z \sim z_{\text{cut}} \ll 1$, the result is **collinear-soft** radiation with $p^- \sim z_i Q$ and $p^+ \sim \theta_i^2 z_i Q$. From [18], these momenta scale like

$$p_{cs} \sim z_{\text{cut}} Q \left(1, \frac{\rho}{z_{\text{cut}}}, \left(\frac{\rho}{z_{\text{cut}}} \right)^{1/2} \right) \quad (3.20)$$

and depend on the single energy scale $\sqrt{\rho z_{\text{cut}}}$. This scale matters in the hemisphere which does not contain the resolved soft gluon.

3.3 Factorization

With the power counting in hand, we are now ready to derive a factorization formula describing the hemisphere mass distribution in the limit $\rho \sim z_{\text{cut}} \ll 1$. First, we should note that it is most straightforward to compute the double differential cross section in the masses of the individual hemispheres, then integrate over them to get the heavy hemisphere mass [38]:

$$\frac{d\sigma}{d\rho} = \int \frac{d^2\sigma}{d\rho_1 d\rho_2} [\delta(\rho - \rho_1)\Theta(\rho_1 - \rho_2) + \delta(\rho - \rho_2)\Theta(\rho_2 - \rho_1)]. \quad (3.21)$$

The integral simply breaks up the two cases $\rho_1 > \rho_2$ and $\rho_2 > \rho_1$ and assigns the correct value of ρ in each case.

Now, in the limit $\rho_1, \rho_2 \ll 1$, we can apply the technology of SCET to factorize the double-differential cross section into a product of hard, soft, and jet contributions [18, 34]. The basic form is

$$\frac{d^2\sigma}{d\rho_1 d\rho_2} = H(Q^2) \otimes S(\rho_1, \rho_2, z_{\text{cut}}) \otimes J_q(\rho_1) \otimes J_g(\rho_1, z_{\text{cut}}) \otimes J_{\bar{q}}(\rho_2). \quad (3.22)$$

The symbol \otimes represents convolution. Here, Q^2 is the squared center-of-mass energy of the collision. $H(Q^2)$ is hard function representing the cross section of $e^+e^- \rightarrow q\bar{q}$ events, $S(\rho_1, \rho_2, z_{\text{cut}})$ is the function representing soft contributions (which are

sensitive to z_{cut}), and $J_i(\rho)$ is a function describing the production of a jet off of particle i (where i is a quark q , antiquark \bar{q} , or gluon g).

As this factorization currently stands, several terms depend on multiple scales and must be refactored. In the limit $\rho \sim z_{\text{cut}} \ll 1$ after mMDT grooming, the soft function consists of global soft emissions which contribute only to the normalization; a resolved soft, wide-angle emission generated by a fixed-order function; and soft radiation which passes the groomer due to the resolved emission. The first two depend only on the scale z_{cut} and can be combined into one function. Therefore, we can write

$$\begin{aligned} \frac{d^2\sigma}{d\rho_1 d\rho_2} = & H(Q^2) \times R(\rho_1, \rho_2, z_{\text{cut}}) \times S_R(\rho - z_{\text{cut}}) \otimes J_{c,q}(\rho_1, z_{\text{cut}}) \\ & \otimes J_{c,g}(\rho_1, z_{\text{cut}}) \otimes J_{c,\bar{q}}(\rho_2, z_{\text{cut}}). \end{aligned} \quad (3.23)$$

Here, $R(\rho_1, \rho_2, z_{\text{cut}})$ describes the resolved emission as well as other soft wide-angle radiation (from which the resolved emission emerged), while $S_R(\rho - z_{\text{cut}})$ describes radiation which passes the groomer in the presence of the resolved emission. We have also re-written the jet functions as $J_{c,i}(\rho, z_{\text{cut}})$ to make explicit their dependence on multiple scales.

Now, as we established in Sec. 3.2.3, radiation collinear to the jet with energy fraction of order 1 depends only on ρ , and radiation with energy fraction much less than 1 depends on the scale $\sqrt{\rho z_{\text{cut}}}$. However, this soft-collinear radiation only matters in the absence of a resolved gluon emission (which stops the mMDT groomer), in which case the jet function factorizes as

$$J_{c,\bar{q}}(\rho, z_{\text{cut}}) = J_{\bar{q}}(\rho) \otimes S_C(\sqrt{\rho z_{\text{cut}}}) \quad (3.24)$$

The result is that we must treat each hemisphere separately, since one contains the resolved emission and the other does not. Moreover, the gluon's jet function J_g only depends on the scale of the gluon's energy, which is a function of ρ and z_{cut} [TODO: **check this**]. Therefore, if we assume, without loss of generality, that $\rho_1 > \rho_2$, the cross section becomes

$$\begin{aligned} \frac{d^2\sigma}{d\rho_1 d\rho_2} = & 2H(Q^2) \times R(\rho_1, \rho_2, z_{\text{cut}}) \times S_R(\rho - z_{\text{cut}}) \otimes J_{c,q}(\rho_1) \\ & \otimes J_{c,g}(\rho_1, z_{\text{cut}}) \otimes [J_{\bar{q}}(\rho_2) \otimes S_C(\sqrt{\rho_2 z_{\text{cut}}})]. \end{aligned} \quad (3.25)$$

This is our final factorization formula for the double differential cross section in each hemisphere mass. The distribution of the heavy hemisphere mass then given by Eq. 3.21. We are now ready to proceed with resummation.

Chapter 4

All-orders calculation

Recall that the goal of our all-orders calculation is to derive an expression which systematically accounts for logarithmic contributions at every order in α_s and with which, if one has sufficient patience and mathematical skill, one could compute the heavy hemisphere mass to arbitrary accuracy in the $\rho \sim z_{\text{cut}} \ll 1$ limit. In this chapter, we will see how this is done.

As we have repeated several times by now,¹ QCD is a scale-invariant theory. However, when we compute something like the groomed heavy hemisphere mass distribution, we impose scale onto the system (such as the hemisphere mass or the groomer energy cut). In QCD, whenever multiple scales appear, say Λ_h and Λ_ℓ , high-order corrections to observables appear with the form [20]

$$\alpha_s^n \log^n \frac{\Lambda_h}{\Lambda_\ell}. \quad (4.1)$$

These logarithms can grow quite large if the scales are far apart, which enhances the size of these contributions [3]. Moreover, since these contributions occur at every order in α_s , they can be difficult to take care of. This leaves us in a quandary — how do we handle large corrections which are, for all intents and purposes, out of computational reach?

The key to an all-orders calculation of the distribution is to keep track of these logarithmic corrections in a systematic way, move them around, and put them back together into a scale-invariant function. This is the process of **resummation**, which we are about to undertake.

4.1 Resummation

The first step towards resummation in SCET is to derive a factorization formula [20], as we have already done in Eq. 3.25. Splitting the cross section into terms, each of which depends only on a single scale, enables resummation of each term [18].

It will be helpful to work in Laplace space, which for a function $f(t)$ is achieved

¹Because it bears repeating!

by the transformation [39]

$$\mathcal{L}\{f\}(s) = \int_0^\infty f(t)e^{-st} dt. \quad (4.2)$$

For notational simplicity, instead of writing $\mathcal{L}\{f\}(s)$ everywhere, we will simply write $f(s)$. That is, whenever a function is written in terms of Laplace variables, we will assume that it is the Laplace-transformed function, and vice versa.

Under Laplace transformation, convolution becomes multiplication, so under the transformation $\rho \rightarrow \nu$, the factorization formula becomes

$$\begin{aligned} \frac{d^2\sigma}{d\nu_1 d\nu_2} &= 2H(Q^2) \times R(\nu_1, \nu_2, z_{\text{cut}}) \times S_R(\nu_1 - z_{\text{cut}}) \times J_q(\nu_1) \times J_g(\nu_1, z_{\text{cut}}) \\ &\quad \times J_{\bar{q}}(\nu_2) \times S_C(\sqrt{\nu_2 z_{\text{cut}}}). \end{aligned} \quad (4.3)$$

The multiplicative factorization in Laplace space allows us to resum each term individually, without worrying about cross-talk between terms [18]. Before moving on, with this calculation, let us study how our resummation strategy will work.

4.1.1 Strategy

Let us consider the simple example of an observable

$$\sigma = F_1 F_2. \quad (4.4)$$

Suppose we are working in $d = 4 - 2\epsilon$ dimensions and have introduced a mass scale μ to compensate for dimensionality changes. We call μ the **renormalization scale**. Since μ is an arbitrary scale introduced to regulate the calculation, the physical quantity σ must be independent of μ at the end of the day:

$$\frac{\partial \sigma}{\partial \mu} = 0. \quad (4.5)$$

In 4 dimensions, this would be true of F_1 and F_2 as well. But in our dimensional regularization scheme, away from 4 dimensions, these functions *do* have μ -dependence. Their departure from μ -independence is described by a quantity called the **anomalous dimension**, so-called because the behavior away from 4 dimensions is anomalous in this sense. If F_1 has an anomalous dimension γ_1 and F_2 has an anomalous dimension γ_2 , then it is a general fact of quantum field theory that [3]

$$\frac{\partial F_1}{\partial \log \mu} = \gamma_1 F_1 \quad \frac{\partial F_2}{\partial \log \mu} = \gamma_2 F_2. \quad (4.6)$$

In fact, many authors (such as the author of Ref. [3]) *define* the anomalous dimension this way. Now notice that this yields, by the product rule,

$$\frac{\partial \sigma}{\partial \log \mu} = (\gamma_1 + \gamma_2) F_1 F_2. \quad (4.7)$$

In order to enforce Eq. 4.5, we demand that

$$\gamma_1 + \gamma_2 = 0. \quad (4.8)$$

This provides constraints on our calculations as well as a strong consistency check — if we have calculated F_1 and F_2 and find that Eq. 4.8 is unsatisfied, then we know a mistake has been made. On the other hand, it means that if we compute the anomalous dimension of F_1 , then we do not need to compute the anomalous dimension of F_2 .

Equations 4.5 and 4.6 are known as **renormalization group equations**.² The overall strategy to resum large logarithms in the cross section σ is to solve the renormalization group equation for each function F_1 and F_2 . As long as σ factorizes as claimed and Eq. 4.8 is satisfied, then this results in an all-orders calculation of σ .

Thus, we have a general two-step strategy for resumming a function F (such as F_1 or F_2 in the example above):

1. Compute the anomalous dimension γ of F . This is done by computing F to some desired order in α_s and pulling out the appropriate terms.
2. Solve the renormalization group equation

$$\frac{\partial F}{\partial \log \mu} = \gamma F = \left(\Gamma_F(\alpha_s) \log \frac{\mu^2}{\mu_1^2} + \gamma_F(\alpha_s) \right) F. \quad (4.9)$$

These steps are explained in more detail below.

4.1.2 Anomalous dimension

In order to solve the renormalization group equation, we need to know more about the anomalous dimensions. In general, for a function F , the anomalous dimension γ can be written as [18]

$$\gamma = \Gamma_F(\alpha_s) \log \frac{\mu^2}{\mu_1^2} + \gamma_F(\alpha_s). \quad (4.10)$$

Here, μ_1 is the remainder of the scale appearing with μ in the logarithm. We call $\Gamma_F(\alpha_s)$ the **cusp anomalous dimension**, and $\gamma_F(\alpha_s)$ is the **non-cusp anomalous dimension**. The cusp anomalous dimension is universal up to normalization and can be written as a series in α_s :

$$\Gamma_F(\alpha_s) = d_F \Gamma_{\text{cusp}}(\alpha_s) = d_F \sum_{n=0}^{\infty} \Gamma_n \left(\frac{\alpha_s}{4\pi} \right)^{n+1}. \quad (4.11)$$

²The renormalization group refers to the symmetry of physical quantities under changes in the techniques used to calculate them. Technically, we are working with the **continuum renormalization group**, which formalizes the independence of observable quantities on μ in dimensional regularization. [3]

The coefficients Γ_n can be pulled from the literature. The relevant terms for our purposes are [18]

$$\begin{aligned}\Gamma_0 &= 4 \\ \Gamma_1 &= 4C_A\left(\frac{67}{9} - \frac{\pi^2}{3}\right) - \frac{80}{9}T_R n_f,\end{aligned}\tag{4.12}$$

where $C_A = 3$ and $T_R = 1/2$ are color factors from QCD and n_f is the number of quarks with energy less than that being considered.

The real work comes from computing the non-cusp anomalous dimension

$$\gamma_F(\alpha_s) = \sum_{n=0}^{\infty} \gamma_n \left(\frac{\alpha_s}{4\pi}\right)^{n+1}.\tag{4.13}$$

An example calculation will be performed in Sec. 4.2. This entails computing the function of interest to the desired accuracy, then peeling off the non-logarithmic contributions to the anomalous dimension. The anomalous dimension can be determined either through inspection, by simply taking the coefficient of $2/\epsilon$, or by computing the appropriate derivative per the renormalization group equation.

4.1.3 Solving the renormalization group equation

To solve the renormalization group equation, Eq. 4.9, it is convenient to rewrite the differential equation not in terms of μ , but in terms of α_s . This is done through the QCD β -function, which describes how α_s depends on the energy scale μ [18]:

$$d \log \mu = \frac{d\mu}{\mu} = \frac{d\alpha_s}{\beta(\alpha_s)}.\tag{4.14}$$

This is a manifestation of the running of the coupling α_s . The β -function is another quantity well-known in the literature as a series in α_s :

$$\beta(\alpha_s) = -2\alpha_s \sum_{n=0}^{\infty} \beta_n \left(\frac{\alpha_s}{4\pi}\right)^{n+1}\tag{4.15}$$

with [18]

$$\begin{aligned}\beta_0 &= \frac{11}{3}C_A - \frac{4}{3}T_R n_f \\ \beta_1 &= \frac{34}{3}C_A^2 - 4T_R n_f \left(C_F + \frac{5}{3}C_A\right),\end{aligned}\tag{4.16}$$

where $C_F = 4/3$ is another QCD color factor. The general solution to the renormalization group equation is then [18]

$$\begin{aligned}F(\mu) = F(\mu_0) \exp \left[2 \int_{\alpha_s(\mu_0)}^{\alpha_s(\mu)} \frac{d\alpha}{\beta(\alpha)} \Gamma_F(\alpha) \int_{\alpha_s(\mu_0)}^{\alpha} \frac{d\alpha'}{\beta(\alpha')} + \int_{\alpha_s(\mu_0)}^{\alpha_s(\mu)} \frac{d\alpha}{\beta(\alpha)} \gamma_F(\alpha) \right. \\ \left. + \log \frac{\mu_0^2}{\mu_1^2} \int_{\alpha_s(\mu_0)}^{\alpha_s(\mu)} \frac{d\alpha}{\beta(\alpha)} \Gamma_F(\alpha) \right].\end{aligned}\tag{4.17}$$

Here, μ_0 is some reference energy scale of our choosing. One way to think about resummation is that it allows us to compute the function F at any scale μ , given the value at a particular scale μ_0 . Moreover, the only place where large logarithms could now live is in $F(\mu_0)$ — it turns out that the logarithms will contain factors of μ_0 , so we can cleverly pick μ_0 in order to eliminate them.

To see that Eq. 4.17 solves the renormalization group equation 4.9, we can simply differentiate it with respect to μ . To do so, first notice that

$$\frac{\partial}{\partial \mu} \int_{\alpha_s(\mu_0)}^{\alpha_s(\mu)} \frac{d\alpha}{\beta(\alpha)} \Gamma_F(\alpha) \int_{\alpha_s(\mu_0)}^{\alpha} \frac{d\alpha'}{\beta(\alpha')} = \frac{\partial \alpha_s(\mu)}{\partial \mu} \frac{\Gamma_F(\alpha_s(\mu))}{\beta(\alpha_s(\mu))} \int_{\alpha_s(\mu_0)}^{\alpha_s(\mu)} \frac{d\alpha}{\beta(\alpha)}. \quad (4.18)$$

By the definition of the β -function in Eq. 4.14,

$$\frac{\partial \alpha_s(\mu)}{\partial \mu} = \frac{\beta(\alpha_s(\mu))}{\mu} \quad (4.19)$$

and

$$\int_{\alpha_s(\mu_0)}^{\alpha_s(\mu)} \frac{d\alpha}{\beta(\alpha)} = \int_{\mu_0}^{\mu} \frac{d\mu'}{\mu'} = \log \frac{\mu}{\mu_0}. \quad (4.20)$$

Thus,

$$\frac{\partial}{\partial \mu} \int_{\alpha_s(\mu_0)}^{\alpha_s(\mu)} \frac{d\alpha}{\beta(\alpha)} \Gamma_F(\alpha) \int_{\alpha_s(\mu_0)}^{\alpha} \frac{d\alpha'}{\beta(\alpha')} = \frac{\Gamma_F(\alpha_s(\mu))}{\mu} \log \frac{\mu}{\mu_0}. \quad (4.21)$$

The second and third integrals of Eq. 4.17 are similar but more straightforward:

$$\int_{\alpha_s(\mu_0)}^{\alpha_s(\mu)} \frac{d\alpha}{\beta(\alpha)} \gamma_F(\alpha) = \frac{\gamma_F(\alpha_s(\mu))}{\mu}, \quad \int_{\alpha_s(\mu_0)}^{\alpha_s(\mu)} \frac{d\alpha}{\beta(\alpha)} \Gamma_F(\alpha) = \frac{\Gamma_F(\alpha_s(\mu))}{\mu}. \quad (4.22)$$

Therefore, differentiating Eq. 4.17 with respect to μ yields, via the chain rule,

$$\begin{aligned} \mu \frac{\partial F(\mu)}{\partial \mu} &= F(\mu) \left[\log \frac{\mu^2}{\mu_0^2} \Gamma_F(\alpha_s) + \gamma_F(\alpha_s) + \log \frac{\mu_0^2}{\mu_1^2} \Gamma_F(\alpha_s) \right] \\ &= F(\mu) \left[\Gamma_F(\alpha_s) \log \frac{\mu^2}{\mu_1^2} + \gamma_F(\alpha_s) \right], \end{aligned} \quad (4.23)$$

where we have assigned $\alpha_s = \alpha_s(\mu)$. This is exactly the renormalization group equation, so the solution works.

Next-to-leading-logarithmic accuracy

In a standard perturbative expansion of a physical quantity

$$f(\lambda) = \sum_{n=0}^{\infty} f_n \lambda^n, \quad (4.24)$$

we might talk about approximating a solution by keeping only, say, the leading-order (LO) term f_0 . If we need higher precision,³ we can take higher-order terms in

³Or are feeling particularly fancy

the series, moving to next-to-leading order (NLO), then next-to-next-to-leading-order (NNLO), and so on.

In the context of a perturbative resummation calculation such as the one at hand, it does not make sense to discuss the order of a result. This is because the exponent of the solution to the renormalization group equation, Eq. 4.17, is itself a series in α_s . To achieve a more accurate result, we want to expand the *exponent* to a fixed order, which means that the quantity itself is *logarithmically* accurate with respect to this expansion. A leading-order exponential expansion yields an overall result accurate to the leading logarithm (LL) of the exponent. Moving to higher accuracy then takes us to the next-to-leading-logarithm (NLL), and so on.

Whereas LL accuracy gives only the vaguest hints about the distribution of an observable, NLL accuracy is the first order which makes meaningful predictions about the shape of the distribution. For this reason, we will explore the process of developing an NLL calculation.

To do this, we have to decide how accurately to calculate each piece of Eq. 4.17. Let

$$K(\mu, \mu_0) \equiv 2 \int_{\alpha_s(\mu_0)}^{\alpha_s(\mu)} \frac{d\alpha}{\beta(\alpha)} \Gamma_F(\alpha) \int_{\alpha_s(\mu_0)}^{\alpha} \frac{d\alpha'}{\beta(\alpha')} + \int_{\alpha_s(\mu_0)}^{\alpha_s(\mu)} \frac{d\alpha}{\beta(\alpha)} \gamma_F(\alpha) \quad (4.25)$$

and

$$\omega(\mu, \mu_0) \equiv \int_{\alpha_s(\mu_0)}^{\alpha_s(\mu)} \frac{d\alpha}{\beta(\alpha)} \Gamma_F(\alpha). \quad (4.26)$$

To achieve NLL accuracy, we want to determine $K(\mu, \mu_0)$ to order $\mathcal{O}(\alpha_s^0)$, while we want $\omega(\mu, \mu_0)$ to order $\mathcal{O}(\alpha_s)$ [18]. It turns out that we need $\Gamma_{\text{cusp}}(\alpha_s)$ to order $\mathcal{O}(\alpha_s^2)$ and $\beta(\alpha_s)$ to order $\mathcal{O}(\alpha_s^3)$, while we only need the non-cusp anomalous dimension $\gamma_F(\alpha_s)$ to order $\mathcal{O}(\alpha_s)$. If we take

$$\Gamma_{\text{cusp}}(\alpha_s) = \Gamma_0 \frac{\alpha_s}{4\pi} + \Gamma_1 \left(\frac{\alpha_s}{4\pi} \right)^2 + \mathcal{O}(\alpha_s^3) \quad (4.27)$$

$$\gamma_F(\alpha_s) = \gamma_0 \frac{\alpha_s}{4\pi} + \mathcal{O}(\alpha_s^2) \quad (4.28)$$

$$\beta(\alpha_s) = -2\beta_0 \frac{\alpha_s^2}{4\pi} - 2\beta_1 \frac{\alpha_s^3}{(4\pi)^2} + \mathcal{O}(\alpha_s^4) \quad (4.29)$$

and let

$$r \equiv \frac{\alpha_s(\mu)}{\alpha_s(\mu_0)}, \quad (4.30)$$

then the first term in the exponent becomes

$$\begin{aligned} K(\mu, \mu_0) &= \frac{d_F \Gamma_0}{2\beta_0^2} \left[\frac{4\pi}{\alpha_s(\mu_0)} \left(\log r + \frac{1}{r} - 1 \right) + \log r \left(\frac{\beta_1}{\beta_0} - \frac{\Gamma_1}{\Gamma_0} \right) + \frac{\beta_1}{2\beta_0} \log^2 r \right] \\ &\quad - \frac{\gamma_0}{2\beta_0} \log r + \mathcal{O}(\alpha_s). \end{aligned} \quad (4.31)$$

while the second is

$$\omega(\mu, \mu_0) = \frac{d_F \Gamma_0}{2\beta_0} \left[\log \frac{1}{r} + \frac{\alpha_s(\mu_0)}{4\pi} (r-1) \left(\frac{\beta_1}{\beta_0} - \frac{\Gamma_1}{\Gamma_0} \right) \right] + \mathcal{O}(\alpha_s^2). \quad (4.32)$$

Recall that $\Gamma_F(\alpha_s) = d_F \Gamma_{\text{cusp}}(\alpha_s)$ for some normalization d_F .

With these expansions in place, we can re-write Eq. 4.17 *in Laplace space* as

$$F(\mu) = F(\mu_0) e^{K(\mu, \mu_0)} \left(\frac{\mu_0^2}{\mu_1^2} \right)^{\omega(\mu, \mu_0)}. \quad (4.33)$$

Everything is now defined in terms of known constants and the anomalous dimension except for $F(\mu_0)$. This quantity is determined by calculating F at some fixed order and then evaluating at the scale μ_0 .⁴ [TODO: explicate the subtle difference between the resummed result and the fixed-order result. Explain why we needed to go through the trouble of resummation in the first place]

4.1.4 Full resummed result

The above process can be completed for every term in the factorization formula, Eq. 4.3. Letting μ_F be the fixed scale at which function F is evaluated and $\mu_{1,F}$ be the natural scale appearing logarithmically in F , we have

$$\begin{aligned} \frac{d^2\sigma}{d\nu_1 d\nu_2} &= 2 \exp \left[K_H(\mu, \mu_H) + K_R(\mu, \mu_R) + K_{S_R}(\mu, \mu_{S_R}) + K_{J_q}(\mu, \mu_{J_q}) \right. \\ &\quad \left. + K_{J_g}(\mu, \mu_{J_g}) + K_{J_{\bar{q}}}(\mu, \mu_{J_{\bar{q}}}) + K_{S_C}(\mu, \mu_{S_C}) \right] \\ &\quad \times H(Q, \mu_H) R(\nu_1, \nu_2, z_{\text{cut}}, \mu_R) S_R(\nu_1, z_{\text{cut}}, \mu_{S_R}) J_q(\nu_1, \mu_{J_q}) \\ &\quad \times J_g(\nu_1, z_{\text{cut}}, \mu_{J_g}) J_{\bar{q}}(\nu_2, \mu_{J_{\bar{q}}}) S_C(\nu_2, z_{\text{cut}}, \mu_{S_C}) \left(\frac{\mu_H}{\mu_{1,H}} \right)^{\omega_H(\mu, \mu_H)} \quad (4.34) \\ &\quad \times \left(\frac{\mu_R}{\mu_{1,R}} \right)^{\omega_R(\mu, \mu_R)} \left(\frac{\mu_H}{\mu_{1,H}} \right)^{\omega_{S_R}(\mu, \mu_{S_R})} \left(\frac{\mu_{J_q}}{\mu_{1,J_q}} \right)^{\omega_{J_q}(\mu, \mu_{J_q})} \\ &\quad \times \left(\frac{\mu_{J_g}}{\mu_{1,J_g}} \right)^{\omega_{J_g}(\mu, \mu_{J_g})} \left(\frac{\mu_{J_{\bar{q}}}}{\mu_{1,J_{\bar{q}}}} \right)^{\omega_{J_{\bar{q}}}(\mu, \mu_{J_{\bar{q}}})} \left(\frac{\mu_{S_C}}{\mu_{1,S_C}} \right)^{\omega_{S_C}(\mu, \mu_{S_C})}. \end{aligned}$$

This result is in Laplace space, but we would like it to be in real space. For the function H , its lack of ν -dependence means that it does not change under inverse Laplace transformation. However, to transform the rest, we need to be sneaky.

For any resummed function F appearing in the factorization formula which takes the form (where we have made the ν -dependence in the scale μ_1 explicit)

$$F(\nu, \mu) = e^{K(\mu, \mu_0)} F(\nu, \mu_0) \left(\frac{\nu^\xi \mu_0}{\mu_1} \right)^{\omega(\mu, \mu_0)}, \quad (4.35)$$

⁴ $F(\mu_0)$ is simply a boundary value for the renormalization group equation.

the fixed-scale function $F(\nu, \mu_0)$ contains logarithms of the form [18]

$$\log^n \frac{\nu^\xi \mu_0}{\mu_1}. \quad (4.36)$$

In fact, all ν -dependence will appear in this way.⁵ We can therefore use the clever relationship [40, 18]

$$\frac{\partial^n}{\partial q^n} \nu^q = \nu^q \log^n \nu \quad (4.37)$$

to re-write the logarithms in the fixed-scale as derivatives. That is, we will take **[TODO: check this]**

$$\log^n \frac{\nu^\xi \mu_0}{\mu_1} \rightarrow \partial_\omega^n, \quad (4.38)$$

a derivative with respect to the function $\omega(\mu, \mu_0)$. Denoting this transformation by $F(L \rightarrow \partial_\omega)$, we have

$$F(\nu, \mu) = e^{K(\mu, \mu_0)} F(L \rightarrow \partial_\omega) \left(\frac{\nu^\xi \mu_0}{\mu_1} \right)^{\omega(\mu, \mu_0)}. \quad (4.39)$$

Now our problem is solved because the inverse Laplace transformation commutes with derivatives and the following transformation is known [18]:

$$\mathcal{L}^{-1}\{\nu^q\} = \frac{\rho^{-q-1}}{\Gamma(-q)} \quad (4.40)$$

where ρ is the transformation partner of ν and $\Gamma(x)$ is the standard gamma function. Hence, the inverse Laplace transformation of $F(\nu, \mu)$ is

$$F(\rho, \mu) = e^{K(\mu, \mu_0)} F(L \rightarrow \partial_\omega) \left[\frac{\mu_0}{\rho^\xi \mu_1} \right]^{\omega(\mu, \mu_0)} \frac{1}{\rho \Gamma(-\xi \omega(\mu, \mu_0))}. \quad (4.41)$$

Performing this operation for every term in Eq. 4.34 that has explicit ν -dependence,

⁵If this seems weird now, do not worry. We will see a concrete example later which makes this point clearer. This will be a ‘proof by example,’ if you will.

we have

$$\begin{aligned}
\frac{d^2\sigma}{d\rho_1 d\rho_2} = & 2 \exp \left[K_H(\mu, \mu_H) + K_R(\mu, \mu_R) + K_{S_R}(\mu, \mu_{S_R}) + K_{J_q}(\mu, \mu_{J_q}) \right. \\
& \left. + K_{J_g}(\mu, \mu_{J_g}) + K_{J_{\bar{q}}}(\mu, \mu_{J_{\bar{q}}}) + K_{S_C}(\mu, \mu_{S_C}) \right] \\
& \times H(Q, \mu_H) R(L \rightarrow \partial_{\omega_R}) S_R(L \rightarrow \partial_{\omega_{S_R}}) J_q(L \rightarrow \partial_{\omega_{J_q}}) \\
& \times J_g(L \rightarrow \partial_{\omega_{J_g}}) J_{\bar{q}}(L \rightarrow \partial_{\omega_{J_{\bar{q}}}}) S_C(L \rightarrow \partial_{\omega_{S_C}}) \left(\frac{\mu_H}{\mu_{1,H}} \right)^{\omega_H(\mu, \mu_H)} \\
& \times \left(\frac{\mu_R}{\mu_{1,R}} \right)^{\omega_R(\mu, \mu_R)} \left(\frac{\mu_{S_R}}{\mu_{1,S_R}} \right)^{\omega_{S_R}(\mu, \mu_{S_R})} \left(\frac{\mu_{J_q}}{\mu_{1,J_q}} \right)^{\omega_{J_q}(\mu, \mu_{J_q})} \\
& \times \left(\frac{\mu_{J_g}}{\mu_{1,J_g}} \right)^{\omega_{J_g}(\mu, \mu_{J_g})} \left(\frac{\mu_{J_{\bar{q}}}}{\mu_{1,J_{\bar{q}}}} \right)^{\omega_{J_{\bar{q}}}(\mu, \mu_{J_{\bar{q}}})} \left(\frac{\mu_{S_C}}{\mu_{1,S_C}} \right)^{\omega_{S_C}(\mu, \mu_{S_C})} \\
& \times \frac{1}{\rho_1 \rho_2} \frac{1}{\Gamma(-\xi_{J_{\bar{q}}} \omega_{J_{\bar{q}}}(\mu, \mu_{J_{\bar{q}}}) - \xi_{S_C} \omega_{S_C}(\mu, \mu_{S_C}))} \\
& \times \frac{1}{\Gamma(-\xi_R \omega_R(\mu, \mu_R) - \xi_{S_R} \omega_{S_R}(\mu, \mu_{S_R}) - \xi_{J_q} \omega_{J_q}(\mu, \mu_{J_q}) - \xi_{J_g} \omega_{J_g}(\mu, \mu_{J_g}))}, \tag{4.42}
\end{aligned}$$

where ξ_F is the exponent of ν in the exponentiated term corresponding to function F . The replacement of $\nu \rightarrow 1/\rho$ in the exponentiated scale ratios is implicit.

As messy as Eq. 4.42 may be, it is remarkable that we can write down the solution in closed form (assuming that we can compute the K and ω functions). All that is left to do now is compute each piece of the cross section to determine the anomalous dimensions and fixed-scale contributions.

Luckily for us, several of the functions — the hard function H , the jet functions J_q , $J_{\bar{q}}$, and J_g , and the collinear-soft function S_C — have already been computed to the necessary order for an NLL calculation of the heavy hemisphere mass [TODO: **would be nice to find/cite these**]. However, the resolved emission function R and the soft function S_R are novel; for these, we must compute their anomalous dimensions and fixed-scale contributions to order α_s . To see how this works, we will compute the soft function S_R in Sec. 4.2.

4.2 Soft function

4.2.1 Setup

Let us first remind ourselves what it is we are calculating. The soft function $S_R(\rho - z_{\text{cut}})$ describes soft radiation which passes the mMDT groomer due to its proximity to the resolved gluon. If the resolved emission occurs at an angle θ from the quark axis, then because of the iterative selection approach of the mMDT grooming algorithm,

any radiation at a smaller angle either from the quark or the gluon will pass the groomer.

We want to compute S_R to order α_s , then use the renormalization group equation to resum the soft function. For the sake of this section, let $\rho_s = \rho - z_{\text{cut}}$ be the contribution of the soft ungroomed emissions to the hemisphere mass.

For now, let the resolved gluon have momentum k_g , let the quark lie along the direction $n_q = (1, 0, 0, 1)$, and consider an extra-soft gluon that has been emitted with momentum k . If this extra-soft gluon is closer to the quark, then its dominant contribution to the mass ρ_s will come from its interaction with the quark:

$$\rho_s = \frac{4k^+}{Q}, \quad (4.43)$$

where $k^+ = n_q \cdot k$ and $k^- = k \cdot (1, 0, 0, -1)$ are light-cone coordinates with respect to the quark axis. On the other hand, if the extra-soft gluon is closer to the resolved gluon, then its dominant contribution comes from this interaction:

$$\rho_s = \frac{4k \cdot n_g}{Q} = \frac{4k \cdot k_g}{E_g Q} \quad (4.44)$$

where n_g is the direction of the resolved gluon and k_g is its energy.

Notice now that the angle between the extra-soft gluon and the quark is given by

$$1 - \cos \theta_{gq} = \frac{k^+}{k_0}, \quad (4.45)$$

while the angle between the extra-soft gluon and the resolved gluon is

$$1 - \cos \theta_{gg} = \frac{k \cdot n_g}{k_0}. \quad (4.46)$$

The case in which the extra-soft gluon is closer to the quark is the case in which $\theta_{gq} < \theta_{gg}$, so $1 - \cos \theta_{gq} < 1 - \cos \theta_{gg}$ and therefore, in turn, $k^+ < k \cdot n_g$. The total measurement function will therefore be

$$\delta_{\rho_s} = \Theta(k \cdot n_g - k^+) \delta\left(\rho - \frac{4k^+}{Q}\right) + \Theta(k^+ - k \cdot n_g) \delta\left(\rho - \frac{4k \cdot n_g}{E_g Q}\right). \quad (4.47)$$

We also need to impose the kinematic constraint that the extra-soft gluon is sufficiently close to the quark or resolved gluon. Saying that the gluon is in the region is equivalent to saying that it is not outside of the region. The gluon is outside of the quark's radius of influence if

$$\frac{k^+}{k_0} = 1 - \cos \theta_{gq} > 1 - \cos \theta = n_g \cdot n_q. \quad (4.48)$$

On the other hand, the gluon is outside the resolved gluon's radius of influence if

$$\frac{k \cdot n_g}{k_0} = 1 - \cos \theta_{gg} > 1 - \cos \theta = n_g \cdot n_q. \quad (4.49)$$

Therefore, the mMDT grooming restriction is

$$\Theta_{\text{mMDT}} = 1 - \Theta(k^+ - k_{0g} \cdot n_q) \Theta(k \cdot n_g - k_0 n_g \cdot n_q). \quad (4.50)$$

In QCD, the gluon carries color charge, so a gluon can be emitted off of any pair of color-charged particles: the quark and antiquark, the quark and resolved gluon, or the antiquark and resolved gluon. The matrix element accounts for all of these possibilities, and in the soft limit in $d = 4 - 2\epsilon$ dimensions it takes the form [36]

$$|\mathcal{M}|^2 = -4\pi\alpha_s\mu^{2\epsilon} \sum_{i < j} \mathbf{T}_i \cdot \mathbf{T}_j \frac{n_i \cdot n_j}{(n_i \cdot k)(n_j \cdot k)}. \quad (4.51)$$

[TODO: are we missing a factor of σ_0 ?] Here i, j range over all the pairs of resolved particles, the n_i are direction vectors, and the \mathbf{T}_i are color charge matrices which account for color correlations. Their precise definition is unimportant, and all we need to know is that $\mathbf{T}_q \cdot \mathbf{T}_{\bar{q}} = -C_F$ [36].

For a complete calculation, we would need to compute the soft function separately for each term of the sum, then combine them all together at the end. However, only one of the terms — emission off of the quark-antiquark pair — is analytically tractable, so for the sake of demonstration we will focus solely on that. This is equivalent, in some sense, to computing the soft function in a theory like quantum electrodynamics, in which the force carrier does not carry charge.⁶ Thus, we will simply take

$$|\mathcal{M}|^2 = 4\pi\alpha_s C_F \mu^{2\epsilon} \frac{n_q \cdot n_{\bar{q}}}{(n_q \cdot k)(n_{\bar{q}} \cdot k)} = 4\pi\alpha_s C_F \mu^{2\epsilon} \frac{2}{k^+ k^-}, \quad (4.52)$$

where $n_{\bar{q}} = (1, 0, 0, -1)$.

Finally, the phase space measure in $d = 4 - 2\epsilon$ dimensions takes the usual form

$$d\Pi = \frac{d^d k}{(2\pi)^{d-1}} \delta(k^2) \Theta(k^+) \Theta(k^- - k^+). \quad (4.53)$$

[TODO: check the power of 2π] Notice that we are enforcing the gluon to be emitted in the hemisphere with the quark by requiring $k^- > k^+$. This is necessary because of the assumption we have made in writing the all-orders result of Eq. 4.42. Note as well that we are only scanning over the momentum of the extra-soft gluon: under the assumption that this gluon is softer than the resolved gluon, the emission does not meaningfully influence the momentum of either the quarks or the resolved gluon.

⁶Of course, this would be a logically incoherent calculation, as the very presence of jet physics is a result of the particular nonlinearities of QCD which lead to the gluon carrying color charge. Nevertheless, we will continue, since the goal of this thesis is, in large part, pedagogical — I warned you that we would have to make sacrifices.

Thus, putting everything together, we find

$$\boxed{S_R(\rho_s) = 4\pi\alpha_s C_F \mu^{2\epsilon} \int \frac{d^d k}{(2\pi)^{d-1}} \delta(k^2) \Theta(k^+) \Theta(k^- - k^+) \frac{2}{k^+ k^-} \\
 \times \left[\Theta(k \cdot n_g - k^+) \delta\left(\rho - \frac{4k^+}{Q}\right) + \Theta(k^+ - k \cdot n_g) \delta\left(\rho - \frac{4k \cdot n_g}{Q}\right) \right] \\
 \times [1 - \Theta(k^+ - k_{0g} \cdot n_q) \Theta(k \cdot n_g - k_{0g} n_g \cdot n_q)]} \quad (4.54)$$

4.2.2 Coordinate choice

If we want to perform any actual calculations, we need to pick a coordinate system in which to evaluate the integral of Eq. 4.54. Notice that, physically, there is an axial symmetry to the problem: nothing depends on the azimuthal angle of the resolved emission about the quark axis. Therefore, we might define our momenta in terms of the **detector coordinates** of transverse momentum $p_\perp \in [0, \infty)$, pseudorapidity $\eta \in [0, \infty)$, and azimuthal angle $\phi \in [0, \pi]$. These are defined in terms of Cartesian coordinates (p_x, p_y, p_z) as

$$p_x = p_\perp \cos \phi \quad p_y = p_\perp \sin \phi \quad p_z = p_\perp \sinh \eta \quad (4.55)$$

$$p_\perp = \sqrt{p_x^2 + p_y^2} \quad \phi = \arctan \frac{p_y}{p_x} \quad \eta = \operatorname{arctanh} \frac{p_z}{|\mathbf{p}|}. \quad (4.56)$$

Notice also that, for an on-shell particle,

$$p_0 = \sqrt{p_x^2 + p_y^2 + p_z^2} = p_\perp \cosh \eta. \quad (4.57)$$

Define the detector coordinates of the extra soft gluon as $k = (k_0, k_\perp, \phi_k, \eta_k)$.

The resolved gluon is fixed from the perspective of the extra-soft gluon, so we can write its momentum in whichever coordinates are most convenient. This turns out to be standard spherical coordinates, in which the gluon is emitted with an azimuthal angle ϕ_g and a polar angle θ_g from the jet axis. Without loss of generality, we can define our coordinate axes so that $\phi_g = 0$.

Now we can transform each term of Eq. 4.54. First, notice that

$$k^+ = k_0 - k_z = k_\perp (\cosh \eta_k - \sinh \eta_k) = k_\perp e^{-\eta_k}, \quad (4.58)$$

and similarly

$$k^- = k_\perp e^{\eta_k}. \quad (4.59)$$

Then the restriction $k^+ > 0$ becomes $k_\perp > 0$ and $k^- > k^+$ becomes $\eta_k > 0$. That is,

$$\Theta(k^+) \Theta(k^- - k^+) = \Theta(k_\perp) \Theta(\eta_k). \quad (4.60)$$

Moreover, the matrix element becomes

$$|\mathcal{M}|^2 = 4\pi\alpha_s C_F \frac{2}{k_\perp^2}. \quad (4.61)$$

Next comes the measurement function. Notice that

$$\begin{aligned} k \cdot n_g &= (k_\perp \cosh \eta_k, k_\perp \cos \phi_k, k_\perp \sin \phi_k, k_\perp \sinh \eta_k) \cdot (1, \sin \theta_g, 0, \cos \theta_g) \\ &= k_\perp [\cosh \eta_k - \cos \phi_k \sin \theta_g - \sinh \eta_k \cos \theta_g]. \end{aligned} \quad (4.62)$$

Therefore

$$\Theta(k^+ - k \cdot n_g) = \Theta\left(\cos \phi_k \cot \frac{\theta_g}{2} - \sinh \eta_k\right) \quad (4.63)$$

and

$$\Theta(k \cdot n_g - k^+) = \Theta\left(\sinh \eta_k - \cos \phi_k \cot \frac{\theta_g}{2}\right). \quad (4.64)$$

The full measurement function becomes

$$\begin{aligned} \delta_{\rho_s} &= \Theta\left(\sinh \eta_k - \cos \phi_k \cot \frac{\theta_g}{2}\right) \delta\left(\rho_s - \frac{4k_\perp e^{-\eta_k}}{Q}\right) \\ &\quad + \Theta\left(\cos \phi_k \cot \frac{\theta_g}{2} - \sinh \eta_k\right) \delta\left(\rho_s - \frac{4k_\perp}{Q} [\cosh \eta_k - \cos \phi_k \sin \theta_g - \sinh \eta_k \cos \theta_g]\right). \end{aligned} \quad (4.65)$$

We also need to transform the mMDT grooming terms. Notice that

$$\Theta(k^+ - k_0 n_g \cdot n_q) = \Theta(\cos \theta_g - \tanh \eta_k) \quad (4.66)$$

and

$$\Theta(k \cdot n_g - k_0 n_g \cdot n_q) = \Theta(\cot \theta_g - e^{\eta_k} \cos \phi_k). \quad (4.67)$$

Therefore,

$$\Theta_{\text{mMDT}} = 1 - \Theta(\cos \theta_g - \tanh \eta_k) \Theta(\cot \theta_g - e^{\eta_k} \cos \phi_k). \quad (4.68)$$

The last thing to transform is the phase space measure. We wish to convert

$$d^d k \delta(k^2) = dk_0 dk_z d^{d-2} \mathbf{k}_\perp \delta(k^2) \rightarrow dk_0 d\eta_k d^{d-2} \mathbf{k}_\perp \delta(k^2), \quad (4.69)$$

where \mathbf{k}_\perp represents the off-axis components of k in $d-2$ dimensions. The first part of the transformation is straightforward, as it simply corresponds to evaluating the Jacobian of the transformation $(k_0, k_z) \rightarrow (k_0, \eta_k)$:

$$dk_0 dk_z = k_\perp \cosh \eta_k dk_0 d\eta_k. \quad (4.70)$$

But how do we transform the term $d^{d-2} \mathbf{k}_\perp$? As we did in the fixed-order calculation, we will siphon the fractional dimensions into an angular term. With $d = 4 - 2\epsilon$, we can write $d^{d-2} \mathbf{k}_\perp$ in spherical coordinates as

$$d^{d-2} \mathbf{k}_\perp = k_\perp^{d-3} dk_\perp \sin^{-2\epsilon} \phi_k d\phi_k d\Omega_{d-3} \quad (4.71)$$

with Ω_{d-3} the solid angle of the $(d-3)$ -dimensional unit sphere. Integrating over the solid angle yields [3]

$$\int d\Omega_{d-3} = \frac{2\pi^{(d-3)/2}}{\Gamma(\frac{d-3}{2})} = \frac{2\pi^{1/2-\epsilon}}{\Gamma(\frac{1}{2}-\epsilon)}. \quad (4.72)$$

Thus, we find that

$$d^{d-2}\mathbf{k}_\perp = dk_\perp d\phi_k k_\perp^{d-3} \sin^{-2\epsilon} \phi_k \frac{2\pi^{1/2-\epsilon}}{\Gamma(\frac{1}{2}-\epsilon)}. \quad (4.73)$$

Also notice that

$$\delta(k^2) = \delta(k_0^2 - k_\perp^2 - k_z^2) = \delta(k_0^2 - k_\perp^2 \cosh^2 \eta_k). \quad (4.74)$$

This simplifies to

$$\delta(k_0^2 - k_\perp^2 \cosh^2 \eta_k) = \frac{1}{k_\perp \cosh \eta_k} \delta(k_0 - k_\perp \cosh \eta_k), \quad (4.75)$$

so we can integrate out k_0 :

$$\int dk_0 \delta(k^2) = \frac{1}{k_\perp \cosh \eta_k}. \quad (4.76)$$

All together the phase space measure is

$$\int \frac{d^d k}{(2\pi)^{d-1}} \delta(k^2) = \frac{(4\pi)^\epsilon}{4\pi^{5/2} \Gamma(\frac{1}{2}-\epsilon)} \int dk_\perp d\phi_k d\eta_k k_\perp^{1-2\epsilon} \sin^{-2\epsilon} \phi_k. \quad (4.77)$$

Under the modified minimal subtraction scheme, we will take $(4\pi)^\epsilon \rightarrow 1$ (and we will also set the Euler-Mascheroni constant $\gamma_E \rightarrow 0$ when it comes up).

Combining Eqs. 4.54, 4.60, 4.61, 4.65, and 4.77 then yields the full integral

$$S_R(\rho_s) = \frac{\pi \alpha_s C_F \mu^{2\epsilon}}{\pi^{5/2} \Gamma(\frac{1}{2}-\epsilon)} \int dk_\perp d\phi_k d\eta_k k_\perp^{1-2\epsilon} \sin^{-2\epsilon} \phi_k \Theta(k_\perp) \Theta(\eta_k) \frac{2}{k_\perp^2}$$

$$\times \left[\Theta\left(\sinh \eta_k - \cos \phi_k \cot \frac{\theta_g}{2}\right) \delta\left(\rho_s - \frac{4k_\perp e^{-\eta_k}}{Q}\right) \right.$$

$$+ \Theta\left(\cos \phi_k \cot \frac{\theta_g}{2} - \sinh \eta_k\right)$$

$$\times \delta\left(\rho_s - \frac{4k_\perp}{Q} [\cosh \eta_k - \cos \phi_k \sin \theta_g - \sinh \eta_k \cos \theta_g]\right) \Big]$$

$$\times [1 - \Theta(\cos \theta_g - \tanh \eta_k) \Theta(\cot \theta_g - e^{\eta_k} \cos \phi_k)]. \quad (4.78)$$

4.2.3 Computation, transformation, and Laurent series

The actual computation of the integral in Eq. 4.78 is fairly involved,⁷ and is therefore relegated to Appendix A. The result, from Eq. A.23, is

$$\begin{aligned}
S_R(\rho_s) = & \frac{2\pi\alpha_s C_F \mu^{2\epsilon}}{\pi^{5/2} \Gamma(\frac{1}{2} - \epsilon)} \left(\frac{Q}{4}\right)^{-2\epsilon} \frac{1}{\rho_s^{1+2\epsilon}} \\
& \times \left[\frac{1}{2\epsilon} \frac{\sqrt{\pi} \Gamma(\frac{1}{2} - \epsilon)}{\Gamma(1 - \epsilon)} - [\pi - \text{arcsec}(1 + \sec \theta_g)] \log \cot \frac{\theta_g}{2} \right. \\
& \quad - \text{arcsec}(1 + \sec \theta_g) \log(2 \cot \theta_g) \\
& \quad - \frac{i}{4} [\text{Li}_2(-e^{-2i \text{arcsec}(1 + \sec \theta_g)}) - \text{Li}_2(-e^{2i \text{arcsec}(1 + \sec \theta_g)})] \\
& \quad + \Theta\left(\theta_g - \frac{\pi}{4}\right) \left[\arccos \cot \theta_g \log(2 \cot \theta_g) \right. \\
& \quad \left. \left. + \frac{i}{4} [\text{Li}_2(-e^{-2i \arccos \cot \theta_g}) - \text{Li}_2(-e^{2i \arccos \cot \theta_g})] \right] \right] + \mathcal{O}(\epsilon^0),
\end{aligned} \tag{4.79}$$

where $\text{Li}_2(z)$ is the dilogarithm function defined in Appendix B. A Laplace transform taking $\rho_s \rightarrow \nu$ has the effect of setting

$$\mathcal{L}\left\{\frac{1}{\rho_s^{1+2\epsilon}}\right\} = \int_0^\infty \frac{d\rho_s}{\rho_s^{1+2\epsilon}} e^{-\rho_s \nu} = \nu^{2\epsilon} \Gamma(-2\epsilon). \tag{4.80}$$

We can then expand the prefactor in ϵ to find

$$\frac{2\pi\alpha_s C_F \mu^{2\epsilon}}{\pi^{5/2} \Gamma(\frac{1}{2} - \epsilon)} \left(\frac{Q}{4}\right)^{-2\epsilon} \nu^{2\epsilon} \Gamma(-2\epsilon) = \frac{\alpha_s C_F}{\pi^2} \left[-\frac{1}{\epsilon} - 2 \log\left(\frac{2\mu\nu}{Q}\right) - 2\epsilon \log^2\left(\frac{2\mu\nu}{Q}\right) \right] + \mathcal{O}(\epsilon). \tag{4.81}$$

We have set the Euler-Mascheroni constant $\gamma_E \rightarrow 0$ when expanding the gamma functions. We have also dropped some order- ϵ terms which are not logarithmically enhanced, as these do not contribute meaningfully to the anomalous dimension. We can also expand the first term in square brackets as

$$\frac{1}{2\epsilon} \frac{\sqrt{\pi} \Gamma(\frac{1}{2} - \epsilon)}{\Gamma(1 - \epsilon)} = \frac{\pi}{2\epsilon} + \pi \log 2 + \mathcal{O}(\epsilon). \tag{4.82}$$

⁷And much too complicated for Mathematica, in case you were wondering

Thus, if we let

$$\begin{aligned}
f(\theta_g) = & \pi \log 2 - [\pi - \text{arcsec}(1 + \sec \theta_g)] \log \cot \frac{\theta_g}{2} \\
& - \text{arcsec}(1 + \sec \theta_g) \log(2 \cot \theta_g) \\
& - \frac{i}{4} [\text{Li}_2(-e^{-2i \text{arcsec}(1 + \sec \theta_g)}) - \text{Li}_2(-e^{2i \text{arcsec}(1 + \sec \theta_g)})] \\
& + \Theta\left(\theta_g - \frac{\pi}{4}\right) \left[\arccos \cot \theta_g \log(2 \cot \theta_g) \right. \\
& \left. + \frac{i}{4} [\text{Li}_2(-e^{-2i \arccos \cot \theta_g}) - \text{Li}_2(-e^{2i \arccos \cot \theta_g})] \right], \tag{4.83}
\end{aligned}$$

we have

$$S_R(\nu) = \frac{\alpha_s C_F}{\pi^2} \left[-\frac{1}{\epsilon} - 2 \log \left(\frac{2\mu\nu}{Q} \right) - 2\epsilon \log^2 \left(\frac{2\mu\nu}{Q} \right) \right] \left[\frac{\pi}{2\epsilon} + f(\theta_g) \right] + \mathcal{O}(\epsilon^0). \tag{4.84}$$

Expanding this out yields the result:

$$\begin{aligned}
S_R(\nu) = & -\frac{\alpha_s C_F}{\pi^2} \left[\frac{\pi}{2\epsilon^2} + \frac{f(\theta_g)}{\epsilon} + \frac{\pi}{\epsilon} \log \left(\frac{2\mu\nu}{Q} \right) + 2f(\theta_g) \log \left(\frac{2\mu\nu}{Q} \right) \right. \\
& \left. + \pi \log^2 \left(\frac{2\mu\nu}{Q} \right) \right] + \mathcal{O}(\epsilon^0).
\end{aligned} \tag{4.85}$$

4.2.4 Anomalous dimension

Recall from Eqs. 4.10, 4.11, and 4.13 that the anomalous dimension takes the form

$$\gamma = \Gamma_F(\alpha_s) \log \frac{\mu^2}{\mu_1^2} + \gamma_F(\alpha_s), \tag{4.86}$$

where

$$\Gamma_F(\alpha_s) = d_F \Gamma_{\text{cusp}}(\alpha_s) \sum_{n=0}^{\infty} \Gamma_n \left(\frac{\alpha_s}{4\pi} \right)^{n+1} \tag{4.87}$$

for some constant d_F and

$$\gamma_F(\alpha_s) = \sum_{n=0}^{\infty} \gamma_n \left(\frac{\alpha_s}{4\pi} \right)^{n+1}. \tag{4.88}$$

We would like to determine the values of d_F and γ_0 (since Γ_0 and Γ_1 are universal and known). The anomalous dimension ends up being the coefficient of $2/\epsilon$, so we can simply read it off: the coefficient of $2/\epsilon$ in Eq. 4.85 is

$$\gamma = -\frac{\alpha_s C_F}{4\pi} \left[\frac{8}{\pi} f(\theta_g) + 4 \log \left(\frac{4\mu^2\nu^2}{Q^2} \right) \right]. \tag{4.89}$$

Thus, we see immediately that

$$\boxed{\gamma_0 = -\frac{8C_F}{\pi} f(\theta_g)} \quad (4.90)$$

and that

$$\boxed{\mu_1 = \frac{Q}{2\nu}.} \quad (4.91)$$

Since, from Eq. 4.12, $\Gamma_0 = 4$, we then have

$$\gamma = \frac{\alpha_s}{4\pi} \left[\gamma_0 - \Gamma_0 C_F \log \frac{\mu^2}{\mu_1^2} \right]. \quad (4.92)$$

Thus, the coefficient on the cusp anomalous dimension is

$$\boxed{d_F = -C_F.} \quad (4.93)$$

Notice that the $\mathcal{O}(\alpha_s)$ calculation of the soft function resulted in the $\mathcal{O}(\alpha_s)$ value of the anomalous dimension. To obtain a more accurate result, we would need to compute the soft function to higher orders in α_s .

Let us now check our work by verifying that, at this fixed order,

$$\frac{\partial S_R}{\partial \log \mu} = \gamma \quad (4.94)$$

if we ignore the pole at $\epsilon = 0$ and then set $\epsilon = 0$.⁸ From Eq. 4.85, we see that, dropping the pole,

$$S_R^{\epsilon=0}(\nu) = -\frac{\alpha_s C_F}{\pi^2} \left[2f(\theta_g) \log \left(\frac{2\mu\nu}{Q} \right) + \pi \log^2 \left(\frac{2\mu\nu}{Q} \right) \right]. \quad (4.95)$$

Then the derivative is, after some light simplification,

$$\frac{\partial S_R^{\epsilon=0}}{\partial \log \mu} = -\frac{\alpha_s C_F}{4\pi} \left[\frac{8}{\pi} f(\theta_g) + 4 \log \left(\frac{4\mu^2\nu^2}{Q^2} \right) \right] = \gamma, \quad (4.96)$$

as desired.

4.2.5 Resumming the soft function

Now, with the anomalous dimension in hand, we can resum the soft function to NLL accuracy using the results of Sec. 4.1.3. For some arbitrary μ_0 and

$$r = \frac{\alpha_s(\mu)}{\alpha_s(\mu_0)}, \quad (4.97)$$

⁸This is acceptable because the pole must eventually cancel in the full resummed result

the exponentiated kernel of Eq. 4.31 becomes

$$\begin{aligned} K(\mu, \mu_0) = & -\frac{C_F \Gamma_0}{2\beta_0^2} \left[\frac{4\pi}{\alpha_s(\mu_0)} \left(\log r + \frac{1}{r} - 1 \right) + \log r \left(\frac{\beta_1}{\beta_0} - \frac{\Gamma_1}{\Gamma_0} \right) + \frac{\beta_1}{2\beta_0} \log^2 r \right] \\ & + \frac{4C_F f(\theta_g)}{\pi\beta_0} \log r + \mathcal{O}(\alpha_s). \end{aligned} \quad (4.98)$$

The other exponentiated term, from Eq. 4.32, is

$$\omega(\mu, \mu_0) = -\frac{C_F \Gamma_0}{2\beta_0} \left[\log \frac{1}{r} + \frac{\alpha_s(\mu_0)}{4\pi} (r-1) \left(\frac{\beta_1}{\beta_0} - \frac{\Gamma_1}{\Gamma_0} \right) \right] + \mathcal{O}(\alpha_s^2). \quad (4.99)$$

Then, from Eq. 4.33, the resummed soft function is

$S_R(\nu, \mu) = S_R(\nu, \mu_0) e^{K(\mu, \mu_0)} \left[\frac{4\nu^2 \mu_0^2}{Q^2} \right]^{\omega(\mu, \mu_0)}.$

(4.100)

From this, it is evident that the natural scale of the soft function is

$$\mu_0 = \frac{Q}{2\nu}. \quad (4.101)$$

To evaluate $S_R(\nu, \mu_0)$, we simply ignore the pole of Eq. 4.85, set $\epsilon = 0$, and set $\mu = \mu_0$:

$$S_R(\nu, \mu_0) = -\frac{\alpha_s C_F}{\pi^2} \left[2f(\theta_g) \log \left(\frac{2\mu_0 \nu}{Q} \right) + \pi \log^2 \left(\frac{2\mu_0 \nu}{Q} \right) \right]. \quad (4.102)$$

Notice that setting $\mu_0 = Q/2\nu$ would eliminate the large logarithms from $S_R(\nu, \mu_0)$ ⁹

Finally, we should convert the soft function back to real space. This is done using the tricks of Sec. 4.1.4. The logarithm-derivative transformation is

$$S_R(L \rightarrow \partial_\omega) = -\frac{\alpha_s C_F}{\pi^2} [2f(\theta_g) \partial_\omega + \pi \partial_\omega^2], \quad (4.103)$$

so from Eq. 4.41 we have

$S_R(\rho_s, \mu) = -\frac{\alpha_s C_F}{\pi^2} e^{K(\mu, \mu_0)} [2f(\theta_g) \partial_\omega + \pi \partial_\omega^2] \left[\frac{4\mu_0^2}{\rho_s^2 Q^2} \right]^{\omega(\mu, \mu_0)} \frac{1}{\rho_s \Gamma(-2\omega(\mu, \mu_0))}.$

(4.104)

This is our NLL resummed result for the soft function. It is plotted in Fig. 4.1, where we have evaluated μ_0 at the natural scale $\mu_0 = Q\rho_s/2$ and taken $\mu = Q = 91.2 \text{ GeV}$, the mass of the Z boson, and $\theta_g = \pi/3$.¹⁰

⁹You might be concerned that it would also set $S_R(\nu, Q/2\nu) = 0$. However, it would also be incorrect to assign the value of μ_0 before performing the inverse Laplace transform, so the point is irrelevant.

¹⁰The particular choice of the Z mass is made because the strong coupling constant α_s has been measured to high precision at this energy scale.

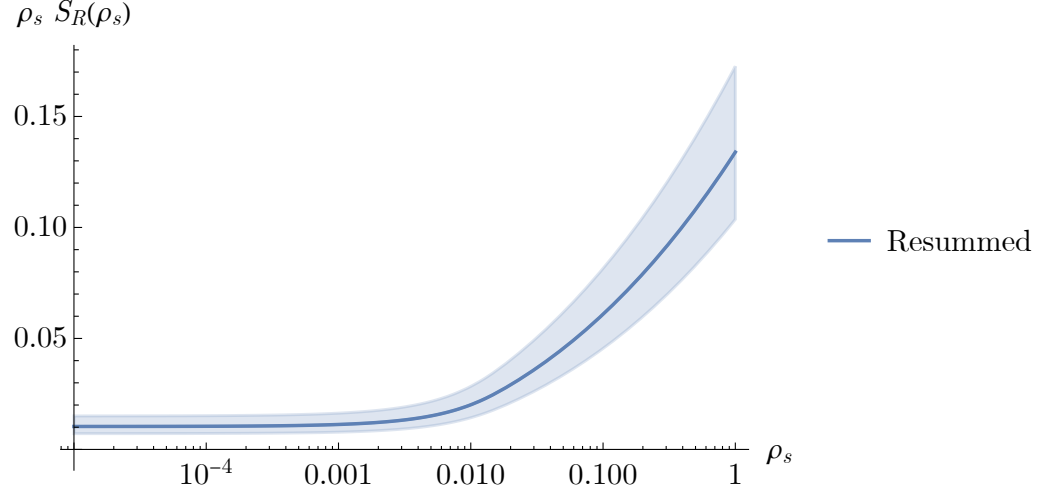


Figure 4.1: NLL resummed distribution of the soft function $S_R(\rho_s)$, from Eq. 4.104. The top figure is the full range of ρ_s , while the bottom is zoomed in for small values of ρ_s . The running of α_s is fixed at the Z boson mass, $\alpha_s(91.2\text{ GeV}) = 0.118$, from [4]. The running is fixed below 1 GeV in order to avoid the Landau pole at 246 MeV [2]. Uncertainty is estimated by varying μ within $\mu = \xi Q$ for $\xi \in [1/2, 2]$.

On its own, the soft function S_R does not have any physical meaning — this much is clear from the manifest dependence on the arbitrary energy scale μ . Physical meaning comes only in the context of the full cross section of Eq. 4.42, where we would expect to find (and, in fact, we would require) that all μ -dependence cancel.¹¹ Unfortunately, this means that until the entire distribution has been calculated, there is little we can do to satisfactorily convince ourselves that Eq. 4.41 is correct. The fact that Fig. 4.1 looks reasonable (i.e., it is smooth and continuous, and the uncertainty is not massive) is, however, a good start.

¹¹This cancellation is a strong cross-check to determine whether we have performed the calculation correctly.

Conclusion

The next steps in completing an NLL calculation of the groomed heavy hemisphere mass distribution would be to perform a similar calculation for the resolved emission function $R(\rho_1, \rho_2, z_{\text{cut}})$ to determine its anomalous dimension, then pull the anomalous dimensions for all the rest of the functions in the factorization theorem of Eq. 4.3. With the anomalous dimensions in hand, we would then be able to complete the explicit calculation of Eq. 4.42 to obtain an NLL prediction for the groomed hemisphere mass. Then we could integrate to find the heavy hemisphere mass:

$$\frac{d\rho}{d\sigma} = \int \frac{d^2\sigma}{d\rho_1 d\rho_2} [\delta(\rho - \rho_1)\Theta(\rho_1 - \rho_2) + \delta(\rho - \rho_2)\Theta(\rho_2 - \rho_1)]. \quad (4.105)$$

Unfortunately, these steps are, to varying degrees, somewhat involved and fairly repetitive, and would take us beyond the pedagogical scope of this thesis. Thus, instead of marching forward, let us recap where we have been — for it was quite an adventure.

Our object of study has been the distribution of the mMDT-groomed heavy hemisphere mass in $e^+e^- \rightarrow \text{hemisphere jets}$ events, in the limit that the heavy hemisphere mass ρ is approximately equal to the mMDT cutoff z_{cut} : $\rho \sim z_{\text{cut}} \ll 1$. As with many calculations in QCD, this distribution must be calculated as a series in the strong coupling α_s . We began our journey in Chapter 2 by studying the leading-order term which contributes to the distribution. This allowed us to practice some important calculational techniques — especially dimensional regularization — and taught us something both about the mathematical structure of the calculation and the physical quantity of interest. We saw the power of the strategy of regions approach, in which the singular limits of the groomed jet mass could be combined to produce the complete distribution in the soft limit of interest. We also saw that the leading-order distribution exhibited a sharp, unphysical cusp, which gave us a clue that there is interesting physics to be studied in this limit.

Nevertheless, fixed-order calculations can only take us so far in the context of our calculation. Not only is it extremely challenging to move beyond the first few terms orders in the strong coupling α_s with fixed-order calculations, but for an exclusive cross section such as $\sigma(e^+e^- \rightarrow \text{hemisphere jets})$, logarithms of energy scales emerge which can become quite large in, say, the $\rho \sim z_{\text{cut}} \ll 1$ limit [2]. We therefore resolved to develop an all-orders calculation which would, through the process of resummation, carefully account for these large logarithms. The result would be a framework without large logarithms, from which one could compute the distribution to arbitrary precision, given inputs with sufficiently high order in α_s .

In Chapter 3, we took our first steps towards this result by developing a factorization formula which broke the full cross section into a convolution of terms, each of which depends only on a single energy scale. To do this, we applied the technology of Soft-Collinear Effective Theory (SCET) after examining the dominant energy scales in each of the singular regions of phase space.¹² The result was the factorization formula Eq. 3.25. The dependence of each term on only a single energy scale meant that each term could be resummed separately, allowing us to achieve resummation of the full cross section.

Finally, we actually performed this resummation in Chapter 4. We began by deriving the sought-after all-orders result in Eq. 4.42. This result can be used to achieve arbitrary accuracy — the inputs are the anomalous dimensions of each function in the factorized cross section, as well as their value at a fixed energy scale for a fixed order in α_s . A given calculation, however, can only be achieved to some fixed accuracy, only here, accuracy increases logarithmically with the order of α_s , in some sense. In order to understand the type of calculation that could go into such a result, we computed one term of the factorized cross section, the soft function $S_R(\rho)$, to next-to-leading-logarithmic (NLL) accuracy.

As discussed above, the obvious next steps for this work would be to compute the remaining terms of the factorization formula to NLL accuracy in order to achieve a full NLL cross section in the $\rho \sim z_{\text{cut}} \ll 1$ limit. One could then match the predictions to extant results at high logarithmic precision in the $\rho \ll z_{\text{cut}} \ll 1$ limit [18, 16, 17], and at high fixed-order precision [19], which should be accurate at high ρ . That would be a very interesting culmination of this work.

Beyond that, the factorized and resummed framework we developed for computing the cross section should, in principle, be useful for even higher-precision calculations. One might dream of eventual comparison between precision predictions of this distribution and experimental measurements, as was performed by ATLAS in Ref. [41].

Until then, I hope that the work of this thesis can provide a helpful example to future students interested in precision calculations in quantum chromodynamics. With luck, you have also developed an appreciation for the techniques that are used in such calculations.

¹²This extended the theme of developing a full result by considering contributions from particular singular regions.

Appendix A

Soft function integral

We would like to compute the soft function of Eq. 4.78,

$$\begin{aligned}
S_R(\rho_s) = & \frac{\pi\alpha_s C_F \mu^{2\epsilon}}{\pi^{5/2} \Gamma(\frac{1}{2} - \epsilon)} \int dk_\perp d\phi_k d\eta_k k_\perp^{1-2\epsilon} \sin^{-2\epsilon} \phi_k \Theta(k_\perp) \Theta(\eta_k) \frac{2}{k_\perp^2} \\
& \times \left[\Theta\left(\sinh \eta_k - \cos \phi_k \cot \frac{\theta_g}{2}\right) \delta\left(\rho_s - \frac{4k_\perp e^{-\eta_k}}{Q}\right) \right. \\
& + \Theta\left(\cos \phi_k \cot \frac{\theta_g}{2} - \sinh \eta_k\right) \\
& \left. \times \delta\left(\rho_s - \frac{4k_\perp}{Q} [\cosh \eta_k - \cos \phi_k \sin \theta_g - \sinh \eta_k \cos \theta_g]\right) \right] \\
& \times [1 - \Theta(\cos \theta_g - \tanh \eta_k) \Theta(\cot \theta_g - e^{\eta_k} \cos \phi_k)],
\end{aligned} \tag{A.1}$$

to a point where we can extract the anomalous dimension. The first step is to integrate out k_\perp , which can be done easily enough using the Dirac delta functions. The first transforms as

$$\delta\left(\rho_s - \frac{4k_\perp e^{-\eta_k}}{Q}\right) = \frac{Q e^{\eta_k}}{4} \delta\left(k_\perp - \frac{Q \rho_s e^{\eta_k}}{4}\right), \tag{A.2}$$

while the second transforms as

$$\begin{aligned}
& \delta\left(\rho_s - \frac{4k_\perp}{Q} [\cosh \eta_k - \cos \phi_k \sin \theta_g - \sinh \eta_k \cos \theta_g]\right) \\
& = \frac{Q}{4(\cosh \eta_k - \cos \phi_k \sin \theta_g - \sinh \eta_k \cos \theta_g)} \\
& \quad \times \delta\left(k_\perp - \frac{Q \rho_s}{4[\cosh \eta_k - \cos \phi_k \sin \theta_g - \sinh \eta_k \cos \theta_g]}\right).
\end{aligned} \tag{A.3}$$

Therefore, integrating out k_\perp from Eq. A.1, we are left with

$$\begin{aligned}
S_R(\rho_s) = & \frac{2\pi\alpha_s C_F \mu^{2\epsilon}}{\pi^{5/2} \Gamma(\frac{1}{2} - \epsilon)} \left(\frac{Q}{4}\right)^{-2\epsilon} \frac{1}{\rho_s^{1+2\epsilon}} \int d\phi_k d\eta_k \sin^{-2\epsilon} \phi_k \Theta(\eta_k) \\
& \times \left[\Theta\left(\sinh \eta_k - \cos \phi_k \cot \frac{\theta_g}{2}\right) e^{-2\epsilon \eta_k} \right. \\
& + \Theta\left(\cos \phi_k \cot \frac{\theta_g}{2} - \sinh \eta_k\right) \\
& \times \left(\frac{1}{\cosh \eta_k - \cos \phi_k \sin \theta_g - \sinh \eta_k \cos \theta_g} \right)^{-2\epsilon} \Big] \\
& \times [1 - \Theta(\cos \theta_g - \tanh \eta_k) \Theta(\cot \theta_g - e^{\eta_k} \cos \phi_k)].
\end{aligned} \tag{A.4}$$

Now, in order to extract the anomalous dimension, we need to determine, in Laplace space, the coefficient of the $2/\epsilon$ term of the Laurent expansion of S_R in ϵ . Under a Laplace transformation taking $\rho_s \rightarrow \nu$, we have

$$\mathcal{L}\left\{\frac{1}{\rho_s^{1+2\epsilon}}\right\} = \nu^{2\epsilon} \Gamma(-2\epsilon) = -\frac{1}{2\epsilon} - \log \nu - \left(\frac{\pi^2}{6} + \log^2 \nu\right)\epsilon + \mathcal{O}(\epsilon^2). \tag{A.5}$$

This means that, in order to compute the anomalous dimension, we will need to keep terms through order $\mathcal{O}(\epsilon^0)$ in the integral.

To actually compute the integral, we will first make a sneaky simplification. Notice that, if we factor out $e^{-2\epsilon \eta_k}$,

$$\begin{aligned}
& \Theta\left(\sinh \eta_k - \cos \phi_k \cot \frac{\theta_g}{2}\right) e^{-2\epsilon \eta_k} \\
& + \Theta\left(\cos \phi_k \cot \frac{\theta_g}{2} - \sinh \eta_k\right) \left(\frac{1}{\cosh \eta_k - \cos \phi_k \sin \theta_g - \sinh \eta_k \cos \theta_g} \right)^{-2\epsilon} \\
= & e^{-2\epsilon \eta_k} \left[\Theta\left(\sinh \eta_k - \cos \phi_k \cot \frac{\theta_g}{2}\right) \right. \\
& \left. + \Theta\left(\cos \phi_k \cot \frac{\theta_g}{2} - \sinh \eta_k\right) \left(\frac{e^{-\eta_k}}{\cosh \eta_k - \cos \phi_k \sin \theta_g - \sinh \eta_k \cos \theta_g} \right)^{-2\epsilon} \right].
\end{aligned} \tag{A.6}$$

This converges as we send $\epsilon_k \rightarrow \infty$, so we can expand the term in brackets to find

$$\begin{aligned}
& \Theta\left(\sinh \eta_k - \cos \phi_k \cot \frac{\theta_g}{2}\right) \\
& + \Theta\left(\cos \phi_k \cot \frac{\theta_g}{2} - \sinh \eta_k\right) \left(\frac{e^{-\eta_k}}{\cosh \eta_k - \cos \phi_k \sin \theta_g - \sinh \eta_k \cos \theta_g} \right)^{-2\epsilon} \\
= & 1 + \mathcal{O}(\epsilon).
\end{aligned} \tag{A.7}$$

We therefore find that

$$\begin{aligned} S_R(\rho_s) &= \frac{2\pi\alpha_s C_F \mu^{2\epsilon}}{\pi^{5/2} \Gamma(\frac{1}{2} - \epsilon)} \left(\frac{Q}{4}\right)^{-2\epsilon} \frac{1}{\rho_s^{1+2\epsilon}} \int d\phi_k d\eta_k \sin^{-2\epsilon} \phi_k \Theta(\eta_k) e^{-2\epsilon\eta_k} \\ &\quad \times [1 - \Theta(\cos \theta_g - \tanh \eta_k) \Theta(\cot \theta_g - e^{\eta_k} \cos \phi_k)] + \mathcal{O}(\epsilon^0). \end{aligned} \quad (\text{A.8})$$

For the first integral, we have (where ϕ_k ranges from 0 to π)

$$\int d\phi_k d\eta_k \sin^{-2\epsilon} \phi_k \Theta(\eta_k) e^{-2\epsilon\eta_k} = \frac{1}{2\epsilon} \frac{\sqrt{\pi} \Gamma(\frac{1}{2} - \epsilon)}{\Gamma(1 - \epsilon)}. \quad (\text{A.9})$$

The second integral is not divergent in η_k if we first set $\epsilon = 0$, so we can do that. Then we are left with

$$\begin{aligned} S_R(\rho_s) &= \frac{2\pi\alpha_s C_F \mu^{2\epsilon}}{\pi^{5/2} \Gamma(\frac{1}{2} - \epsilon)} \left(\frac{Q}{4}\right)^{-2\epsilon} \frac{1}{\rho_s^{1+2\epsilon}} \left[\frac{1}{2\epsilon} \frac{\sqrt{\pi} \Gamma(\frac{1}{2} - \epsilon)}{\Gamma(1 - \epsilon)} \right. \\ &\quad - \int d\phi_k d\eta_k \Theta(\eta_k) \Theta(\cos \theta_g - \tanh \eta_k) \\ &\quad \left. \times \Theta(\cot \theta_g - e^{\eta_k} \cos \phi_k) \right] + \mathcal{O}(\epsilon^0). \end{aligned} \quad (\text{A.10})$$

To evaluate the remaining integral, we need to establish our region of integration. We can simplify the bounds as

$$\begin{aligned} &\Theta(\cos \theta_g - \tanh \eta_k) \Theta(\cot \theta_g - e^{\eta_k} \cos \phi_k) \\ &= \Theta\left(\frac{1}{1 + \sec \theta_g} - \cos \phi_k\right) \Theta\left(\cot \frac{\theta_g}{2} - e^{\eta_k}\right) \\ &\quad + \left[\Theta\left(\cos \phi_k - \frac{1}{1 + \sec \theta_g}\right) \Theta(\cot \theta_g - \cos \phi_k) \right. \\ &\quad \left. \times \Theta(\cot \theta_g \sec \phi_k - e^{\eta_k}) \right]. \end{aligned} \quad (\text{A.11})$$

Now, because

$$\text{arcsec}(1 + \sec \theta_g) < \frac{\pi}{2} \quad (\text{A.12})$$

for $0 < \theta_g < \pi/2$, we can split the first term up for positive and negative values of $\cos \phi_k$:

$$\Theta\left(\frac{1}{1 + \sec \theta_g} - \cos \phi_k\right) = \Theta\left(\frac{\pi}{2} - \phi_k\right) \Theta(\sec \phi_k - 1 - \sec \theta_g) + \Theta\left(\phi_k - \frac{\pi}{2}\right). \quad (\text{A.13})$$

Then evaluating the first part of the integral yields

$$\begin{aligned} &\int d\phi_k d\eta_k \Theta(\eta_k) \left[\Theta\left(\frac{\pi}{2} - \phi_k\right) \Theta(\sec \phi_k - 1 - \sec \theta_g) + \Theta\left(\phi_k - \frac{\pi}{2}\right) \right] \Theta\left(\cot \frac{\theta_g}{2} - e^{\eta_k}\right) \\ &= [\pi - \text{arcsec}(1 + \sec \theta_g)] \log\left(\cot \frac{\theta_g}{2}\right). \end{aligned} \quad (\text{A.14})$$

The second part is a little more complicated. We can first integrate in η_k to find

$$\begin{aligned} \int d\phi_k d\eta_k \Theta(\eta_k) \Theta\left(\cos \phi_k - \frac{1}{1 + \sec \theta_g}\right) \Theta(\cot \theta_g - \cos \phi_k) \Theta(\cot \theta_g \sec \phi_k - e^{\eta_k}) \\ = \int d\phi_k \Theta\left(\cos \phi_k - \frac{1}{1 + \sec \theta_g}\right) \Theta(\cot \theta_g - \cos \phi_k) \log(\cot \theta_g \sec \phi_k). \end{aligned} \quad (\text{A.15})$$

To solve the remaining integral, first notice that

$$\cot \theta_g > 1 \implies \cot \theta_g > \cos \phi_k \quad (\text{A.16})$$

for $0 < \theta_g < \pi/4$. Therefore,

$$\Theta(\cot \theta_g - \cos \phi_k) = \Theta\left(\frac{\pi}{4} - \theta_g\right) + \Theta\left(\theta_g - \frac{\pi}{4}\right) \Theta(\cot \theta_g - \cos \phi_k). \quad (\text{A.17})$$

Now that we have established the bounds, we can evaluate the indefinite integral:

$$\int d\phi_k \log(\cot \theta_g \sec \phi_k) = \frac{i\phi_k^2}{2} + \phi_k \log(2 \cot \theta_g) - \frac{i}{2} \text{Li}_2(-e^{2i\phi_k}), \quad (\text{A.18})$$

where $\text{Li}_2(x)$ is the dilogarithm function. This function is explored in Appendix B. From Eq. B.8, we have

$$\frac{i}{2} \text{Li}_2(-e^{2i\phi_k}) = -\frac{i\pi^2}{24} + \frac{i\phi_k^2}{2} - \frac{i}{4} [\text{Li}_2(-e^{-2i\phi_k}) - \text{Li}_2(-e^{2i\phi_k})]. \quad (\text{A.19})$$

Then Eq. A.18 becomes

$$\int d\phi_k \log(\cot \theta_g \sec \phi_k) = \phi_k \log(2 \cot \theta_g) + \frac{i}{4} [\text{Li}_2(-e^{-2i\phi_k}) - \text{Li}_2(-e^{2i\phi_k})] + \frac{i\pi^2}{24}. \quad (\text{A.20})$$

The imaginary part of this integral is manifestly a constant, $i\pi^2/24$, and therefore drops out when we perform a definite integral. Now notice that

$$\arccos\left(\frac{1}{1 + \sec \theta_g}\right) = \text{arcsec}(1 + \sec \theta_g). \quad (\text{A.21})$$

Thus, we can combine Eqs. A.15, A.17, and A.20 to find

$$\begin{aligned} \int d\phi_k \Theta\left(\cos \phi_k - \frac{1}{1 + \sec \theta_g}\right) \Theta(\cot \theta_g - \cos \phi_k) \log(\cot \theta_g \sec \phi_k) \\ = \text{arcsec}(1 + \sec \theta_g) \log(2 \cot \theta_g) + \frac{i}{4} \left[\text{Li}_2(-e^{-2i \text{arcsec}(1 + \sec \theta_g)}) \right. \\ \left. - \text{Li}_2(-e^{2i \text{arcsec}(1 + \sec \theta_g)}) \right] \\ - \Theta\left(\theta_g - \frac{\pi}{4}\right) \left[\arccos \cot \theta_g \log(2 \cot \theta_g) \right. \\ \left. + \frac{i}{4} [\text{Li}_2(-e^{-2i \arccos \cot \theta_g}) - \text{Li}_2(-e^{2i \arccos \cot \theta_g})] \right]. \end{aligned} \quad (\text{A.22})$$

We can therefore conclude that the full soft function through order $\mathcal{O}(\epsilon^{-1})$ is

$$\begin{aligned}
S_R(\rho_s) = & \frac{2\pi\alpha_s C_F \mu^{2\epsilon}}{\pi^{5/2} \Gamma(\frac{1}{2} - \epsilon)} \left(\frac{Q}{4}\right)^{-2\epsilon} \frac{1}{\rho_s^{1+2\epsilon}} \\
& \times \left[\frac{1}{2\epsilon} \frac{\sqrt{\pi} \Gamma(\frac{1}{2} - \epsilon)}{\Gamma(1 - \epsilon)} - [\pi - \text{arcsec}(1 + \sec \theta_g)] \log \cot \frac{\theta_g}{2} \right. \\
& \quad - \text{arcsec}(1 + \sec \theta_g) \log(2 \cot \theta_g) \\
& \quad - \frac{i}{4} [\text{Li}_2(-e^{-2i \text{arcsec}(1 + \sec \theta_g)}) - \text{Li}_2(-e^{2i \text{arcsec}(1 + \sec \theta_g)})] \\
& \quad + \Theta\left(\theta_g - \frac{\pi}{4}\right) \left[\arccos \cot \theta_g \log(2 \cot \theta_g) \right. \\
& \quad \left. \left. + \frac{i}{4} [\text{Li}_2(-e^{-2i \arccos \cot \theta_g}) - \text{Li}_2(-e^{2i \arccos \cot \theta_g})] \right] \right] + \mathcal{O}(\epsilon^0).
\end{aligned} \tag{A.23}$$

This has been a long calculation, and it would be nice to confirm that we did it right. We can compare our analytic result to numeric results after first fixing the values of the constants. Let $Q = 91.2$ GeV (the mass of the Z boson), at which $\alpha_s = 0.118$ [4]. Then take $C_F = 4/3$, and arbitrarily take $\mu = 10$ GeV and $\rho_s = 0.1$. Finally, since our analytic result is only accurate through order $\mathcal{O}(\epsilon^{-1})$, we should take ϵ to be small so that higher-order corrections are small. Thus, let us take $\epsilon = 0.0001$. The result is displayed in Fig. A.1. There is good agreement between the numerical result and the analytic one, which helps us feel confident that we performed the integral correctly.

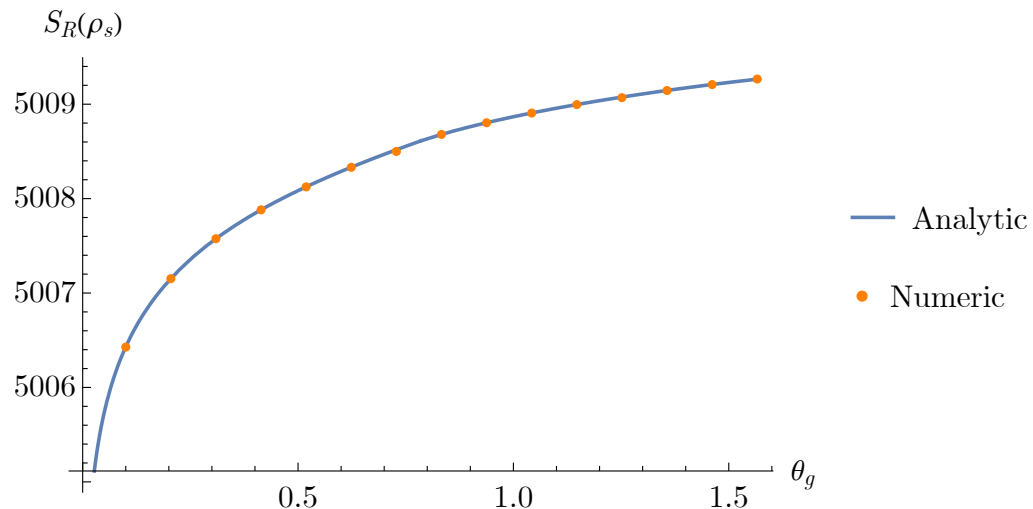


Figure A.1: Analytic (blue curve) and numeric (orange dots) results for the soft function $S_R(\rho_s)$. The analytic curve is from Eq. A.23, while the numeric result comes from evaluating Eq. A.4. Constants are fixed to values described in the text.

Appendix B

The dilogarithm function

The dilogarithm function is defined by the power series [42]

$$\text{Li}_2(z) = \sum_{k=1}^{\infty} \frac{z^k}{k^2}, \quad \text{for } |z| < 1. \quad (\text{B.1})$$

It is an identity of the dilogarithm that [43]

$$\text{Li}_2(z) + \text{Li}_2\left(\frac{1}{z}\right) = -\frac{\pi^2}{6} - \frac{1}{2} \log^2(-z). \quad (\text{B.2})$$

The dilogarithm of exponentials in which we are interested is

$$\text{Li}_2(-e^{2i\phi}) = \sum_{k=1}^{\infty} \frac{(-1)^k e^{2ik\phi}}{k^2} = \sum_{k=1}^{\infty} \frac{(-1)^k \cos(2k\phi)}{k^2} + i \sum_{k=1}^{\infty} \frac{(-1)^k \sin(2k\phi)}{k^2}. \quad (\text{B.3})$$

The real part can be re-written in terms of dilogarithms:

$$\begin{aligned} \sum_{k=1}^{\infty} \frac{(-1)^k \cos(2k\phi)}{k^2} &= \frac{1}{2} \left[\sum_{k=1}^{\infty} \frac{(-1)^k e^{-2ik\phi}}{k^2} + \sum_{k=1}^{\infty} \frac{(-1)^k e^{2ik\phi}}{k^2} \right] \\ &= \frac{1}{2} [\text{Li}_2(-e^{2i\phi}) + \text{Li}_2(-e^{-2i\phi})]. \end{aligned} \quad (\text{B.4})$$

By Eq. B.2, we see that

$$\text{Li}_2(-e^{2i\phi}) + \text{Li}_2(-e^{-2i\phi}) = -\frac{\pi^2}{6} - \frac{1}{2} \log^2(e^{2i\phi}) = -\frac{\pi^2}{6} - 2\phi^2. \quad (\text{B.5})$$

Therefore, the real part of Eq. B.3 is

$$\text{Re}[\text{Li}_2(-e^{2i\phi})] = -\frac{\pi^2}{12} + \phi^2. \quad (\text{B.6})$$

The imaginary part is

$$\begin{aligned} \sum_{k=1}^{\infty} \frac{(-1)^k \sin(2k\phi)}{k^2} &= \frac{i}{2} \left[\sum_{k=1}^{\infty} \frac{(-1)^k e^{-2ik\phi}}{k^2} - \sum_{k=1}^{\infty} \frac{(-1)^k e^{2ik\phi}}{k^2} \right] \\ &= \frac{i}{2} [\text{Li}_2(-e^{-2i\phi}) - \text{Li}_2(-e^{2i\phi})], \end{aligned} \quad (\text{B.7})$$

which is more difficult to simplify.¹ Therefore, we conclude that

$$\text{Li}_2(-e^{2i\phi}) = -\frac{\pi^2}{12} + \phi^2 - \frac{1}{2} [\text{Li}_2(-e^{-2i\phi}) - \text{Li}_2(-e^{2i\phi})]. \quad (\text{B.8})$$

The portion in square brackets is purely imaginary.

¹To the best of my knowledge, no straightforward identity exists.

References

- [1] M. Cush, *Standard Model of Elementary Particles*, Sept., 2019, https://commons.wikimedia.org/wiki/File:Standard_Model_of_Elementary_Particles.svg.
- [2] A.J. Larkoski, *Elementary Particle Physics: An Intuitive Introduction*, Cambridge University Press, Cambridge, United Kingdom; New York, NY (2019).
- [3] M.D. Schwartz, *Quantum Field Theory and the Standard Model*, Cambridge University Press, New York (2014).
- [4] Particle Data Group, *Review of Particle Physics, Progress of Theoretical and Experimental Physics* **2020** (2020) .
- [5] Super-Kamiokande Collaboration, *Evidence for oscillation of atmospheric neutrinos*, *Phys. Rev. Lett.* **81** (1998) 1562.
- [6] J.J. Aubert, U. Becker, P.J. Biggs, J. Burger, M. Chen, G. Everhart et al., *Experimental observation of a heavy particle J*, *Phys. Rev. Lett.* **33** (1974) 1404.
- [7] J.E. Augustin, A.M. Boyarski, M. Breidenbach, F. Bulos, J.T. Dakin, G.J. Feldman et al., *Discovery of a narrow resonance in e^+e^- annihilation*, *Phys. Rev. Lett.* **33** (1974) 1406.
- [8] D0 Collaboration, *Observation of the top quark*, *Phys. Rev. Lett.* **74** (1995) 2632 [[hep-ex/9503003](#)].
- [9] CDF Collaboration, *Observation of top quark production in $\bar{p}p$ collisions*, *Phys. Rev. Lett.* **74** (1995) 2626 [[hep-ex/9503002](#)].
- [10] ATLAS Collaboration, *Observation of a new particle in the search for the Standard Model Higgs boson with the ATLAS detector at the LHC*, *Phys. Lett. B* **716** (2012) 1.
- [11] C. Collaboration, *Observation of a new boson at a mass of 125 GeV with the CMS experiment at the LHC*, *Physics Letters B* **716** (2012) 30 [[1207.7235](#)].
- [12] CERN AC, *Layout of ATLAS. Dessin representant le detecteur ATLAS*, Mar., 1998, <https://cds.cern.ch/record/39038>.

- [13] T. Sakuma and T. McCauley, *Detector and Event Visualization with SketchUp at the CMS Experiment*, *J. Phys.: Conf. Ser.* **513** (2014) 022032.
- [14] ATLAS Outreach, *ATLAS Fact Sheet: To raise awareness of the ATLAS detector and collaboration on the LHC*, 2012,
<http://cds.cern.ch/record/1457044>.
- [15] M. Dasgupta, A. Fregoso, S. Marzani and G.P. Salam, *Towards an understanding of jet substructure*, *J. High Energ. Phys.* **2013** (2013) 29.
- [16] A. Kardos, A.J. Larkoski and Z. Trócsányi, *Groomed jet mass at high precision*, *Physics Letters B* **809** (2020) 135704.
- [17] A. Kardos, A.J. Larkoski and Z. Trócsányi, *Two- and three-loop data for the groomed jet mass*, *Phys. Rev. D* **101** (2020) 114034.
- [18] C. Frye, A.J. Larkoski, M.D. Schwartz and K. Yan, *Factorization for groomed jet substructure beyond the next-to-leading logarithm*, *J. High Energ. Phys.* **2016** (2016) 64.
- [19] A. Kardos, G. Somogyi and Z. Trócsányi, *Soft-drop event shapes in electron-positron annihilation at next-to-next-to-leading order accuracy*, *Physics Letters B* **786** (2018) 313 [[1807.11472](https://arxiv.org/abs/1807.11472)].
- [20] T. Becher, A. Broggio and A. Ferroglia, *Introduction to Soft-Collinear Effective Theory*, vol. 896 of *Lecture Notes in Physics*, Springer International Publishing, Cham (2015), 10.1007/978-3-319-14848-9.
- [21] ATLAS Collaboration, “Event Displays from Run 2 physics analyses.” <https://twiki.cern.ch/twiki/bin/view/AtlasPublic/EventDisplayRun2Physics>.
- [22] M.G. Holloway and C.P. Baker, *How the barn was born*, *Physics Today* **25** (1972) 9.
- [23] ATLAS Collaboration, “Event displays from collision data.” <https://twiki.cern.ch/twiki/bin/view/AtlasPublic/EventDisplayRun2Collisions>.
- [24] Y.L. Dokshitzer, G.D. Leder, S. Moretti and B.R. Webber, *Better jet clustering algorithms*, *J. High Energy Phys.* **1997** (1997) 001.
- [25] M. Wobisch and T. Wengler, *Hadronization corrections to jet cross-sections in deep inelastic scattering*, in *Workshop on Monte Carlo Generators for HERA Physics (Plenary Starting Meeting)*, (Hamburg, Germany), pp. 270–279 (1998), <https://arxiv.org/abs/hep-ph/9907280>.
- [26] A.J. Larkoski, *Improving the Understanding of Jet Grooming in Perturbation Theory*, *arXiv:2006.14680 [hep-ex, physics:hep-ph]* (2020) [[2006.14680](https://arxiv.org/abs/2006.14680)].

- [27] C.W. Bauer, S. Fleming and M. Luke, *Summing Sudakov logarithms in $B \rightarrow X_s + \gamma$ in effective field theory*, *Phys. Rev. D* **63** (2000) 014006 [[hep-ph/0005275](#)].
- [28] C.W. Bauer, S. Fleming, D. Pirjol and I.W. Stewart, *An effective field theory for collinear and soft gluons: Heavy to light decays*, *Phys. Rev. D* **63** (2001) 114020.
- [29] C.W. Bauer and I.W. Stewart, *Invariant operators in collinear effective theory*, *Physics Letters B* **516** (2001) 134.
- [30] C.W. Bauer, D. Pirjol and I.W. Stewart, *Soft-collinear factorization in effective field theory*, *Phys. Rev. D* **65** (2002) 054022.
- [31] M. Beneke, A.P. Chapovsky, M. Diehl and T. Feldmann, *Soft-collinear effective theory and heavy-to-light currents beyond leading power*, *Nuclear Physics B* **643** (2002) 431 [[hep-ph/0206152](#)].
- [32] M. Beneke and T. Feldmann, *Multipole-expanded soft-collinear effective theory with non-abelian gauge symmetry*, *Physics Letters B* **553** (2003) 267 [[hep-ph/0211358](#)].
- [33] R.J. Hill and M. Neubert, *Spectator Interactions in Soft-Collinear Effective Theory*, *Nuclear Physics B* **657** (2003) 229 [[hep-ph/0211018](#)].
- [34] S.D. Ellis, C.K. Vermilion, J.R. Walsh, A. Hornig and C. Lee, *Jet shapes and jet algorithms in SCET*, *J. High Energ. Phys.* **2010** (2010) 101.
- [35] G. 't Hooft and M. Veltman, *Regularization and renormalization of gauge fields*, *Nuclear Physics B* **44** (1972) 189.
- [36] S. Catani and M. Grazzini, *Infrared factorization of tree-level QCD amplitudes at the next-to-next-to-leading order and beyond*, *Nuclear Physics B* **570** (2000) 287 [[hep-ph/9908523](#)].
- [37] R.K. Ellis, W.J. Stirling and B.R. Webber, *QCD and Collider Physics*, Cambridge Monographs on Particle Physics, Nuclear Physics and Cosmology, Cambridge University Press, Cambridge (1996), 10.1017/CBO9780511628788.
- [38] Y.-T. Chien and M.D. Schwartz, *Resummation of heavy jet mass and comparison to LEP data*, *J. High Energ. Phys.* **2010** (2010) 58.
- [39] M.L. Boas, *Mathematical Methods in the Physical Sciences*, Wiley, Hoboken, NJ, 3rd ed ed. (2006).
- [40] T. Becher, M. Neubert and B.D. Pecjak, *Factorization and Momentum-Space Resummation in Deep-Inelastic Scattering*, *J. High Energy Phys.* **2007** (2007) 076 [[hep-ph/0607228](#)].

- [41] ATLAS Collaboration, *A measurement of soft-drop jet observables in $\$pp\$$ collisions with the ATLAS detector at $\$sqrt{s} = 13\$$ TeV*, *Phys. Rev. D* **101** (2020) 052007 [[1912.09837](#)].
- [42] *The Hypergeometric Functions*, in *Special Functions*, G.E. Andrews, R. Roy and R. Askey, eds., Encyclopedia of Mathematics and Its Applications, (Cambridge), pp. 61–123, Cambridge University Press (1999).
- [43] D. Zagier, *The Dilogarithm Function*, in *Frontiers in Number Theory, Physics, and Geometry II: On Conformal Field Theories, Discrete Groups and Renormalization*, P. Cartier, P. Moussa, B. Julia and P. Vanhove, eds., (Berlin, Heidelberg), pp. 3–65, Springer (2007).